

ABSTRACT

KHARE, NIDHI. Phosphate Sorption in Single and Mixed Fe- and Al-oxide Systems.

(Under the direction of Dr. Dean L. Hesterberg)

The interaction of phosphate with Fe(III) and Al(III) is important in soils, wastes and other systems of environmental significance. The goal of this research was to characterize phosphate sorption in single- and mixed Fe- and Al-oxide systems using XANES (X-ray absorption near edge structure spectroscopy). The specific objectives of this research were: 1) To determine the quantitative distribution of phosphate between Fe- and Al-oxide minerals in mixtures containing these minerals; 2) To assign XANES spectral features for phosphate associated with Fe(III) or Al(III) to specific electronic transitions; and 3) To characterize adsorption versus surface precipitation in single- and binary mixtures of Fe- and Al-oxide minerals. Phosphate was sorbed in single-mineral aqueous suspensions of ferrihydrite [Fe(OH)₃], boehmite (γ -AlOOH), goethite (α -FeOOH), or non-crystalline (non-xl) Al-hydroxide [Al(OH)₃] and mixtures of ferrihydrite/boehmite, goethite/boehmite, and ferrihydrite/non-xl Al-hydroxide at pH 6. Samples were reacted at 22 °C for 42 h. Phosphate sorption isotherm trends for mixed-mineral systems were L-curves and were intermediate to those of the respective minerals in the mixture. Phosphorus K-XANES spectra for PO₄ on Fe- vs. Al-oxide minerals differed in that a weak doublet peak was observed for Fe-oxides on the low-energy side of the P K-edge, i.e., in the pre-edge region. The quantitative distribution of phosphate between ferrihydrite and boehmite in mixtures of these minerals was determined using linear combination

fitting (LCF) analysis of the XANES pre-edge region. Results showed that PO_4 essentially distributed itself in proportion to the maximum PO_4 sorption capacity of each of these minerals. Using a XANES fitting procedure, PO_4 was found to show a greater apparent preference for boehmite and non-xl Al-hydroxide minerals in goethite/boehmite and ferrihydrite/non-xl Al-hydroxide mixtures, respectively. To interpret XANES spectra based on molecular bonding configuration, spectral features were assigned to specific electronic transitions using bonding arguments supported by extended Huckel (EH) model computations of molecular orbital energies (projected density of states-PDOS). Experimental evidence (both XANES and UV-visible spectroscopy) was given for the white-line peak in Fe(III)/phosphate systems being caused by a dipole allowed transition of a P 1s electron to a P(3p)-O(2p) antibonding molecular orbital. Similarly, the white-line peak in Al-phosphate systems was assigned to a dipole allowed transition into a Al(3p)-O(2p)-P(3p) antibonding molecular orbital. The pre-edge feature in XANES spectra was assigned to a dipole allowed transition into a Fe(4p)-O(2p) antibonding molecular orbital. Using these XANES spectral assignments, the increase in FWHM (full width at half maximum height) of the white-line peak in XANES spectra indicated precipitation. Based on a linear increase in FWHM with increasing sorbed PO_4 concentration, Al-phosphate surface precipitation occurred in boehmite and non-xl Al-hydroxide systems. On the contrary, no evidence was found for Fe-phosphate precipitation in single-mineral systems of goethite and ferrihydrite. Surface precipitation occurred in goethite/boehmite mixtures following similar trends as in boehmite, but no evidence for surface precipitation was found in ferrihydrite/non-xl Al-hydroxide mixtures over

the range of phosphate studied (up to 1230 mmol kg⁻¹). In these mixtures, mineral interactive effects apparently inhibited Al-phosphate precipitation as occurred when phosphate was reacted with non-xl Al-hydroxide alone. Furthermore, phosphate showed a trend of affinity preference for non-xl Al-hydroxide with increasing adsorbed P concentrations in the ferrihydrite/non-xl Al-hydroxide mixtures.

**PHOSPHATE SORPTION IN SINGLE AND MIXED Fe- and Al-OXIDE
SYSTEMS**

**by
Nidhi Khare**

A dissertation submitted to the Graduate Faculty of
North Carolina State University
in partial fulfillment of the
requirements for the Degree of
Doctor of Philosophy

Soil Science

Raleigh

2003

APPROVED BY:

Chair of Advisory Committee

DEDICATION

All the good that comes out of this work is from Allah (swt) (the one true GOD, in arabic) alone! The most loving, and compassionate, the owner of knowledge and wisdom who gave me the patience, guidance, and perseverance needed to complete this work and put mercy and compassion in the hearts of human beings who helped toward this work.

BIOGRAPHY

The author of this work was born in India and completed her Btech. (Hons.) degree in Agricultural Engineering from Indian Institute of Technology (Kharagpur, India) in June of 1995. After graduating, she worked at city corp. overseas software limited as a software engineer. In August 1995, she came to North Carolina State University to start a Master's degree in Biological and Agricultural Engineering addressing hog waste disposal. She then, worked in the area of animal waste management developing software to evaluate different waste treatment technologies. During the spring of 1999, she became interested in the area of soil chemistry. In July of 2000, she started her doctoral degree in the department of Soil Science under the guidance of Dr. Dean L. Hesterberg. Her goal is to use her abilities toward building bridges in an increasingly fragmented world.

ACKNOWLEDGMENTS

Acquire knowledge because its acquisition is God-consciousness, its search is worship and jihad (struggle), its teaching is charity and imparting it to those who are worthy is meritorious. It is a friend in journey, companion in solitude, guide to religion, and light in happiness and misfortune. It is a bosom friend to a stranger and beacon to the path of paradise.

Translated from a part of the saying of prophet Muhammad (Peace be upon him)

This work would not have been possible without the kindness of a great many individuals. It is not possible to give thanks truly due to them; this is simply a token of the appreciation of their efforts.

I am very grateful to my advisor Dr. Dean L. Hesterberg for his guidance and intense involvement in my research. His expertise and dedication to soil physical chemistry helped steer this work to completion. He spent many hours in the laboratory instilling in me the thoroughness and consistency required for making good quality samples. I am very grateful for the many nights he spent teaching me the details of data collection and analysis at the National Synchrotron Light Source (Brookhaven National Lab). His passion and love for learning helped me to continuously improve this work. Many of the best ideas in this work are his. He was a great support to me during the difficult times of my job search and his encouragement was invaluable. Above, all his kindness and patience in teaching me were critical in my education.

A special thanks is owed to Dr. Martin, my chemistry professor. His contribution helped take this dissertation a step up. All ideas about molecular orbital theory are his. Many thanks are due to him for the hours he spent guiding this work, particularly the second and third chapter of this dissertation. His experience inspired me to persist and complete this work.

I benefited tremendously from Dr. Sayers expertise in XANES spectroscopy. His pre-lim-oral questions helped me dig deeper into the area of molecular environmental sciences. I am very grateful for his encouragement and personal interest in guiding my job search.

I owe my understanding of thermodynamics, surface complexation modeling, and soil analysis techniques to Dr. Robarge. We have had many interesting discussions about my research. His availability to brainstorm helped this work greatly.

Special thanks are due to Dr. Suzanne Beauchemin without whose help I could not have completed data collection for my dissertation. She was a source of support and encouragement and her experience as a woman scientist was a source of inspiration to me.

Dr. Shan-Li Wang, a previous postdoctoral scientist (in Dr. Hesterberg's group) was a catalyst for this research. I owe my knowledge of IR spectroscopy and single-crystal work to him; his help is gratefully acknowledged. I also want to thank Dr. Roger Sullivan (Dr. Martin's previous doctoral student) for the many stimulating discussions we had about my research.

Ms. Kim Hutchison taught me some of the basic lab procedures and I am very grateful for her assistance during sample preparation before data analysis. She often went out of her way to help with this research and her generosity will be remembered. Ms. Daphine McKinney, my colleague and officemate often lightened the burden; this Ph.D. would not have been possible without her support and

friendship. Roberta-Miller Haraway's help with my power-point presentations is greatly appreciated. Thanks are due to Melissa Massengill, Dee Ann Cooper, and Angela Nicholson of the Soil Science administrative staff who went out of their way to help smooth things. Also, many thanks are owed to all faculty and staff who supported and assisted in this work.

My parents instilled in me a love for learning since my early childhood; I owe this work to the education and upbringing they imparted and their and constant encouragement and support. During the ~8 years of my graduate study, I looked to (my friend and family) Dr. Azza H. Mahmoud as a role model. My friend Dr. Mouna Nakkas was a constant source of support and good advice. Another friend, Dr. Afaf J. Khogeer taught me the value of hard work and commitment to perfection! My uncle and tant (french for aunt) Salah and Soad Elshafie opened their home and hearts to me and shared with me the pain and joy of this struggle. Their home was my refuge during the most difficult times of this work. My friend Sahar Elshafie's experience as a teacher and support came in use when it was most needed.

TABLE OF CONTENTS

	Page
LIST OF TABLES	ix
LIST OF FIGURES	x
1. INTRODUCTION.....	1
2. XANES ANALYSIS OF ADSORBED PHOSPHATE DISTRIBUTION BETWEEN FERRIHYDRITE AND BOEHMITE IN MIXED-MINERAL SYSTEMS.....	8
Introduction.....	8
Materials and Methods.....	11
Results and Discussion.....	18
Conclusions.....	29
References.....	30
Table.....	35
Figure Captions.....	36
Figures.....	38
3. ASSIGNMENT OF PHOSPHORUS K-XANES SPECTRAL FEATURES TO ELECTRONIC TRANSITIONS IN Fe- AND Al-PHOSPHATE SYSTEMS.....	45
Introduction.....	45
Methods.....	48
Results	54
Discussion	56
Conclusions.....	67
References.....	69
Figure Captions.....	74
Figures.....	76
4. XANES INVESTIGATION OF METAL PHOSPHATE PRECIPITATION IN SINGLE AND BINARY MIXTURES OF Fe- and Al-OXIDE MINERALS.....	90
Introduction.....	90
Materials and Methods.....	93

TABLE OF CONTENTS (continued)

Results and Discussion.....	99
Conclusions.....	108
References	109
Tables.....	113
Figure Captions.....	115
Figures	117
5. CONCLUSIONS AND IMPLICATIONS	129

LIST OF TABLES

	Page
2.1 Distribution of PO ₄ between boehmite and ferrihydrite in 1:1 (mass basis) mixtures of these minerals at pH 6.0 ± 0.1 calculated using linear combination fitting of edge normalized phosphorus K-XANES spectra.....	35
4.1 Phosphate associated with Fe and Al in 1:1 (mass basis) mixtures of goethite and boehmite calculated using linear combination fitting of edge normalized phosphorus K-XANES spectra.....	113
4.2 Phosphate associated with Fe and Al in 1:1 (mass basis) mixtures of ferrihydrite and non-xl Al-hydroxide calculated using linear combination fitting of edge normalized phosphorus K-XANES spectra.....	114

LIST OF FIGURES

	Page
<p>2.1 Adsorption isotherms for phosphate on boehmite, ferrihydrite, and mixed boehmite/ferrihydrite (1:1 mass basis) at pH 6.0 ± 0.1, along with Freundlich isotherm models as solid lines for the Jun02 data. Data for the mixed mineral isotherm for Jun 02 are fit using a mass weighted (1:1) linear combination of Freundlich models from the single-mineral systems (dashed line, see text). Some additional data collected in Oct 02 for PO_4 adsorbed on mixed-mineral systems are shown. q_f, q_m, q_b, denote the Freundlich model predicted PO_4 adsorption for ferrihydrite (f), mineral mixtures (m), and boehmite (b) as a function of dissolved PO_4 concentration (c).</p>	38
<p>2.2 Edge-normalized, stacked phosphorus K-XANES spectra for phosphate adsorbed on boehmite, ferrihydrite (ferri.) or mixed-mineral systems (Jun 02 at pH 6.0 ± 0.1) at selected concentrations. Numbers in the legend denote adsorbed PO_4 in mmol kg^{-1}.</p>	39
<p>2.3 Edge-normalized phosphorus K-XANES spectra for strengite versus variscite and ensemble-averaged spectra for phosphate adsorbed on ferrihydrite (ferri.) versus boehmite at pH 6.0 ± 0.1, showing a pre-edge feature for PO_4 associated with Fe(III).</p>	40
<p>2.4 Comparison of the pre-edge region for edge-normalized XANES spectra for PO_4 adsorbed in mixed-mineral systems (Jun 02) at selected concentrations with spectra for averaged standards for PO_4 adsorbed on boehmite or ferrihydrite at pH 6.0 ± 0.1. Least square linear fits to the mixed-mineral systems using a combination of the averaged standards for PO_4 adsorbed on boehmite or ferrihydrite are also included. Numbers in the legend denote adsorbed PO_4 concentrations in mmol kg^{-1}.</p>	41
<p>2.5 Pre-edge region in edge-normalized phosphorus K-XANES spectra for phosphate adsorbed on ferrihydrite (ferri.–Jun 02 and Oct 02 data) or boehmite at various concentrations at pH 6.0 ± 0.1 along with averaged standards for PO_4 adsorbed on each mineral. Numbers in the legend denote adsorbed PO_4 concentrations in mmol kg^{-1}.</p>	42
<p>2.6 Concentration of PO_4 adsorbed on ferrihydrite (as calculated from XANES fitting analysis) plotted as a function of total adsorbed phosphate concentration in ferrihydrite-boehmite mixtures. (a) Linear regression fits for Jun 02 and Oct 02 data; (b) Comparison of Jun 02 data with a no-preference line based on distribution of adsorbed PO_4 between the minerals in direct proportion to their relative contributions to the maximum adsorption capacity of the mixed systems.</p>	43

	Page
3.1 Metal (M = Fe or Al) phosphate clusters in different idealized bonding configurations used for extended Huckel computations are illustrated: a) monodentate complex; b) bidentate complex.	76
3.2 Edge-normalized phosphorus K-XANES spectra for phosphate associated with Fe(III) in aqueous, sorbed (on ferrihydrite), and mineral (strengite) complexes versus phosphate associated with Al(III) in sorbed (on boehmite) and mineral (variscite) complexes.	78
3.3 Phosphorus K-XANES spectra for aqueous Fe (III)-phosphate solutions at Fe/P molar ratios of 0 to 2 (50 mmol P kg ⁻¹ ; pH~0.5). The intensity of the pre-edge feature increased with increasing Fe/P ratio and the white-line peak shifted toward higher energy: a) overall spectra in -10 to 25 eV relative energy range; b) rescaled white-line region.	79
3.4 Pre-edge region in phosphorus K-XANES spectra for aqueous Fe (III) Phosphate solutions at Fe/P molar ratios of 0 to 2 (50 mmol P kg ⁻¹ ; pH~0.5). Pre-edge peaks are denoted as a and b.	81
3.5 UV-visible absorption spectra for aqueous Fe (III)-phosphate solutions (50 mmol P kg ⁻¹ ; pH~0.5) at Fe/P molar ratios of 0 to 2. The peak shifted to lower energies with increasing Fe/P ratio.	82
3.6 Energies of peaks in the phosphorus K-XANES spectra (white-line) and UV-visible spectra as a function of Fe/P molar ratio.	83
3.7 Comparison of the energies of valence atomic orbitals and corresponding core orbitals (dotted), bonding molecular orbitals, (dashed), and antibonding molecular orbitals (solid) expected for Fe/PO ₄ and Al/PO ₄ systems: a) atomic orbital energies for Fe, Al, P, and O; b) P(1s) core orbitals and molecular orbitals.	84
3.8 The projected density of states (PDOS) of antibonding molecular orbitals computed for Fe-PO ₄ and Al-PO ₄ in idealized monodentate and bidentate geometries using the Extended Huckel approximation: (a) monodentate FePO ₄ complex; (b) bidentate Fe-PO ₄ complex; (c) monodentate Al-PO ₄ complex; (d) bidentate Al-PO ₄ complex.	86
4.1 Sorption isotherms for phosphate on single- and mixed-mineral systems (1:1 mass basis) at pH 6.0 ± 0.1, along with Freundlich isotherm models. (a) goethite/boehmite systems; (b) ferrihydrite/non-xl Al-hydroxide systems. Data for the mixed mineral isotherm are also compared with mass weighted (1:1) linear combination of Freundlich models from the single-mineral systems (dashed line). Model parameters q _i and c _i denote the Freundlich model predicted sorbed and dissolved PO ₄ concentrations respectively for boehmite (B), goethite (G), non-xl Al- hydroxide (A)	

	Page
ferrihydrite (F), and mineral mixtures (M), calculated from the data.	117
4.2 Normalized, stacked phosphorus K-XANES spectra for phosphate sorbed on goethite, boehmite, or mixed-mineral systems at pH 6.0 ± 0.1 at selected concentrations. Numbers in the legend denote adsorbed PO_4 in mmol kg^{-1} . A pre-edge feature between -5 and -1 eV relative energy is apparent in the goethite and mixed-mineral spectra.	118
4.3 Normalized, stacked phosphorus K-XANES spectra for phosphate sorbed on ferrihydrite, non-xl Al-hydroxide, or mixed-mineral systems at pH 6.0 ± 0.1 at selected concentrations. Numbers in the legend denote adsorbed PO_4 in mmol kg^{-1} . A pre-edge feature between -5 and -1 eV relative energy is apparent in the ferrihydrite and mixed-mineral spectra.	119
4.4 The projected density of states (PDOS) computed for Al- PO_4 complex and variscite using the Extended Huckel approximation: (a) PDOS for monodentate Al- PO_4 ; (b) PDOS for the mineral variscite.	121
4.5 Comparison of the pre-edge region for normalized XANES spectra for PO_4 sorbed in mixed-mineral systems at selected concentrations with spectra for averaged standards for PO_4 sorbed on Fe-oxide or Al-oxide at pH 6.0 ± 0.1 . Numbers in the legend denote adsorbed PO_4 concentrations in mmol kg^{-1} : (a) goethite/boehmite mixtures; (b) ferrihydrite/non-xl Al-hydroxide mixtures.. . . .	123
4.6 Concentration of PO_4 sorbed on the Fe-oxide component of Fe- and Al-oxide mixtures (as calculated from XANES fitting analysis) plotted as a function of total sorbed phosphate concentration for mixtures: (a) goethite/boehmite mixtures; (b) ferrihydrite/non-xl Al-hydroxide mixtures. The apparent no-preference line was determined based on the maximum observed sorption capacities of the single minerals in Fig. 1, assuming no surface precipitation (see Chapter 2). Regression fits to the data are also included.	125
4.7 The full width at half maximum height (FWHM) of the white-line peak in XANES spectra for phosphate sorbed on mixtures, and the respective single-mineral components as a function of sorbed PO_4 concentration: (a) goethite/boehmite mixtures; (b) ferrihydrite/non-xl Al-hydroxide mixtures.	127

1. INTRODUCTION

Phosphorus has been intensively studied due to its role in the eutrophication of surface waters and status as a plant macronutrient. It has currently gained importance due to the USDA-USEPA policy to limit phosphorus input to soils with animal waste and fertilizers (Sharpley et al., 2000). Although, phosphorus sorbs strongly to soil and has mainly been a concern for surface water quality, in deep sandy, organic-matter rich, or P-enriched soils, P can also leach and deteriorate sub-surface water quality (Sims et al., 1997). Soil phosphate concentration, its matrix composition (e.g. mineralogy, and organic matter content), pH, and redox potential are considered the main factors affecting soil phosphate dissolution. In acid soils and sediments, Fe- and Al-oxide minerals are considered the main phosphate sorbents (Beauchemin and Simard, 1999; Sallade and Sims, 1997; Pierzynski et al., 1990a; 1990b). Hence, the goal of this research was to characterize the interaction of ortho-phosphate with Fe and Al-oxide minerals relevant to soils. Pure and mixed-mineral systems were used as these can be controlled and characterized and can provide an understanding of fundamental interactions of ortho- PO_4 with Fe(III) and Al(III) bearing minerals. Goethite, boehmite, ferrihydrite, and non-crystalline Al-hydroxide were chosen for this research because ferrihydrite, boehmite, and non-crystalline Al-hydroxide minerals are poorly crystalline and non-crystalline analogues of Fe- and Al-oxide minerals in soil, and goethite is ubiquitous in soils and sediments.

Past work has involved P-sorption on a single sorbent, or competitive sorption of multiple sorbates on a single sorbent, for example competitive

sorption of PO_4 and AsO_4 on oxide minerals (Violante et al., 1997). Although, some studies (Ioannou et al., 1998; Papadopoulos et al., 1998) have characterized phosphate sorption on multiple sorbents, only equilibrium adsorption isotherms and kinetic measurements were used. Hence, one unresolved issue was to determine phosphate solid state speciation in single- and mixed Fe- and Al-oxide systems. This is important because dissolution of phosphate during soil reduction has been explained by the release of phosphate associated with Fe(III)-phosphate and Fe(III)-oxide minerals (Patrick et al., 1973; Hongve, 1997; Reddy et al., 1998). However, Al-oxide minerals are considered redox inactive, so any associated phosphate may be less susceptible to release during soil reduction. Hence, the relative distribution of phosphate between Fe- and Al-oxide minerals may affect its dissolution. Phosphate solid-state speciation as adsorbed vs. surface precipitated forms is also important because surface precipitation (compared to strictly adsorption) can cause greater amounts of phosphate to be associated with oxide minerals and can also retard its release.

Several molecular-scale techniques including nuclear magnetic resonance (NMR), X-ray photoelectron (XPS), and X-ray absorption fine structure (XAFS) spectroscopies were considered to determine phosphate solid state speciation. It was important that the technique was able to characterize phosphate sorption in-situ (aqueous samples) and be element specific. Nuclear magnetic resonance (NMR) and XPS techniques were element specific but required sample drying. Furthermore, paramagnetic ions such as Fe(III) cause peak broadening in NMR spectra. X-ray absorption fine structure spectroscopy is element specific, and can

be done in moist samples and hence, may be used for studying phosphate sorption in-situ. X-ray absorption fine structure spectroscopy comprises X-ray absorption near edge structure (XANES) and extended X-ray absorption fine structure (EXAFS) techniques. Although EXAFS can provide bonding information of phosphorus with oxide minerals, significant improvement in signal to noise ratio is needed to fully exploit the EXAFS region at the P K-edge (Bradley et al., 1997). Hesterberg et al., (1999) showed that P K-XANES could be used to study sorbed PO_4 and precipitated Fe- and Al-phosphates. Hence, for our research XANES was selected to characterize phosphate sorption in single- and mixed Fe- and Al-oxide systems.

XANES spectroscopy involves the excitation of an electron from a core atomic orbital into bound molecular orbitals or into the continuum (Durham, 1988) and provides information on geometrical arrangements of atoms in a local cluster around the absorbing atom (Bianconi, 1988). Phosphorus K-XANES spectra may be interpreted via fingerprinting by comparing XANES spectra of the compounds investigated with a series of standards or via theoretical density of states (DOS) computations. The fingerprinting approach is limited and relies on the availability of suitable standards, while DOS computations can be used for assigning XANES spectral features to specific electronic transitions that can allow interpretation of spectral trends to obtain solid-state speciation information. Although some P K-XANES studies (Franke and Hormes, 1995; Okude et al., 1999) have provided information on assignment of P K-XANES spectral features, this information was limited and not based on theoretical computations.

My goal was to characterize the molecular-scale bonding of phosphate on Fe- and Al-oxide mixtures using phosphorus K-XANES analysis as a spectroscopic tool. The specific objectives of this research were: (1) To develop a method to quantify the distribution of phosphate between Fe- and Al-oxides in mixtures of these minerals (Chapter 2); (2) To assign P K-XANES spectral features to specific electronic transitions in Fe- and Al-phosphate systems (Chapter 3); and (3) To investigate the transition from adsorption to surface precipitation in single- and mixed Fe- and Al-oxide systems (Chapter 4).

REFERENCES

Beauchemin, S. and R.R. Simard. 1999. Soil phosphorus saturation degree: review of some indices and their suitability for P management in Quebec, Canada. *Can. J. Soil Sci.* 79:615-625.

Bianconi, 1988. XANES. p 150-190. In D.C. Koningsberger and R. Prins (ed.) *X-ray absorption: principles, applications, techniques of EXAFS, SEXAFS, and XANES*. John Wiley & Sons, New York.

Bradley, S.M., S. Djajanti, S. Thomson, R.F. Howe. 1997. Soft X-ray absorption spectroscopy of microporous materials. SSRL activity report.

Franke, R. and J. Hormes. 1995. The P K-near edge absorption spectra of phosphates. *Physica B.* 216:85 - 95.

Hesterberg, D.L., W. Zhou, K.J. Hutchison, S. Beauchemin, and D.E. Sayers. 1999. XAFS study of adsorbed and mineral forms of phosphate. *J. Synchrotron Rad.* 6:636-638.

Hongve, D. 1997. Cycling of iron, manganese, and phosphate in a meromictic lake. *Limnol. Oceanogr.* 42:635-647.

Ioannou, A., A. Dimirkou, and P. Papadopoulos. 1998. Phosphate sorption by goethite and kaolinite-goethite (K-G) systems as described by isotherms. *Commun. Soil Sci. Plant Anal.* 29:2175-2190.

Okude, N., M. Nagoshi, H. Noro, Y. Baba, H. Yamamoto, T.A. Sasaki. 1999. P and S K-edge XANES of transition metal phosphates and sulfates. *J. Electron Spectrosc. Relat. Phenom.* 101-103: 607-610.

Papadopoulos, P., A. Dimirkou, and A. Ioannou. 1998. Kinetics of phosphorus sorption by goethite and kaolinite-goethite (K-G) Systems. *Commun. Soil Sci. Plant Anal.* 29:2191-2206.

Patrick, W.H., S. Gotoh, and B.G. Williams. 1973. Strengite dissolution in flooded soils and sediments. *Science* 179: 564-565.

Pierzynski, G.M., T.J. Logan, S.J. Traina, and J.M. Bigham. 1990a. Phosphorus chemistry and mineralogy in excessively fertilized soils: quantitative analysis of phosphorus-rich particles. *Soil Sci. Soc. Am. J.* 54:1576-1583.

Pierzynski, G.M., T.J. Logan, S.J. Traina, and J.M. Bigham. 1990b. Phosphorus chemistry and mineralogy in excessively fertilized soils: descriptions of phosphorus-rich particles. *Soil Sci. Soc. Am. J.* 54:1583-1589.

Pote D. H., T.C. Daniel, A.N. Sharpley, P.A. Moore, Jr. D.R. Edwards, and D.J. Nichols. 1996. Relating extractable soil phosphorus to phosphorus losses in runoff. *Soil Sci. Soc. Am. J.* 60:855-859.

Reddy, K.R., G.A.O.' Connor, and P.M. Gale. 1998. Phosphorus sorption capacities of wetland soils and stream sediments impacted by dairy effluent. *J. Environ. Qual.* 27: 438-447.

Sallade, Y.E., and J.T. Sims. 1997. Phosphorus transformations in the sediments of Delaware's agricultural drainageways: II. Effect of reducing conditions on phosphorus release. *J. Environ. Qual.* 26: 1579-1588.

Sharpley, A.N. 1995. Dependence of runoff phosphorus on extractable soil phosphorus. *J. Environ. Qual.* 24:920-926.

Sims, J.T., Simard R.R., and Joern, B.C. 1998. Phosphorus loss in agricultural drainage: Historical perspective and current research. *J. Environ. Qual.* 27:277-293.

Violante, A., and M. Pigna. 2002. Competitive sorption of arsenate and phosphate on different clay minerals and soils. *Soil Sci. Soc. Am. J.* 66:1788-1796.

2. XANES ANALYSIS OF ADSORBED PHOSPHATE DISTRIBUTION BETWEEN FERRIHYDRITE AND BOEHMITE IN MIXED-MINERAL SYSTEMS

INTRODUCTION

Phosphorus has been intensively studied due to its importance as a plant macronutrient, and more recently because of its negative role in the eutrophication of surface waters. In deep sandy soils, soils rich in organic matter, or soils with elevated phosphorus concentrations from long-term fertilization, phosphorus can also be leached through the soil profile and eventually be discharged with subsurface flow to surface waters (Sims et al., 1998). Soil phosphorus has recently gained much attention due to the USDA-USEPA policy to limit phosphorus input with animal waste and fertilizers (Sharpley et al., 2000).

Soil phosphate concentration, soil matrix composition (e.g. mineralogy, and organic matter content), pH, and redox potential are considered to be the main soil properties affecting phosphate dissolution and mobility. Phosphate typically binds strongly with soils. However, soil P concentration was positively correlated with dissolved PO_4 concentration in runoff water, and this relationship was soil specific (Sharpley, 1995; Pote et al., 1996). Being able to predict phosphate dissolution and mobility in different soils or under varying soil conditions would help in developing soil management practices that decrease detrimental environmental impacts of P. Soil phosphate speciation, i.e., the chemical forms of phosphate in a soil, dictates the effects of soil phosphate concentration, mineralogy, pH, and redox potential on phosphate binding and dissolution.

Phosphate adsorption in soils has been correlated with a number of indices derived from chemical extractions (Beauchemin and Simard, 1999). For example, the phosphate sorption capacity of soils has been related to various indices based on acid oxalate extractable Fe and Al, suggesting that poorly crystalline Fe- and Al-oxides are largely responsible for phosphate retention in acidic soils (Beauchemin and Simard, 1999). Similarly, chemical extraction analyses of Sallade and Sims (1997) suggested that phosphate in sediments collected from drainage ditches adjacent to agricultural fields was associated with Fe- and Al-oxide minerals. Ferrihydrite, a poorly crystalline Fe-oxide mineral is often found in sediments or hydromorphic soils as a precursor of other Fe-oxide minerals (Schwertmann and Cornell, 1991). Furthermore, transmission electron microscopy with energy dispersive x-ray analysis (TEM/EDX) showed association of phosphate with Al and Fe in isolated particles from different soils (Pierzynski et al., 1990a; 1990b)

Phosphate dissolution in soils may depend on the relative distribution of phosphate between Fe- and Al-oxide minerals. For example, dissolution of phosphate during soil reduction has been explained by release of phosphate associated with Fe(III)-phosphate and Fe(III)-oxide minerals (Patrick et al., 1973; Hongve, 1997; Reddy et al., 1998). However, Al-oxide minerals are considered redox inactive, so any associated phosphate should be less susceptible to release during soil reduction.

One barrier to evaluating such hypotheses is the lack of a direct method for quantifying phosphate distribution between Fe- and Al-oxide minerals when

these minerals occur as a mixture (as in soils). Past research characterizing phosphate adsorption in mineral mixtures, specifically kaolinite and goethite, used equilibrium adsorption isotherms and kinetic measurements (Ioannou et al., 1998; Papadopoulos et al., 1998). However, definitive information about the distribution of phosphate between these two minerals could not be obtained from empirical modeling (Langmuir and Freundlich fits) of the macroscopic adsorption data. In this research, we characterized the distribution of phosphate between ferrihydrite and boehmite using phosphorus K-XANES analysis.

Hesterberg et al. (1999) identified unique features in P K-XANES spectra of strengite ($\text{FePO}_4 \cdot 2\text{H}_2\text{O}$) and variscite ($\text{AlPO}_4 \cdot 2\text{H}_2\text{O}$), which indicated the possibility of distinguishing adsorbed phosphate in mixed Fe- and Al-oxide systems. For example, due to electron orbital configurations and electronic transitions at the x-ray absorption edge, phosphate associated with Fe(III) and some other transition metals in phosphate minerals produces a distinct pre-edge feature on the low energy side of an intense white-line peak near 2150 eV in the P K-XANES spectrum (Behrens, 1992; Hesterberg et al., 1999; Franke and Hormes, 1995; Okude et al, 1999). This feature is absent in spectra of Al-phosphates. Because of the ability of XANES to distinguish phosphate bound to Fe(III) versus Al(III), this technique was considered suitable for characterizing phosphate on Fe- and Al-oxide minerals.

The objective of this research was to utilize XANES spectroscopy to quantify the distribution of phosphate between ferrihydrite and boehmite in mixtures of these minerals, and thereby determine the relative affinity of phosphate for each

mineral in the mixture. Two-line ferrihydrite ($\text{Fe}_5\text{HO}_8 \cdot 4\text{H}_2\text{O}$) and poorly crystalline boehmite ($\gamma\text{-AlOOH}$) were chosen because we expected that their high (and comparable) phosphate sorption capacities (relative to, e.g., goethite and gibbsite) would allow better detection of subtle changes in XANES spectra of the mixtures. Ferrihydrite is representative of poorly crystalline Fe-oxides in soils, and boehmite is a finely-divided, crystalline analog of non-crystalline Al-hydroxides relevant to soils.

MATERIALS AND METHODS

Mineral Synthesis and Characterization

Two-line ferrihydrite was synthesized by hydrolyzing Fe(III) with KOH according to the method of Schwertmann and Cornell (1991) and aging for 6 months before use. Poorly-crystalline boehmite was purchased from Reheis Co. (Berkeley Heights, NJ) in gel form under the trade name Rehydragel HPA. Both ferrihydrite and boehmite were analyzed before experiments using X-ray powder diffraction to determine mineralogical purity. The X-ray diffraction pattern for ferrihydrite showed only two broad peaks at 0.15 and 0.24 nm, which is characteristic of two-line ferrihydrite. More crystalline Fe-oxides, if present, were not detected. The X-ray diffraction pattern for the boehmite sample showed all peaks reported for boehmite, and no peaks for gibbsite or any other crystalline Al-oxide minerals. The maximum adsorption capacities of boehmite and ferrihydrite remained constant within 3% between Jun 2002 and Jun 2003, indicating that aging did not affect PO_4 adsorption on these minerals.

Ferrihydrite was washed thrice with 1 mol L⁻¹ KCl solution and further washed with 0.01 mol L⁻¹ KCl to obtain a 0.01 mol L⁻¹ KCl background electrolyte. Boehmite gel in deionized water was brought into a 0.01 mol L⁻¹ KCl background by adding 1 mol L⁻¹ KCl solution. Both minerals were stored as stock aqueous suspensions of known (measured) solids concentration in 0.01 mol L⁻¹ KCl (see Alcacio et al., 2001) containing 40.2 g ferrihydrite kg⁻¹ and 14.1 g boehmite kg⁻¹. The mean crystalline dimensions of poorly crystalline boehmite used in this study were previously determined to be 4.5, 2.2 and 10 nm along the crystal a, b and c axes respectively, and the BET H₂O surface area reported for this mineral was 514 m²g⁻¹ (Wang et al. 2003). Water adsorption was previously used to avoid sample drying and because this small, polar molecule can access the internal surfaces present in a poorly crystalline material such as boehmite (Wang et al. 2003). Because a temperature-induced structural change in poorly crystalline materials (such as boehmite and ferrihydrite) has been observed at 100-110°C (Wang et al., 2003), the N₂ BET surface areas of these minerals were not measured.

Adsorption Isotherms

Adsorption isotherm experiments for ferrihydrite, boehmite and mixed ferrihydrite-boehmite (1:1 mass ratio) suspensions were conducted at pH 6.0 in 250-mL polycarbonate centrifuge bottles following the basic procedure described by Oh et al. (1999).

All samples had a suspended solids concentration of 1.50 g kg⁻¹, constant

ionic strength of 0.01 mol L^{-1} KCl, and total sample mass of $133.34 \pm 0.01 \text{ g}$. Aqueous solutions for adsorption experiments (KCl, HCl, KOH, and KH_2PO_4 , all at 0.01 mol L^{-1} concentrations) were prepared using analytical grade reagents and degassed (heated and N_2 purged) deionized water. Stock mineral suspensions were shaken on a reciprocating shaker at a rate of 1 s^{-1} for at least 1 h before use. Two to eight grams of ferrihydrite, boehmite, or a 1:1 (by mass) mixture of ferrihydrite and boehmite prepared gravimetrically from stock suspensions were weighed while vigorously stirring a suspension on a magnetic stirrer, and brought to about 70% of the final sample mass with 0.01 mol L^{-1} KCl. An appropriate aliquot of 0.01 mol L^{-1} KH_2PO_4 was slowly added to each vigorously-stirred sample in random chronological order using a micropipetter. The pH was adjusted to pH 6.0 using 0.01 mol L^{-1} HCl or 0.01 mol L^{-1} KOH, and the sample headspace was flushed with N_2 gas. Samples were shaken for 42 h on a reciprocating water bath shaker at a rate of 0.5 s^{-1} and 22°C . Kinetics of phosphate sorption is complex, and this operationally chosen time of 42 h should be sufficiently long to complete fast sorption reactions (Li and Stanforth, 2000).

After about 16 h of shaking, the pH varied by an average of 0.2 units and was again adjusted to pH 6.0 and each sample was brought to its final mass. The pH was again checked after 40 h of equilibration and minor adjustments (usually <0.1 units) were made if needed. After equilibration, samples were centrifuged at $\sim 6000 \times g$ for 15 minutes, and the supernatant solutions were decanted. The pH was measured in a portion of the supernatant solution before filtering and was found to be 6.0 ± 0.1 for all samples. The remaining solutions were filtered under

vacuum using 0.2- μm Millipore Isopore polycarbonate filter membranes (Millipore Corporation, Bedford MA). Dissolved PO_4 was measured in the supernatant solutions using the molybdate colorimetric (Murphy-Riley) procedure (Olsen and Sommers, 1982). The concentration of PO_4 adsorbed on samples was determined as the difference between total added phosphate and PO_4 measured in supernatant solutions. Samples were analyzed on a Shimadzu Model UV 2101-PC spectrophotometer using a 1-cm (for higher-P samples) or 5-cm path length cell. Additional isotherm data for the single and mixed ferrihydrite/boehmite (mixed-mineral) systems were obtained on scaled down samples of 30 g total in 50 mL polycarbonate centrifuge tubes prepared under identical constraints and following an analogous procedure as outlined above. Isotherm results from both procedures were integrated.

XANES Data Collection and Analysis

Sample Preparation

For XANES analysis, each sedimented mineral sample from the 250-mL centrifuge bottles used for concurrent isotherm experiments was rinsed into 50-mL polycarbonate centrifuge tubes using a portion of its supernatant solution, and centrifuged at $\sim 20,000 \times g$ for 15 minutes. Because the supernatant solution in equilibrium with the solids from the prior centrifugation was used, no adsorption or desorption was expected. Supernatant solutions were decanted and each sedimented mineral sample was homogenized by mixing thoroughly with a clean teflon spatula in the 50-mL tube. The moist paste was de-watered to

a clay:water ratio of about 1:2 by placing it on a 0.2 μm Millipore filter, under vacuum, for < 60 s. Samples were loaded into labeled, acrylic sample holders and covered with 5 μm polypropylene X-ray film (Spex Industries, Metuchen, NJ) and secured with chemically-pure Kapton tape (Budnick Converting, Inc., Columbia, IL). Individually mounted samples were covered with a second piece of acrylic to protect the sample during transport, and sealed into a labeled low-density polyethylene plastic bag. All samples were sealed into a second plastic bag with a moist paper towel to prevent desiccation. Experiments were timed so that sample preparation was completed a maximum of three days in advance of XANES data collection. All XANES data for single, and mixed-mineral systems were collected in June 2002 (Jun 02) during a single synchrotron beam time (a data collection period) except for five additional samples of mixed-mineral systems (100, 570, 760, 920, and 1190 $\text{mmol PO}_4 \text{ kg}^{-1}$) collected in October 2002 (Oct 02) to determine reproducibility of results.

Data Collection

Phosphorus K-XANES data acquisition was done at Beamline X-19A at the National Synchrotron Light Source, Brookhaven National Laboratory in Upton, NY. The electron beam energy was 2.5 GeV and the maximum beam current was 300 mA. The synchrotron radiation was monochromatized by a germanium [Ge(111)] monochromator. The monochromator was calibrated to 2149 eV at the edge (maximum peak in the 1st-derivative spectrum) of variscite. A variscite reference for monochromator calibration could not be placed behind samples

because of the low energy (low penetrating power) of the X-rays at the P K-edge. For example, we calculate based on absorption coefficients (McMaster et al., 1969) that >99% of the X-ray intensity at 2150 eV would be attenuated by a 10 μm thickness of iron oxide. Samples of thickness $\ll 10 \mu\text{m}$ would be required for collecting data in transmission mode, which was not practical. Moreover thin samples can desiccate quickly, thus defeating the purpose of using XANES analysis for moist samples to determine phosphate distribution in-situ. Therefore, a 0.1 mm thick moist paste was used for data collection to maintain sample moisture. XANES spectra were collected at photon energies between 2079 and 2248 eV, with a minimum step size of 0.2 eV between 2099 to 2174 eV. Two to four scans with consistent baselines were ensemble averaged.

Spectra were collected in fluorescence mode using a PIPS (Passivated Implanted Planar Silicon) detector mounted into a He-filled sample chamber. XANES data were also collected for variscite and strengite standards diluted to 400 mmol P kg^{-1} in boron nitride. Self-absorption effects can distort XANES spectra collected in fluorescence mode, particularly at low X-ray energies as used here, and at high concentrations of the analyte (P in this case) (Troger et al., 1992). Hesterberg et al. (1999) calculated that self-absorption at the phosphorus K-edge was <10% for phosphate mineral samples diluted to 800 mmol kg^{-1} in boron nitride. If self-absorption significantly affected our XANES spectra, we would expect to see a decrease in the white-line peak intensity with increasing adsorbed P. However, the white-line peak intensities for PO_4 adsorbed on ferrihydrite remained essentially constant between 100 and 1680

mmol P kg⁻¹ (Fig. 2-discussed below), indicating that self-absorption did not measurably impact our results.

Data Normalization

The photon energy scale was normalized to a relative energy scale by subtracting the calibration energy of 2149 eV from all spectra (Hesterberg et al., 1999). The data were baseline corrected using a linear regression between -40 and -10 eV relative energy (Sayers and Bunker, 1988). To quantitatively analyze the pre-edge region of the spectra, baselines were further refined by adjusting all spectra in a set to a common fluorescence yield value at -8 eV. To remove P concentration effects on the edge step, single-point background normalization (Sayers and Bunker, 1988) was done in three ways, using the fluorescence yield at each of three energies: (1) at the maximum peak between 10 and 18 eV in the first derivative XANES spectrum (edge normalized), (2) at the maximum of a post white-line resonance feature between 14 and 18 eV, and (3) at 30 eV relative energy in a flat portion of the spectrum. In each case, the fluorescence yields over the entire spectrum were divided by the fluorescence yield at the given normalization energy.

Linear Combination Fitting

The proportions of total phosphate adsorbed on each mineral in the mixed-mineral suspensions were determined using least squares linear combination fitting (Vairavamurthy et al., 1997; Hutchison et al., 2001), with

spectra for adsorbed PO_4 in the single-mineral systems serving as standards. Fitting results were judged according to their chi-square (goodness of fit) values.

XANES spectra for PO_4 adsorbed in single- and mixed-mineral systems at lower concentrations were noisier than spectra at higher adsorbed PO_4 concentrations. Therefore, standards for single-mineral samples of lower concentration ($\leq 100 \text{ mmol PO}_4 \text{ kg}^{-1}$ ferrihydrite or $\leq 200 \text{ mmol kg}^{-1}$ boehmite) were used for mixed-mineral samples of lower concentration ($100 \text{ mmol PO}_4 \text{ kg}^{-1}$). Similarly, standards for single-mineral samples of higher adsorbed concentration ($> 100 \text{ mmol PO}_4 \text{ kg}^{-1}$ ferrihydrite or $> 200 \text{ mmol kg}^{-1}$ boehmite) were used for mixed-mineral samples of higher concentration ($> 100 \text{ mmol PO}_4 \text{ kg}^{-1}$). Further details about the rationale for choosing single-mineral standards for fitting analysis are included in the Results and Discussion section.

RESULTS AND DISCUSSION

Adsorption Isotherms

Adsorption isotherms for ferrihydrite, boehmite and mixtures of ferrihydrite and boehmite (Fig. 2.1) were L-curves that could be fit with Freundlich models (Sposito, 1984). The phosphate adsorption isotherm for the mixed-mineral system was intermediate between those of the single-mineral systems. The maximum levels of adsorption observed were about 1860, 1420, and 850 mmol kg^{-1} for ferrihydrite, mixed-mineral, and boehmite systems. Because of the shapes of the isotherms, these levels were considered as maximum adsorption

capacities for the purposes of this study.

Freundlich isotherm models were used to determine whether PO₄ adsorption in the mixed-mineral system could be fit as a linear combination of adsorption in the single-mineral systems. The predicted adsorption for the 1:1 mixture based on a linear combination of Freundlich models for the single-mineral systems ($q_{\text{mixed, predicted}}$) was taken as

$$q_{\text{mixed, predicted}} = 0.5q_f + 0.5q_b = 0.5 (A_f c_f^{\beta(f)} + A_b c_b^{\beta(b)}) \quad (1),$$

where q_f and q_b denote the model-predicted adsorption in single-mineral systems for a given aqueous concentration (c_f and c_b) weighted by a factor of 0.5 for the 1:1 (mass basis) mixture, and $A_f, \beta(f); A_b, \beta(b)$ are Freundlich model parameters for ferrihydrite and boehmite, respectively. For dissolved PO₄ concentrations between 100 and 1400 $\mu\text{mol L}^{-1}$ in the mixed system, $q_{\text{mixed, predicted}}$ (dashed line, Fig. 2.1) deviated by $\leq 10\%$ on the low side of q_m , the predicted concentration determined by a direct fit of the Freundlich model to the mixed mineral isotherm (solid lines in Fig. 2.1). The isotherm fitting results indicated that adsorption in the mixed-mineral system essentially behaved (within about 10% variation) as a linear combination of adsorption in the single-mineral systems. That is, there was no interaction between the minerals that notably affected PO₄ adsorption.

In general, one cannot determine from the isotherm data how PO₄ is distributed between ferrihydrite and boehmite at any given adsorbed PO₄ concentration in the mixed-mineral systems. Therefore, XANES spectroscopy was used to determine PO₄ distribution in the mixed-mineral systems.

Phosphorus K-XANES

Adsorbed PO₄ in Single- and Mixed-Mineral Systems

Figure 2.2 shows examples of edge-normalized XANES spectra for PO₄ adsorbed at different concentrations on ferrihydrite, boehmite or mixed-mineral systems. All spectra were characterized by an intense resonance (white-line) near 2150 eV (1 eV relative energy), and weaker oscillations between 5 and 15 eV (relative energy). The white-line peak intensity of XANES spectra for PO₄ on boehmite or ferrihydrite did not change systematically with adsorbed PO₄ concentration (Fig. 2.2). However, a statistically significant difference ($p < 0.05$) between the mean white-line peak intensity for PO₄ on boehmite (4.36 ± 0.02) versus ferrihydrite (4.00 ± 0.10) was observed. The spectra for PO₄ in mixed-mineral systems showed some differences in the white-line peak intensity, but no trend with concentration (Fig. 2.2). The spectra for PO₄ on ferrihydrite showed a pre-edge feature near -4 eV, which was not present in the spectra for PO₄ on boehmite as discussed in more detail below. XANES spectra for phosphate adsorbed in mixed-mineral systems (Jun 02) also showed a pre-edge feature (Fig. 2.2), which tended to diminish in intensity with increasing adsorbed phosphate concentration (discussed below).

XANES spectral features arise from electronic transitions during X-ray absorption, as influenced by the atomic coordination environment around the absorbing atom (P in this case). Features are due to electronic transitions into bound states (pre-edge features) or to photoelectron backscattering from surrounding atoms (post edge features) (Franke and Hormes, 1995; Stohr,

1996). For K-shell spectra, the observed peaks typically correspond to dipole-allowed transitions of a 1s electron to π and σ antibonding orbitals (Stohr, 1996). The absorption edge is usually defined as the energy at which the 1s electron from the K shell escapes into the continuum, and is estimated in practice by the most intense peak in the 1st derivative XANES spectra (Stohr, 1996; Sayers and Bunker, 1988). However, in the phosphorus XANES, an intense peak (white-line) resulting from electronic transitions of the core electron into unoccupied p like valence electronic states occurs at an energy less than the absorption edge (Franke and Hormes, 1995). Therefore, we defined the edge as shown in Fig. 2.2, at the energy yielding a relative maximum in the 1st derivative XANES spectrum on the high-energy side of the white-line peak. XANES spectra for phosphate adsorbed on ferrihydrite and boehmite had edges at 12 and 14 eV respectively (Fig. 2.2).

Normalized XANES spectra for PO₄ adsorbed on boehmite at concentrations ≤ 200 mmol kg⁻¹ (data not shown) and PO₄ adsorbed on ferrihydrite at concentrations ≤ 100 mmol kg⁻¹ (data not shown) were noisier than XANES spectra for these minerals at higher adsorbed PO₄ concentrations because of their lower concentration-dependent edge step. Data normalized to the maximum fluorescence yield at the post edge feature and at 30 eV followed similar trends and are not shown. Hereafter, data for edge-normalized spectra will be shown and discussed, unless otherwise noted.

Comparison with Fe(III) and Al(III)-phosphates

For our research on adsorbed PO₄ species, strengite and variscite served as standards of known molecular structure of Fe (III) vs. Al (III)-bound phosphate. The XANES spectrum for strengite showed a pronounced pre-edge feature at 2146 eV, whereas the variscite spectrum showed no such pre-edge feature (Fig. 2.3). The pre-edge resonance observed for Fe (III)-coordinated PO₄ as in strengite has been previously ascribed to hybridization of Fe(3d), O(2p), and P(3p) valence orbitals giving some p character to the d like unoccupied states from Fe(III) (Franke and Hormes, 1995; Behrens, 1992; Okude et al., 1999). The lack of a pre-edge resonance in variscite is due to the absence of d orbitals in Al. Thus, differences in electron orbital configuration resulted in differences in the pre-edge region of XANES spectra for strengite and variscite. Similarly, XANES spectra for PO₄ adsorbed on ferrihydrite (Fe-oxide) at different adsorbed PO₄ concentrations showed a pre-edge feature while XANES spectra for PO₄ adsorbed on boehmite (Al-oxide) did not show such a pre-edge feature (average spectra from Fig. 2.2 shown in Fig. 2.3). Thus, the pre-edge feature could be used for distinguishing PO₄ associated with ferrihydrite versus boehmite.

Because the pre-edge feature for P K-XANES spectra of strengite has been attributed to P-O-Fe(III) coordination (Franke and Hormes, 1995; Behrens, 1992; Okude et al., 1999), a similar pre-edge feature observed in XANES spectra for PO₄ adsorbed on ferrihydrite provided direct evidence for inner sphere complexation of PO₄ on the surface of ferrihydrite. Also, note that the pre-edge feature for strengite was stronger (and the white-line peak weaker) than that for

PO₄ on ferrihydrite (Fig. 2.3), likely because of more P-O-Fe bonds in the bulk mineral. The weaker pre-edge for PO₄ on ferrihydrite indicated that phosphate was dominantly adsorbed (not precipitated).

PO₄ adsorbed in Mixed-Mineral Systems (Pre-edge)

Because the pre-edge feature has been used to differentiate P associated with ferrihydrite versus boehmite, we focused on the pre-edge region as a means for characterizing adsorbed PO₄ in the mixed-mineral systems. With increasing concentration of total adsorbed PO₄ in the mixed-system, the pre-edge feature intensity showed a trend from being similar to PO₄ on ferrihydrite, towards having intensity intermediate between that of PO₄ on ferrihydrite and PO₄ on boehmite (Fig. 2.4). XANES spectra for mixed-mineral systems from Oct 02 (data not shown) generally followed the same trend. This trend indicated that with increasing adsorbed PO₄ concentration in mixed-mineral systems, an increasingly greater proportion of PO₄ was adsorbed on boehmite.

Because XANES analysis probes the weighted average of all P bonding environments in a sample (Beauchemin et al., 2002), the XANES spectra for PO₄ adsorbed in mixed-mineral systems were considered to be a linear combination of the spectra for PO₄ adsorbed on boehmite and PO₄ adsorbed on ferrihydrite. Furthermore, because fitting of adsorption isotherms for the mixed-mineral system could be done within 10% as a combination of isotherms for single-mineral systems, we assumed that no species of PO₄ unique to the mixed-mineral system were present in detectable quantities. Hence, linear combination

fitting (LCF) analysis was used to quantitatively assess the relative distribution of adsorbed PO_4 between the two minerals in the mixed-mineral systems.

Rationale For Selecting Fitting Standards

The pre-edge region of XANES spectra for PO_4 adsorbed on boehmite ($>200 \text{ mmol kg}^{-1}$) and PO_4 adsorbed on ferrihydrite ($>100 \text{ mmol kg}^{-1}$) is magnified in Fig. 2.5. The pre-edge region of the XANES spectra for PO_4 adsorbed on boehmite ($>200 \text{ mmol kg}^{-1}$) were essentially identical (Fig. 2.5). Hence, all data were ensemble averaged to generate a mean spectral standard for boehmite for fitting spectra from the mixed-mineral systems collected in Jun 02 and Oct 02.

The XANES spectra for PO_4 adsorbed on ferrihydrite at 200 to 1680 mmol kg^{-1} (Jun 02 data) were essentially identical in the pre-edge region (Fig. 2.5). Hence, these spectra were ensemble averaged to generate a mean spectral standard for fitting Jun 02 or Oct 02 mixed-mineral systems containing $>100 \text{ mmol PO}_4\text{kg}^{-1}$

A different set of XANES spectra for single-mineral systems were used for fitting spectra from mixed-mineral systems at lower concentration. XANES spectra for PO_4 on boehmite at concentrations $\leq 200 \text{ mmol kg}^{-1}$ (data not shown), on ferrihydrite at concentrations $\leq 100 \text{ mmol kg}^{-1}$ or on mixed-mineral systems at concentrations $\leq 100 \text{ mmol kg}^{-1}$ (Jun 02 and Oct 02) (data not shown) were noisier than XANES spectra for samples with higher adsorbed PO_4 concentrations. Also, PO_4 adsorbed on ferrihydrite (Jun 02) at concentrations of 50 and 100 mmol kg^{-1} (data not shown) had a more intense pre-edge than the

XANES spectra for PO_4 adsorbed at concentrations of 200 to 1680 mmol kg^{-1} (Fig. 2.5). Principal component analysis (Beauchemin et al., 2002) performed for the dataset of the seven spectra and restricted to the pre-edge region for PO_4 adsorbed on ferrihydrite (Jun 02) showed two significant components, suggesting the presence of two different species. A t-test carried out on the averaged fluorescence yields at -4.5 eV for the two suspected groups (50 to 100 vs. 200 to 1680) also indicated a significant difference ($p < 0.001$). Hence, for fitting analysis of the mixed-mineral system from Jun 02 or Oct 02 at a concentration of 100 $\text{mmol PO}_4 \text{ kg}^{-1}$, ensemble averaged standards for ferrihydrite containing 50 and 100 $\text{mmol PO}_4 \text{ kg}^{-1}$ and for boehmite containing 50, 100, and 200 $\text{mmol PO}_4 \text{ kg}^{-1}$ were used.

XANES Fitting Results

Two approaches to LCF of XANES spectra for mixed-mineral systems were evaluated. The data were fit either in the pre-edge region (-7 to -2 eV) or over an expanded energy range of -7 to 5 eV to include the white-line peak. LCF results that included the white-line peak did not yield consistent trends with level of adsorbed PO_4 apparently because the white-line peak region dominated the fitting relative to the pre-edge region. LCF results limited to the pre-edge region showed consistent trends for all concentrations of adsorbed PO_4 in the mixed-mineral system. In addition, regardless of the background normalization method, spectral fitting results using the pre-edge region yielded similar (within 6% variation) distributions of PO_4 between ferrihydrite and boehmite in the mixed-

mineral system. Hence, only the fitting results for edge-normalized data are presented here (Table 2.1).

For adsorbed PO_4 concentrations up to 400 mmol kg^{-1} in the mixed-mineral system (Jun 02 data), XANES fitting indicated that 68 to 97% of adsorbed PO_4 was on ferrihydrite. At adsorbed PO_4 concentrations of 600 and $1310 \text{ mmol kg}^{-1}$ (Jun 02 data), 64 and 59% of PO_4 respectively was adsorbed on ferrihydrite (Table 2.1). Fitting results for XANES spectra collected on mixed-mineral systems in Oct 02 showed that for adsorbed PO_4 of 100 mmol kg^{-1} , 62% was adsorbed on ferrihydrite (Table 2.1). At adsorbed PO_4 concentrations of 570 to $1190 \text{ mmol kg}^{-1}$, results showed that 51 to 38% of PO_4 was adsorbed on ferrihydrite (Table 2.1).

Based on the percentages of total PO_4 on ferrihydrite (versus boehmite) in the mixed-mineral systems (Table 2.1) and the known amounts of total adsorbed PO_4 , we calculated the concentration of adsorbed PO_4 on ferrihydrite for each mixed-mineral system in Jun 02 and Oct 02. Linear relationships between the amount of PO_4 adsorbed on ferrihydrite as a function of total PO_4 adsorbed in the mixed-mineral systems depict the reproducibility of trends in PO_4 distribution between each mineral (Fig. 2.6a). Both sets of samples showed linear trends with nearly equivalent slopes, indicating that with increasing inputs, PO_4 is distributed at a near constant proportion between ferrihydrite and boehmite. However, the fitting results for the Oct 02 samples showed lower amounts of PO_4 on ferrihydrite relative to boehmite (Fig. 2.6a). We attribute this discrepancy to the lack of a complete set of fitting standards analyzed along with these samples

in Oct 02. So, we have more confidence in the accuracy of the results from Jun 02 samples.

Mixed-mineral systems from Jun 02 were used to assess the relative affinity of PO_4 for ferrihydrite versus boehmite in mineral-mixtures. Relative affinity was quantitatively estimated by including a thermodynamic no-preference line for the Jun 02 data (Fig. 2.6b). This no-preference line is based on the maximum observed concentrations of PO_4 adsorbed on ferrihydrite ($1860 \text{ mmol kg}^{-1}$) versus boehmite (850 mmol kg^{-1}) – Fig. 2.1, assuming that the no-preference distribution of PO_4 on each mineral in the mixed-system would be in proportion to the contribution of that mineral to the total adsorption capacity of the system. From a molecular perspective, no preference in the binding affinity of PO_4 implies that the PO_4 would be adsorbed in proportion to the number of binding sites on each mineral. Because ferrihydrite has a 2.2 fold greater PO_4 adsorption capacity than boehmite, one would expect a distribution of 69% of PO_4 on ferrihydrite and 31% on boehmite in a 1:1 mixture of these minerals if there was no thermodynamic preference for either mineral.

A comparison of calculated concentrations of PO_4 on ferrihydrite in the mixed-mineral systems versus the no-preference line showed that PO_4 had greater affinity for ferrihydrite compared to boehmite at the lowest total adsorbed concentration ($100 \text{ mmol PO}_4 \text{ kg}^{-1}$) (Fig. 2.6b). At intermediate total adsorbed PO_4 concentrations ($200 - 600 \text{ mmol PO}_4 \text{ kg}^{-1}$), the proportion of PO_4 adsorbed on ferrihydrite (64 to 78% of total) deviated by $\leq 9\%$ from the no-preference distribution (Table 2.1). Therefore at intermediate adsorbed PO_4 concentrations,

the adsorbed level on either mineral could be predicted solely on the basis of the relative contribution of that mineral to the total PO_4 adsorption capacity of the system (Fig. 2.6b).

At the greatest level of total adsorbed PO_4 in the mixed system depicted in Fig. 2.6b ($1310 \text{ mmol kg}^{-1}$), PO_4 was at (near) maximum adsorption capacity for the system. Therefore, PO_4 should be distributed between ferrihydrite and boehmite in proportion to the maximum adsorption capacity of each mineral, regardless of the affinity preference of PO_4 for either mineral. If so, then the data point for $1310 \text{ mmol PO}_4 \text{ kg}^{-1}$ should fall on the no-preference line, corresponding to 69% of total PO_4 on ferrihydrite (31% on boehmite). However, fitting results showed that at this adsorbed concentration, 59% of PO_4 was on ferrihydrite, which was within 10% of the expected distribution based strictly on adsorption as the only phosphate binding mechanism. The initiation of a surface precipitate at this high-adsorbed PO_4 concentration could explain any negative deviation from the no-preference line beyond experimental error.

The adsorption preference trends in Fig. 2.6b, particularly the high affinity preference of PO_4 for ferrihydrite at 100 mmol kg^{-1} total adsorbed PO_4 , suggests the presence of a limited number of high affinity binding sites on ferrihydrite. If so, then with increasing levels of PO_4 these sites are filled first and then PO_4 distributes more to boehmite in the mixture. An analogous trend was observed for Pb (II) by Templeton et al. (2001), where Pb (II) sorption at low levels was dominated by complexation to high-affinity metal-oxide surface sites in biofilm coated hematite and corundum surfaces. Finally, to the extent that the limited

results of our study on pure, binary mixtures can be extended to slightly-acid soils, our findings suggest that soil phosphate would mostly be distributed between poorly crystalline Fe- and Al-oxides in proportion to the PO₄ sorption capacity of each mineral.

CONCLUSIONS

Phosphate adsorption at pH 6 and 22°C in a 1:1 mixed suspension of ferrihydrite and boehmite could be modeled within 10% as a linear combination of adsorption in each single-mineral system, indicating that mineral interaction effects that influence PO₄ adsorption were minimal in the mixture. Phosphorus K-XANES spectra for phosphate adsorbed on ferrihydrite or boehmite were distinctly different in the pre-edge region between -7 to -2 eV relative energy. The presence of a pre-edge feature in the XANES spectra for PO₄ adsorbed on ferrihydrite was similar to that found in the spectrum for strengite, and gave direct evidence for inner-sphere surface complexation of PO₄ on ferrihydrite. Linear combination fitting results for mixed-mineral systems containing between 100 mmol kg⁻¹ and 1310 mmol PO₄ kg⁻¹ (near maximum capacity), showed that phosphate was typically adsorbed on both ferrihydrite and boehmite. Between 200 and 600 mmol kg⁻¹, phosphate distribution between boehmite and ferrihydrite was in direct proportion to each mineral's relative contribution to the maximum adsorption capacity of the mixture, indicating that neither mineral had an affinity preference for PO₄.

REFERENCES

Alcacio, T.E., D. Hesterberg, J.W. Chou, J.D. Martin, S. Beauchemin, and D.E. Sayers. 2001. Molecular scale characteristics of Cu(II) bonding in goethite-humate complexes. *Geochim. Cosmochim. Acta.* 65:1355-1366.

Beauchemin, S. and R.R. Simard. 1999. Soil phosphorus saturation degree: review of some indices and their suitability for P management in Quebec, Canada. *Can. J. Soil Sci.* 79:615-625.

Beauchemin S., D.L. Hesterberg and M. Beauchemin. 2002. Principal component analysis approach for modeling sulfur K-XANES spectra of humic Acids. *Soil Sci. Soc. Am. J.* 66:83-91.

Behrens, P.1992. X-ray absorption spectroscopy in chemistry II. X-ray absorption near edge structure. *Trends Anal. Chem.* 11:237-244.

Franke, R. and J. Hormes. 1995. The P K-near edge absorption spectra of phosphates. *Physica B.* 216:85 - 95.

Hesterberg, D.L., W. Zhou, K.J. Hutchison, S. Beauchemin, and D.E. Sayers. 1999. XAFS study of adsorbed and mineral forms of phosphate. *J. Synchrotron Rad.* 6:636-638.

Hongve, D. 1997. Cycling of iron, manganese, and phosphate in a meromictic

lake. *Limnol. Oceanogr.* 42:635-647.

Hutchison K.J., and D.L. Hesterberg. 2001. Stability of reduced organic sulfur in humic acid as affected by aeration and pH. *Soil Sci. Soc. Am. J.* 65:704-709.

Ioannou, A., A. Dimirkou, and P. Papadopoulos. 1998. Phosphate sorption by goethite and kaolinite-goethite (K-G) systems as described by isotherms. *Commun. Soil Sci. Plant Anal.* 29:2175-2190.

Li, L., and R. Stanforth. 2000. Distinguishing adsorption and surface precipitation of phosphate on goethite (α -FeOOH). *J. Colloid Interface Sci.* 230:12-21

McMaster, W. H, N. Kerr del Grande, J. H. Mallet, and J. H. Hubell. 1969. *Compilation of x-ray cross sections.* Lawrence Radiation Laboratory.

Oh, Y.-M., D. Hesterberg, and P. V. Nelson. 1999. Phosphate adsorption on clay minerals as a pre-plant source of phosphorus in soilless root media. *Commun. Soil Sci. Plant Anal.* 30:747-756.

Okude, N., M. Nagoshi, H. Noro, Y. Baba, H. Yamamoto, T.A. Sasaki. 1999. P and S K-edge XANES of transition metal phosphates and sulfates. *J. Electron Spectrosc. Relat. Phenom.* 101-103: 607-610.

Olsen, S.R., and L.E. Sommers, 1982. Phosphorus. p 403-430. *In* Al.

Page et al. (ed.) Methods of soil analysis Part 2, 2nd Ed. SSSA, Madison, WI.

Papadopoulos, P., A. Dimirkou, and A. Ioannou. 1998. Kinetics of phosphorus sorption by goethite and kaolinite-goethite (K-G) Systems. Commun. Soil Sci. Plant Anal. 29:2191-2206.

Patrick, W.H., S. Gotoh, and B.G. Williams. 1973. Strengite dissolution in flooded soils and sediments. Science 179: 564-565.

Pierzynski, G.M., T.J. Logan, S.J. Traina, and J.M Bigham. 1990a. Phosphorus chemistry and mineralogy in excessively fertilized soils: quantitative analysis of phosphorus-rich particles. Soil Sci. Soc. Am. J. 54:1576-1583.

Pierzynski, G.M., T.J. Logan, S.J. Traina, and J.M Bigham. 1990b. Phosphorus chemistry and mineralogy in excessively fertilized soils: descriptions of phosphorus-rich particles. Soil Sci. Soc. Am. J. 54:1583-1589.

Pote D. H., T.C. Daniel, A.N. Sharpley, P.A. Moore, Jr. D.R. Edwards, and D.J Nichols. 1996. Relating extractable soil phosphorus to phosphorus losses in runoff. Soil Sci. Soc. Am. J. 60:855-859.

Reddy, K.R., G.A.O.' Connor, and P.M. Gale. 1998. Phosphorus sorption capacities of wetland soils and stream sediments impacted by dairy effluent. J.

Environ. Qual. 27: 438-447.

Sallade, Y.E., and J.T. Sims. 1997. Phosphorus transformations in the sediments of Delaware's agricultural drainageways: II. Effect of reducing conditions on phosphorus release. *J. Environ. Qual.* 26: 1579-1588.

Sayers D.E., B.A. Bunker. 1988. Data analysis. p 211-253. *In* D.C. Koningsberger and R. Prins (ed.) X-ray absorption: principles, applications, techniques of EXAFS, SEXAFS, and XANES. John Wiley & Sons, New York.

Schwertmann, U. and R.M. Cornell. 1991. Iron oxides in the laboratory: preparation and characterization. VCH Publ. Co., Weinheim, Germany.

Sharpley, A.N. 1995. Dependence of surface runoff phosphorus on extractable soil phosphorus. *J. Environ. Qual.* 24:920-926.

Sharpley, A.N., B. Foy, and P. Withers. 2000. Practical and innovative measures for the control of agricultural losses to water: an overview. *J. Environ. Qual.* 29: 1-9.

Sims, J.T., R.R. Simard, and Joern, B.C. 1998. Phosphorus loss in agricultural drainage: Historical perspective and current research. *J. Environ. Qual.* 27:277-293.

Sposito, G. 1984. The surface chemistry of soils. Oxford Univ. Press, New York.

Stohr, J. 1996. NEXAFS spectroscopy. Springer Publications, New-York.

Templeton, A.S., T.P. Trainor, S.J. Traina, A.M. Spormann, and G.E. Brown.
2001. Pb(II) distributions at biofilm-metal oxide interfaces. Proc. Natl. Acad.
Sci. USA. 98:11897-11902.

Troger, L., D. Arvanitis, K. Baberschke, H. Michaelis, U. Grimm, and E. Zschech.
1992. Full correction of the self absorption in soft fluorescence extended x-ray
absorption fine structure. Phys. Rev. B. 46:3283-3289.

Vairavamurthy, M.A., D. Maletic, S. Wang, B. Manowitz, T. Eglinton, and T.
Lyons, 1997. Characterization of sulfur-containing functional groups in
sedimentary humic substances by X-ray absorption near-edge spectroscopy.
Energy fuels 11:546-553.

Wang, S.L., C.T. Johnston, D.L. Bish, J.L. White, and S.L. Hem. 2003. Water-
vapor adsorption and surface area measurement of poorly crystalline boehmite.
J. Colloid Interface Sci. 260: 26-35.

Table 2.1: Distribution of PO₄ between boehmite and ferrihydrite in 1:1 (mass basis) mixtures of these minerals at pH 6.0 ± 0.1 calculated using linear combination fitting of edge normalized phosphorus K-XANES spectra †

Level of Adsorbed PO ₄ (mmol kg ⁻¹)	Date	% on Ferrihydrite	% on Boehmite	χ ²
100	Jun 02	97 ± 3	3 ± 6	0.0016
200	Jun 02	70 ± 2	30 ± 5	0.0010
300	Jun 02	76 ± 1	24 ± 3	0.0002
400	Jun 02	68 ± 1	32 ± 3	0.0002
600	Jun 02	64 ± 1	36 ± 3	0.0002
1310	Jun 02	59 ± 2	41 ± 5	0.0009
100	Oct 02	62 ± 4	38 ± 6	0.0027
570	Oct 02	38 ± 3	62 ± 5	0.0017
760	Oct 02	48 ± 1	52 ± 2	0.0001
920	Oct 02	51 ± 1	49 ± 2	0.0001
1190	Oct 02	44 ± 1	56 ± 2	0.0002

†Standard errors shown were calculated by the fitting program (Kaliedagraph, Synergy Software Co., Reading, PA).

Figure Captions

Fig. 2.1 Adsorption isotherms for phosphate on boehmite, ferrihydrite, and mixed boehmite/ferrihydrite (1:1 mass basis) at pH 6.0 ± 0.1 , along with Freundlich isotherm models as solid lines for the Jun02 data. Data for the mixed mineral isotherm for Jun 02 are fit using a mass weighted (1:1) linear combination of Freundlich models from the single-mineral systems (dashed line, see text). Some additional data collected in Oct 02 for PO_4 adsorbed on mixed-mineral systems are shown. q_f , q_m , q_b , denote the Freundlich model predicted PO_4 adsorption for ferrihydrite (f), mineral mixtures (m), and boehmite (b) as a function of dissolved PO_4 concentration (c).

Fig. 2.2 Edge-normalized, stacked phosphorus K-XANES spectra for phosphate adsorbed on boehmite, ferrihydrite (ferri.) or mixed-mineral systems (Jun 02 at pH 6.0 ± 0.1) at selected concentrations. Numbers in the legend denote adsorbed PO_4 in mmol kg^{-1} .

Fig. 2.3 Edge-normalized phosphorus K-XANES spectra for strengite versus variscite and ensemble-averaged spectra for phosphate adsorbed on ferrihydrite (ferri.) versus boehmite at pH 6.0 ± 0.1 , showing a pre-edge feature for PO_4 associated with Fe(III).

Fig. 2.4 Comparison of the pre-edge region for edge-normalized XANES spectra for PO_4 adsorbed in mixed-mineral systems (Jun 02) at selected concentrations

with spectra for averaged standards for PO₄ adsorbed on boehmite or ferrihydrite at pH 6.0 ± 0.1. Least square linear fits to the mixed-mineral systems using a combination of the averaged standards for PO₄ adsorbed on boehmite or ferrihydrite are also included. Numbers in the legend denote adsorbed PO₄ concentrations in mmol kg⁻¹.

Fig. 2.5 Pre-edge region in edge-normalized phosphorus K-XANES spectra for phosphate adsorbed on ferrihydrite (ferri.–Jun 02 and Oct 02 data) or boehmite at various concentrations at pH 6.0 ± 0.1 along with averaged standards for PO₄ adsorbed on each mineral. Numbers in the legend denote adsorbed PO₄ concentrations in mmol kg⁻¹.

Fig. 2.6 Concentration of PO₄ adsorbed on ferrihydrite (as calculated from XANES fitting analysis) plotted as a function of total adsorbed phosphate concentration in ferrihydrite-boehmite mixtures. (a) Linear regression fits for Jun 02 and Oct 02 data; (b) Comparison of Jun 02 data with a no-preference line based on distribution of adsorbed PO₄ between the minerals in direct proportion to their relative contributions to the maximum adsorption capacity of the mixed systems.

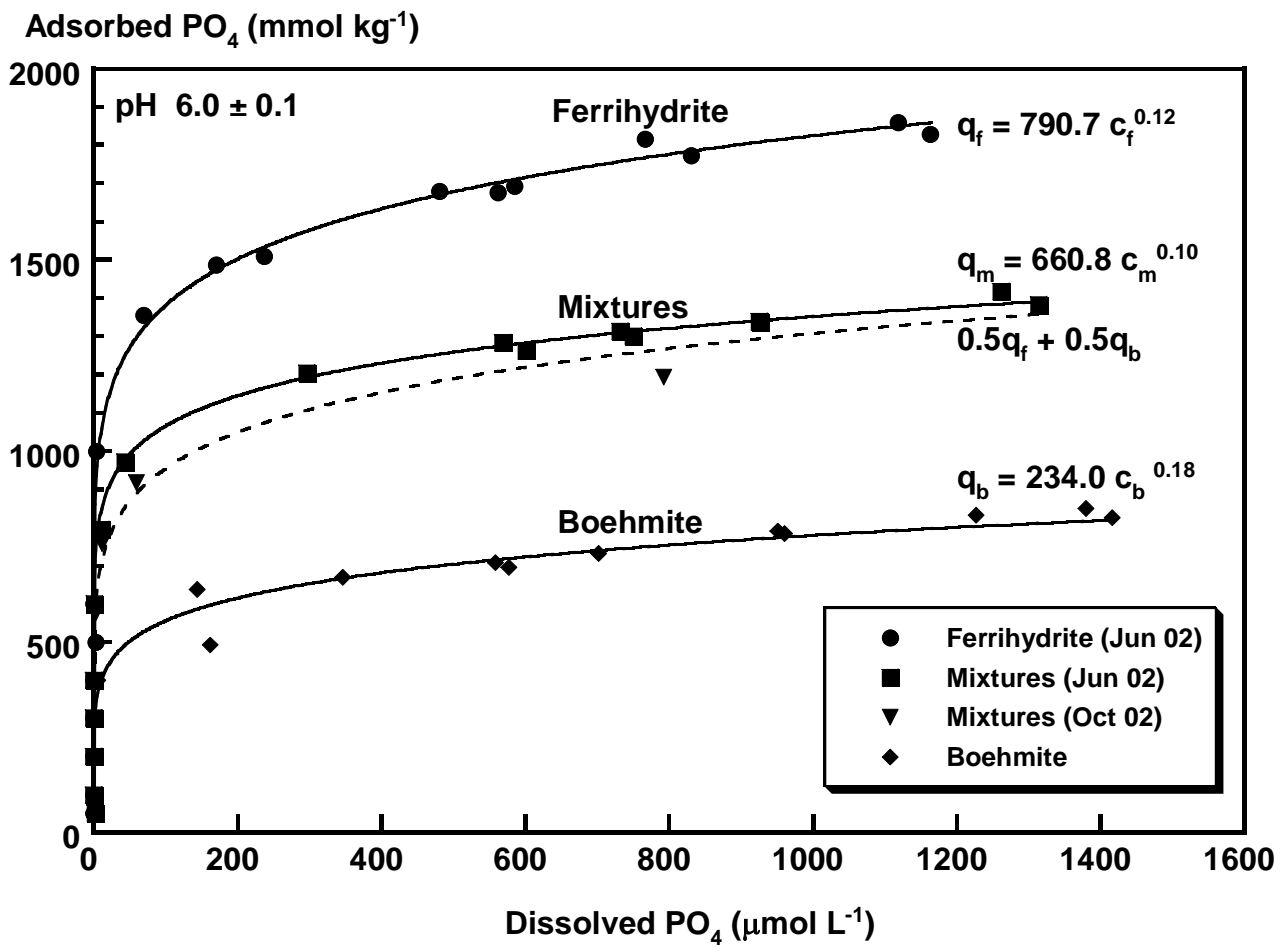


Fig. 2.1

Normalized Fluorescence Yield

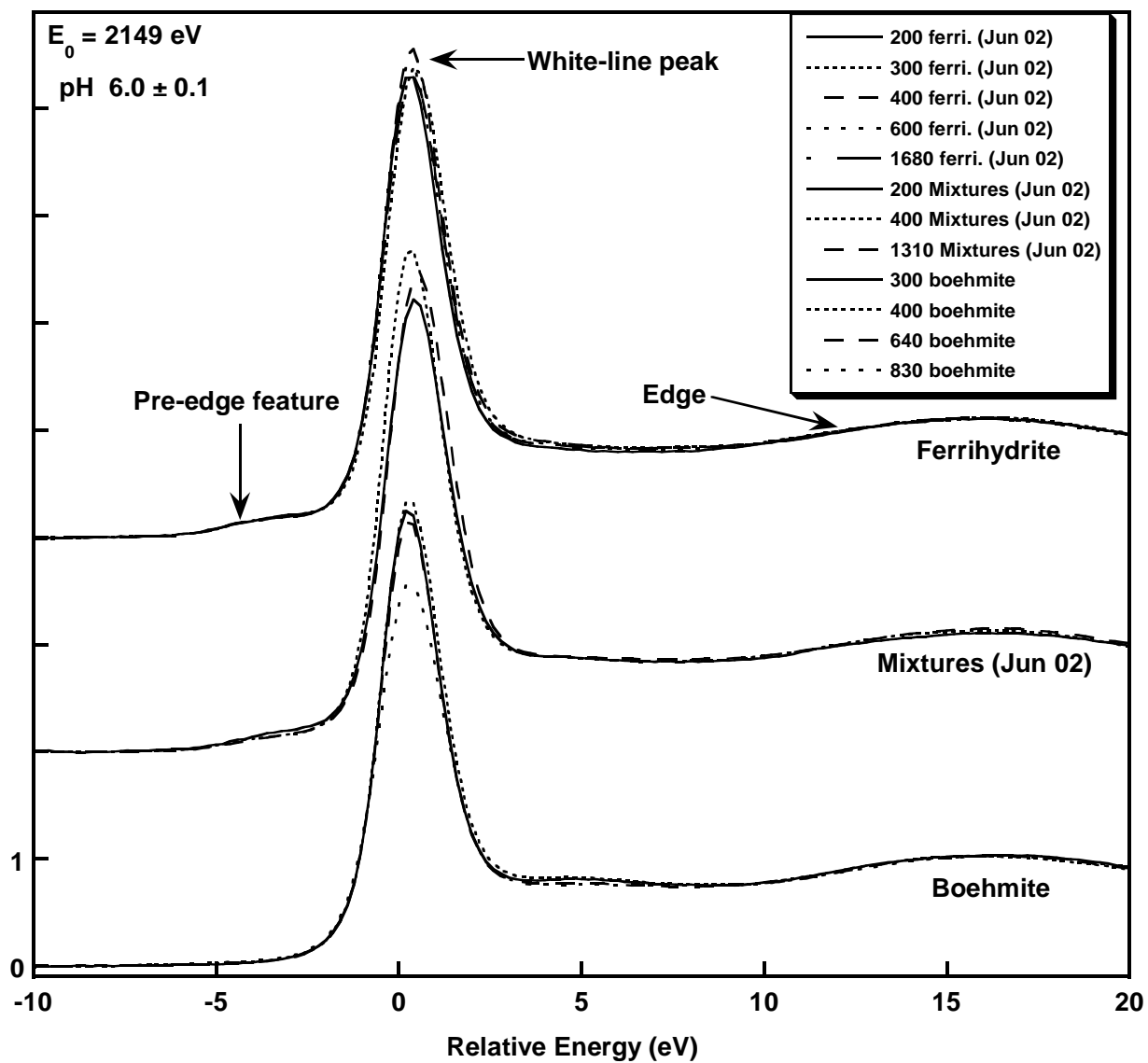


Fig. 2.2

Normalized Fluorescence Yield

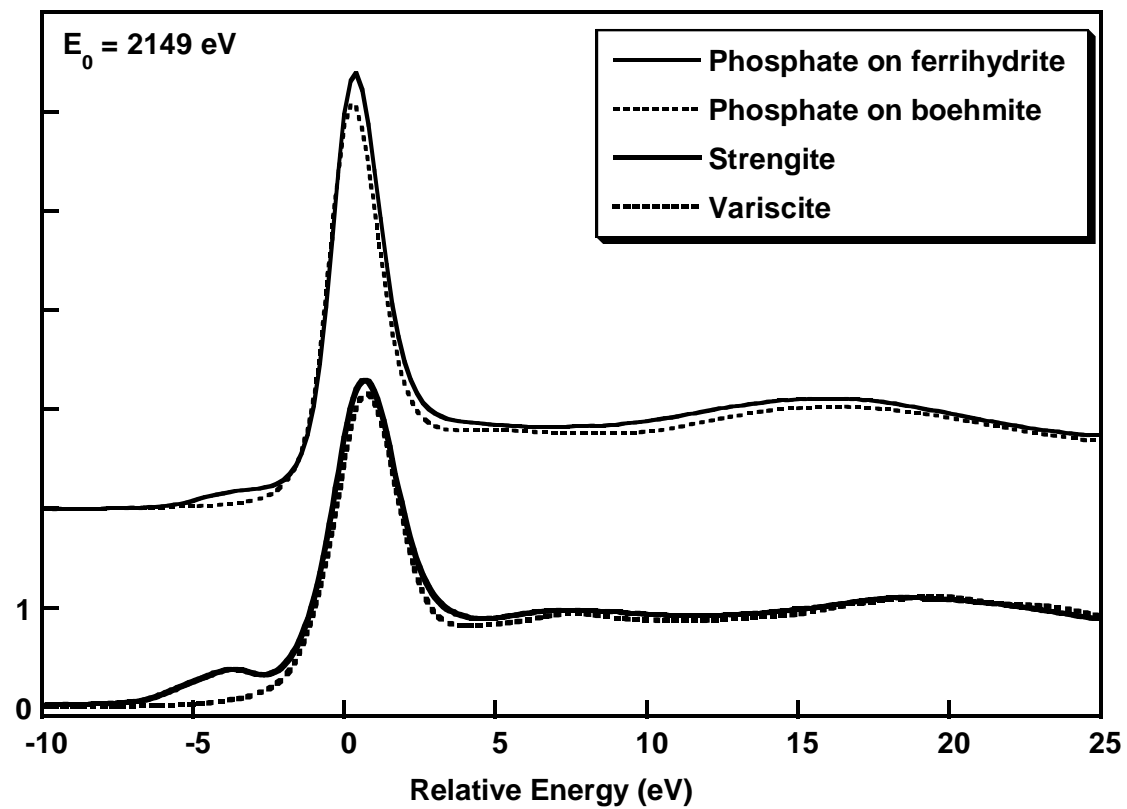


Fig. 2.3

Normalized Fluorescence Yield

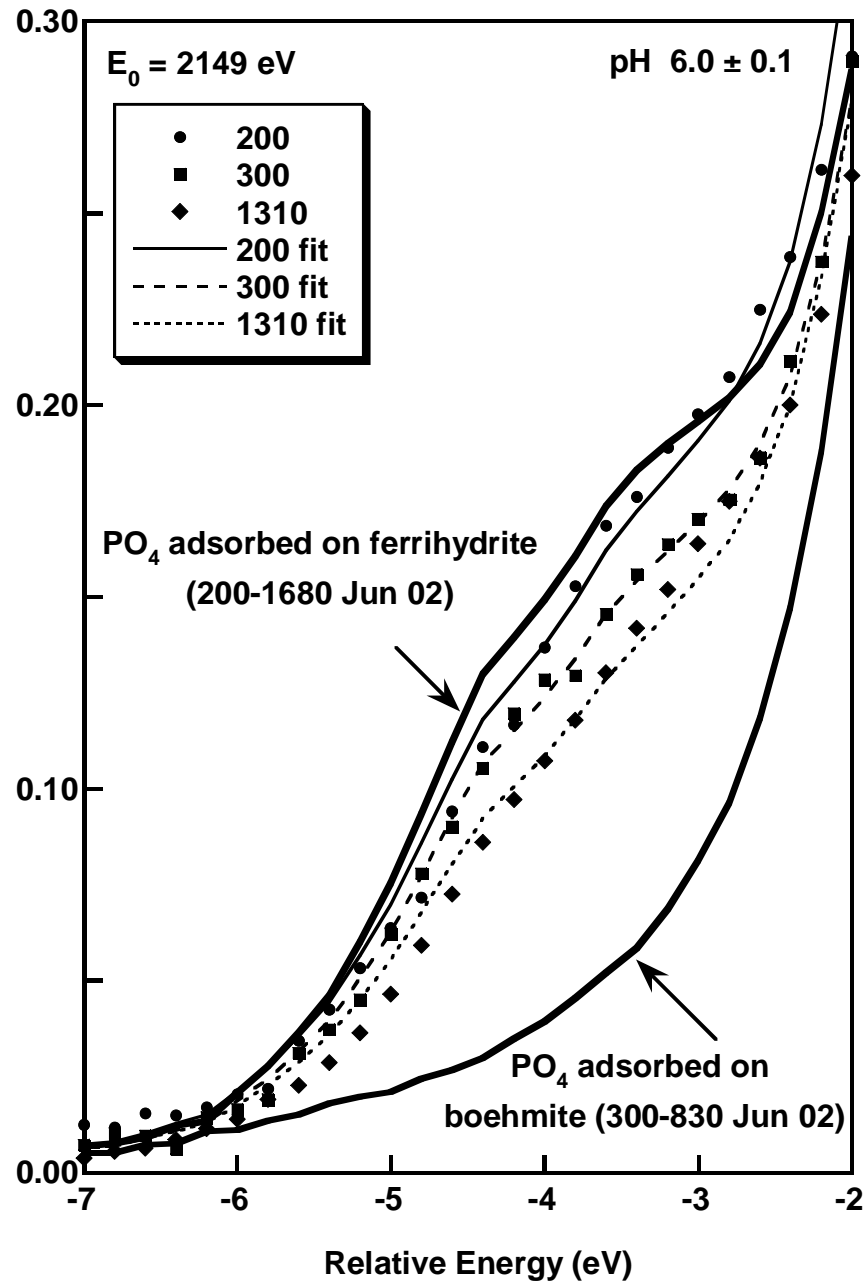


Fig. 2.4

Normalized Fluorescence Yield

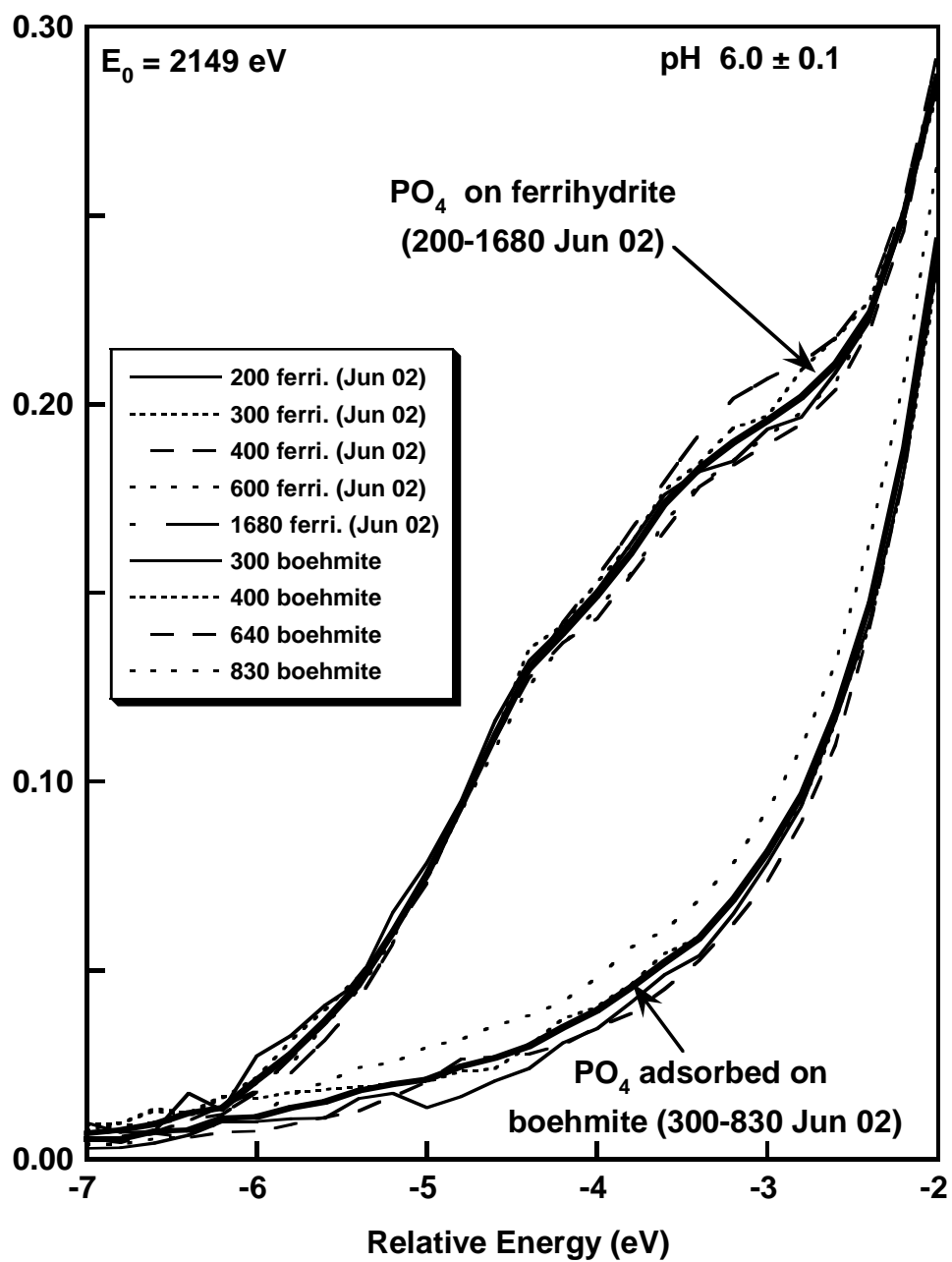


Fig. 2.5

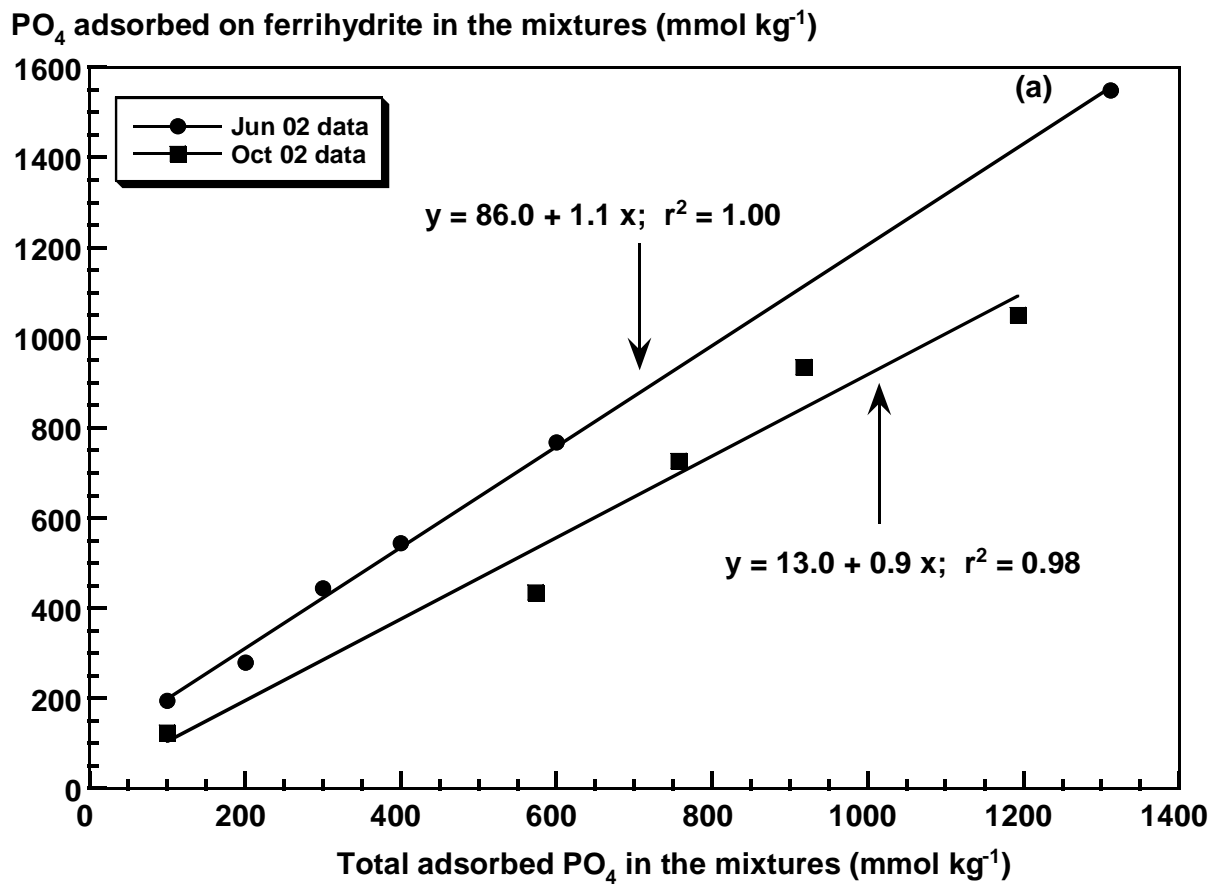


Fig. 2.6a

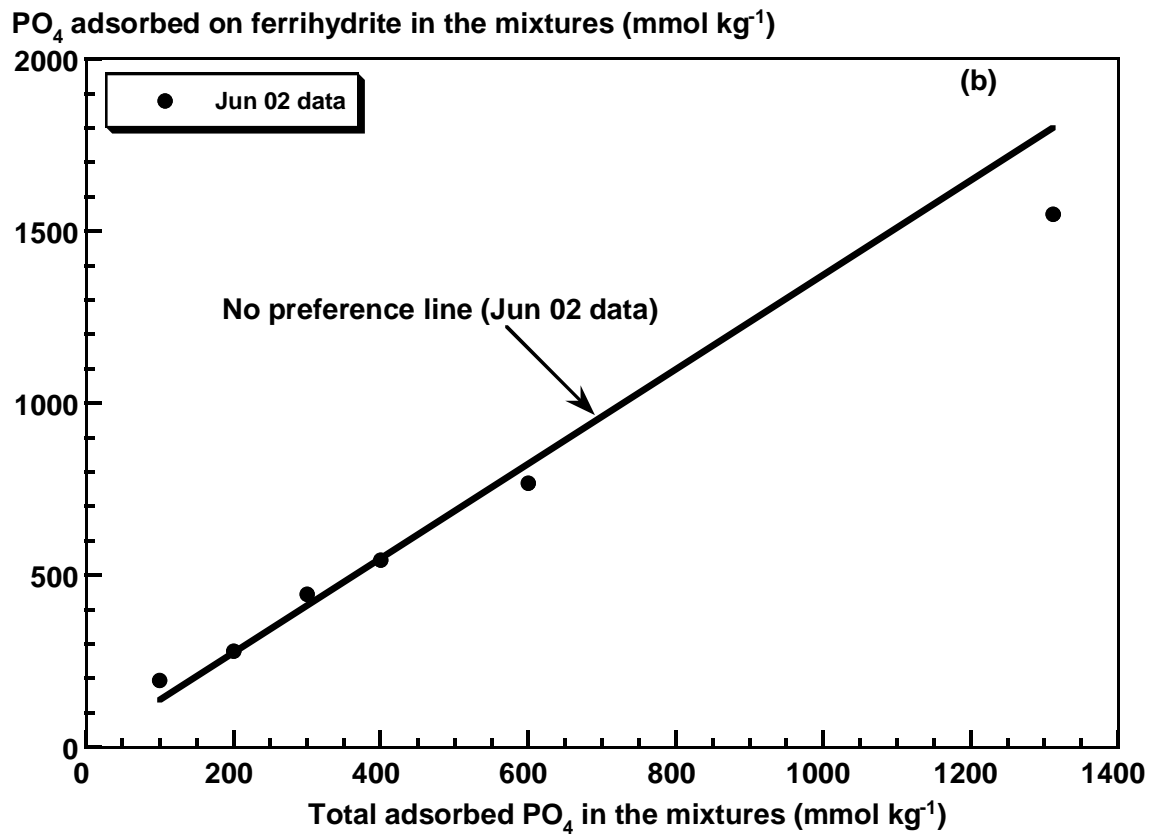


Fig. 2.6b

3. ASSIGNMENT OF PHOSPHORUS K-XANES SPECTRAL FEATURES TO ELECTRONIC TRANSITIONS IN Fe- AND Al-PHOSPHATE SYSTEMS

INTRODUCTION

The association of phosphate with iron and aluminum in adsorbed or precipitated phases is important for regulating P retention in soils, sediments, and waste materials (Beauchemin and Simard, 1999; Sallade and Sims, 1997; Pierzynski et al., 1990a; 1990b; Fendorf et al., 1994). The atomic structure of FePO_4 glasses is also critical to their use in vitrifying high-level nuclear wastes and needs to be characterized (Marasinghe et al., 1997). Furthermore, because the structure of phosphate surface complexes on metal oxide minerals in aqueous systems affects the reactivity of the oxides towards dissolution (Biber and Stumm, 1994), the molecular configuration of adsorbed phosphate has been a topic of continued interest.

Much research has been done toward determining the binding mode of phosphate on Fe- and Al-oxide minerals that serve as models for soil, including goethite, ferrihydrite, boehmite and non-crystalline Al-hydroxide. Approaches used included vibrational (infrared) spectroscopy, XPS (X-ray photoelectron spectroscopy), NMR (nuclear magnetic resonance) spectroscopy, and macroscopic studies on phosphate adsorption kinetics and hydroxyl release. Infrared spectroscopic studies on phosphate sorption on goethite (Persson et al., 1995; Tejedor-Tejedor et al., 1989; Parfitt and Atkinson, 1976; and Parfitt et al., 1975) have differed regarding whether bidentate or monodentate surface complexes are shown

by IR spectra. For example, Parfitt et al. (1975) and Parfitt and Atkinson (1976) interpreted IR spectra to show binuclear bidentate complexation of phosphate sorbed on goethite. However, the infrared analyses were performed on mineral samples after drying, which may alter the structure of the surface species. Infrared studies reported by Tejedor-Tejedor et al. (1989) on moist goethite pastes provided evidence for protonated and non-protonated binuclear bidentate as well as non-protonated monodentate complexes. Persson et al. (1995) interpreted their spectra as showing only monodentate surface complexes of PO_4 on goethite. Hence, despite the importance of binding mechanisms of phosphate on soil components such as oxide minerals, these are not definitively understood. Because X-ray absorption near edge structure (XANES) spectroscopy probes the local molecular structure around an element such as phosphorus, this technique has the potential to provide additional insights on phosphate bonding to oxide mineral surfaces.

XANES spectroscopy involves the excitation of an electron from a core atomic orbital into bound molecular orbitals or into the continuum (Durham, 1988). The technique provides information on geometrical arrangements of atoms in a local cluster around the absorbing atom (Bianconi, 1988) and it can be performed on moist (aqueous) samples. Consequently, phosphorus K-XANES is an effective and non-invasive tool for investigating the local chemical environment of the P atoms in-situ. Phosphorus K-XANES spectra have been interpreted via fingerprinting by comparing XANES spectra of the compounds investigated with a series of standards chosen to provide a step-wise change in a structure or electronic parameter (Behrens, 1992; Chapter 2). Although the fingerprinting approach is powerful, it

relies on the availability of suitable standards (Behrens, 1992). Yet, for sorbed species where the coordination and structure of the sorbed phase is unknown, the fingerprinting approach is limited. For example, a recent study by Khare et al. (in press) (Chapter 2) used spectral fingerprinting to determine the amounts of phosphate associated with Fe vs. Al in phosphated mixtures of Fe- and Al-oxide minerals. However, information on phosphate bonding configuration at the mineral surfaces was not obtained. To interpret XANES spectra in terms of phosphate bonding configuration on oxide mineral surfaces, an assignment of spectral features to electronic transitions from a P 1s core orbital into specific antibonding molecular orbitals is needed.

Calculating density of states (DOS) (via quantum chemistry) and relating XANES spectral features to the unoccupied part of the DOS via dipole selection rules (Behrens, 1992) is one way to assign spectral features to specific electronic transitions. For example, spectral features in metal K-XANES for transition metal compounds have been assigned based on molecular orbital computations of metal-oxygen octahedron clusters by Tossell et al. (1974), Best (1966), and Seka and Hanson (1969). However, assignment of the main features (white-line peak, and pre-edge peak) in P K-XANES spectra for PO_4 associated with Fe(III) or Al(III) has not been made on the basis of theoretical computations. For example, the pre-edge feature in P K-XANES spectra for $\text{Fe}_3(\text{PO}_4)_2$ and other transition metal phosphates was ascribed to the transition of a P 1s electron to a Fe(3d)-O(2p)-P(3p) hybrid orbital, as the latter was considered to be the lowest unoccupied orbital available

(Franke and Hormes, 1995; Okude et al., 1999). However, the supporting evidence for this interpretation was weak.

In this study we used a combination of bonding arguments and extended Huckel (EH) computations to study aqueous and solid phase systems containing PO_4 associated with Fe(III) or Al(III). Complexation in Fe/ PO_4 solutions at different Fe/P molar ratio has been studied using UV-visible spectroscopy (Filatova et al., 1976), and EXAFS (Rose et al., 1996). For Fe/P molar ratio of 2, a bidentate Fe- PO_4 complex ($\text{Fe}_2\text{HPO}_4^{4+}$) was proposed based on UV-visible spectroscopy and at lower Fe/P molar ratio there was evidence for monodentate Fe- PO_4 complexes (Filatova et al., 1976; Rose et al., 1996). Hence, the approach involved developing a consistent theory for explaining XANES spectra for Fe(III)- or Al(III)-phosphate associations in aqueous, adsorbed, and mineral phases based on a combination of known bonding configurations and supporting EH molecular orbital DOS calculations. The specific objective of this study was to assign features in XANES spectra for PO_4 associated with Fe(III) or Al(III) to specific electronic transitions of the core (K-shell) electron.

METHODS

Aqueous Fe(III) PO_4

Phosphorus K-XANES spectra probe the unoccupied antibonding valence states in a system. Aqueous solutions containing Fe(III) and PO_4 complexes in monodentate and bidentate bonding configurations were prepared for XANES analysis using a procedure similar to that described in Filatova et al., 1976. All

solutions contained 50 mM PO_4 and 0 to 100 mM Fe(III) (Fe/P molar ratio = 0 to 2) in a 0.2 M ClO_4^- background. PO_4 was added as a 1M H_3PO_4 solution and Fe(III) as 0.2 M $\text{Fe}(\text{ClO}_4)_3 \cdot x\text{H}_2\text{O}$ in 0.1 M HClO_4 background. The remaining ClO_4^- to make the solutions as 0.2 M ClO_4^- was added as 4 M HClO_4 solution. Molar H_3PO_4 solution was prepared by diluting concentrated phosphoric acid, and 4 M HClO_4 was prepared from concentrated, standardized HClO_4 solution. A 0.2 M $\text{Fe}(\text{ClO}_4)_3 \cdot x\text{H}_2\text{O}$ was prepared by diluting the salt with a standardized 0.1 M HClO_4 solution. In each 100-mL volumetric flask, 5 mL of 1 M H_3PO_4 was added to about 25 mL of DI water and the required amount of 4 M HClO_4 was added to bring solutions to a 0.2 M ClO_4^- background. While stirring with a magnetic stirrer, the required volume of Fe(III) solution was added. A pH meter standardized with pH 1 and 4 standards was used to adjust the final solution to approximately pH 0.5 using 4 M HClO_4 . Each sample was mixed and carefully brought to volume with DI water.

Solid Fe- or Al- PO_4 Sample Preparation

The procedure for preparing samples for phosphate sorbed on Fe- or Al-oxides has been described in Chapter 2. A purchased variscite ($\text{AlPO}_4 \cdot 2\text{H}_2\text{O}$) standard and synthetic strengite ($\text{FePO}_4 \cdot 2\text{H}_2\text{O}$) standard used in this study were those reported by Hesterberg et al. (1999).

P K-XANES data collection and analysis

The XANES spectra for aqueous Fe(III)-PO₄ complexes were collected at Beamline X-19A at the National Synchrotron Light Source, Brookhaven National Laboratory in Upton, NY. A Ge(111) monochromator was used for most samples, but aqueous solution samples were collected using a Si(111) monochromator. The monochromator was calibrated to 2149 eV at the edge (maximum peak in the 1st-derivative spectrum) of variscite (Chapter 2). The spectra were collected in fluorescence mode over an energy range 2069 to 2249 eV. The photon energy scale was normalized to a relative energy scale by subtracting the calibration energy of 2149 eV from all spectra (Chapter 2). Data collected with a Si(111) monochromator were limited to -20 eV (relative energy) at the low energy end. Multiple scans of each sample were collected to obtain at least two spectra with consistent baseline slopes (Chapter 2).

Averaged scans were analyzed using the plotting and data analysis software Kaleidagraph (Synergy Software, Reading PA) following details reported in Chapter 2. Baseline corrections were made by calculating a linear regression through each spectrum between -40 and -10 eV (-20 to -10 eV for Si(111) monochromator) then subtracting the calculated fluorescence yield for each energy across the entire spectrum (Sayers and Bunker, 1988). To normalize spectra to a common edge step and remove P concentration effects, single-point background normalization (Sayers and Bunker, 1988) was done using the fluorescence yield at the energy of the maximum peak between 10 and 18 eV in the first derivative XANES spectrum (edge

normalized) (Chapter 2). The fluorescence yields over the entire spectrum were divided by the fluorescence yield at the given normalization energy (Chapter 2).

UV Visible Data collection and analysis

The UV-visible spectra were recorded on a dual beam Shimadzu SF-16 spectrophotometer (Shimadzu Corp., Columbia, MD) in the range of 300-500 nm at room temperature using 0.2 M HClO_4^- as reference. Because, the Fe/PO_4 solutions were colored, they showed d-d electronic transitions in the visible region, and UV-visible spectra could be obtained (Bellhausen and Gray, 1965). Samples and reference solutions were contained in matched quartz cells of 1 cm pathlength. After collection, the wavelength scale (λ) in nm was converted to energy (E) in electron volt ($E = 1240.70/\lambda$) and molar absorptivity (absorptivity = absorbance/molarity of Fe) was calculated from absorbance and sample concentrations of Fe(III).

Projected Density of States Calculations

Coordinates for idealized fragments

The projected density of states (PDOS: density of states projected onto the contributing atoms and atomic orbitals) were used to study the distribution of metal [Fe(4p) or Al(3p)], P(3p), and Fe(3d) atomic orbital contributions in systems containing PO_4 associated with Fe(III) or Al(III). Iron and Al- PO_4 complexes in idealized monodentate and bidentate configurations were used to model PO_4 associated with Fe(III) or Al(III). Identical metal-metal, metal-oxygen, and phosphorus-oxygen distances were used to calculate the fractional coordinates for

each bonding configuration in Fe- and Al-PO₄ complexes. The monodentate complexes (Metal₂O₉PO₄H₉)⁶⁻ and the bidentate complexes (Metal₂O₈PO₄H₈)⁵⁻ are illustrated in Figs. 3.1a and 3.1b.

As shown, a metal dimer where M = Fe(III) or Al(III) was used in both monodentate and bidentate configurations to solely focus on the differences in PDOS due to the change in bonding configuration. Projected density of states calculations for Fe-PO₄ or Al-PO₄ complexes in monodentate configuration with only one metal center rather than two centers shown in Figs. 3.1a and 3.1b produced essentially the same molecular orbital description. Thus, the PDOS trends were unaffected by the size of the idealized cluster evaluated.

Geometrical optimization required for EH PDOS calculations was achieved by assuming an ideal octahedral symmetry for metal-O, and ideal tetrahedral symmetry for PO₄ fragments. The bond distances, Fe-O (0.200 nm), and Fe-Fe (0.300 nm) used for Fe-O octahedral cluster for both monodentate and bidentate configurations were those of goethite (α -FeOOH). The P-O (0.150 nm) bond distance, and the Fe-O-P bond angle (135°) was an average of P-O bond distance in 20 Fe-PO₄ monodentate complexes from the literature (ICSD-Inorganic Crystal Structure Database). For Fe- or Al-PO₄ monodentate complexes, the PO₄ fragment bound by a single metal-O bond was free to rotate (See Fig. 3.1a). For the purposes of determining fractional coordinates, one of the oxygens of PO₄ was fixed in the center of two in-plane Fe-O bonds (projecting outward) to minimize O-O repulsion. In the bidentate configuration, the PO₄ fragment was fixed in space with two out of-plane metal-O bonds. To accommodate the smaller O-O distance (0.283 nm) in the PO₄

tetrahedron compared to the metal-metal distance (0.300 nm), the metal-oxygen bonds were $<90^\circ$ in the bidentate configurations, causing a slight distortion in the otherwise perfect octahedral symmetry. Distortions have been reported for Al-oxide ($\alpha\text{-Al}_2\text{O}_3$) surfaces, on which Al-O distances have contracted relative to the bulk mineral (Eng et al., 2000). All oxygens bound to the metal were protonated and projected out linearly from the Fe-O bonds with O-H bond length of 0.096 nm (not shown); however, the oxygens bound to phosphate were not protonated. Identical geometry (fractional coordinates) as in monodentate Fe-PO₄ and bidentate Fe-PO₄ complexes were used for monodentate Al-PO₄ and bidentate Al-PO₄ complexes respectively to focus on the difference in PDOS by Al(III) vs. Fe(III) binding to PO₄.

Extended-Huckel calculations

The EH calculations for Fe-PO₄ and Al-PO₄ complexes in idealized monodentate and bidentate configurations were carried out using the CESAR suite of programs developed by W.H. Whangbo (Whangbo, 2000; Ren et al., 1988). The EH calculations are low level calculations that use slater type atomic orbital wave functions for hydrogenic one-electron atoms to estimate overlap integrals (Whangbo, 2000). The EH calculations are not reliable in predicting the optimum structure of a system however, they can be invaluable for systems of known geometry (Whangbo, 2000). In addition, these calculations do not account for electron-electron interactions within the x-ray absorbing atom as a core electron is excited into a bound state (Teo, 1986) during XANES analysis. Hence, the PDOS energies determined from EH calculations are not expected to quantitatively match the

energies of XANES spectral features. Although the approximate electronic structures calculated by EH method may not be used for quantitative predictions, they are adequate for providing a qualitative trend in energy distribution of the various antibonding molecular orbitals (Whangbo, 2000) and corresponding XANES features arising from core electron excitation into a bound state. The metal orbital energies H_{ii} and the orbital exponents employed were the default values throughout. For Fe or Al- PO_4 monodentate or bidentate complexes, molecular orbitals and PDOS were computed using the calculated fractional coordinates (described above).

RESULTS

Phosphorus K-XANES spectra for PO_4 sorbed on ferrihydrite versus boehmite, compared to XANES spectra for strengite ($FePO_4 \cdot 2H_2O$) versus variscite ($AlPO_4 \cdot 2H_2O$) are shown in Fig. 3.2. XANES spectra for PO_4 associated with Fe(III) either as a sorbed or a mineral phase, showed a pre-edge feature between -5 eV to -2 eV in addition to the white-line peak at about 1 eV (relative energy). The pre-edge feature in XANES spectra for strengite was more intense (and the white-line peak less intense) than those for PO_4 sorbed on ferrihydrite. The Al(III) bonded PO_4 did not show a pre-edge feature.

Aqueous solutions containing Fe(III) and PO_4 were characterized by both XANES and UV visible spectroscopy. The P K-XANES spectra for aqueous Fe(III)/phosphate solutions at different Fe/P molar ratios are shown in Figs. 3.3a, 3.3b and 3.4. XANES spectra exhibited a strong white-line peak and pre-edge peak.

The white-line peak for Fe/PO₄ solutions exhibited a systematic shift of 0.4 eV to higher energy with increasing Fe concentrations as shown in the magnified white-line region in Fig. 3.3b. In addition to the white-line peak, the P K-XANES spectra for Fe/PO₄ solutions showed two distinct pre-edge peaks on the lower energy side of the white-line peak as shown in Fig. 3.4. The pre-edge peak 'a' is present at all Fe/P molar ratios ≥ 0.5 in Fe/PO₄ solutions. The pre-edge peak 'b' appears at Fe/P molar ratio ≥ 0.5 and increases considerably in intensity for Fe/P molar ratio of 2. The corresponding UV-visible spectra for Fe/PO₄ solutions shown in Fig. 3.5 exhibited a single peak between 2.9 and 3.0 eV that systematically shifted to lower energy (~0.05 eV shift) with increasing Fe/P molar ratio in UV visible spectra for Fe/PO₄ solutions.

Filatova et al. (1976) used UV-visible spectrometry to characterize the transition from monodentate to bidentate Fe/PO₄ bonding in aqueous Fe(III)-phosphate solutions. A peak at 425 nm (2.92 eV) found at Fe/P = 2 was attributed to bidentate bonding, and a less intense peak at 413 nm (3.0 eV) was attributed to monodentate bonding (Filatova et al., 1976). Thus, the shift in peak from 2.96 to 2.92 eV and increasing absorptivity with increasing Fe/P ratio (Fig. 3.5) indicate a transition from monodentate to bidentate aqueous Fe/PO₄ complexes.

Figure 3.6 shows the trends in energy of the white-line peak in XANES spectra compared with that of the peak in UV-visible spectra as a function of Fe/P molar ratio for aqueous Fe/PO₄ solutions. Between Fe/P = 0 to 0.5, peak positions for both types of spectra were constant. For Fe/P > 0.5, the white-line peak of XANES spectra shifted to higher energy while the peak in the UV-visible spectrum showed a

symmetric shift to lower energy. The pre-edge feature in P K-XANES spectra for PO_4 associated with Fe(III), and shifts in the white-line and UV-visible peaks are due to specific types of core- or valence-electron transitions into antibonding molecular orbitals as affected by the mode of bonding (monodentate or bidentate). In the following discussion, we propose electronic transitions that are consistent with both the XANES and UV-visible results.

DISCUSSION

Possible Assignment of P K-XANES Spectral Features

XANES spectra in the pre-edge region are caused by the electronic transition from 1s core orbitals to bound molecular orbitals or the continuum (Durham, 1988). To assign spectral features to specific electronic transitions in Fe/ PO_4 or Al/ PO_4 systems, the electronic structure of these systems needs to be known. The molecular electronic structure may be approximated by molecular orbitals calculated as a linear combination of valence atomic orbitals of constituent atoms via symmetry and energy overlap (Bellhausen and Gray, 1965). Only valence atomic orbitals are used since the electrons in the core orbitals are tightly bound and hence do not participate in bonding. The positive overlap of atomic orbitals denoted as bonding molecular orbitals leads to lowering of energy, causing these orbitals to be occupied by electrons (Bellhausen and Gray, 1965). The negative atomic orbital overlap leads to the formation of antibonding molecular orbitals that are higher in energy and hence available for electronic transition from core orbitals (Bellhausen and Gray,

1965).

The white-line peak observed in P K-XANES spectra for Fe/PO₄ and Al/PO₄ systems (Fig. 3.2) has been previously attributed to the dipole allowed electronic transition from a P 1s core orbital to a P(3p) antibonding orbital (Franke and Hormes, 1995; Okude et al., 1999). The pre-edge peak observed in P K-XANES spectra for Fe/PO₄ systems (Fig. 3.2) (absent from the spectra for Al/PO₄ systems) was previously attributed to a 1s transition into a Fe(3d)-O(2p) hybridized orbital. This assignment of the pre-edge peak was based on Fe(3d)-O(2p) orbital being the lowest un-occupied orbital available for transition (Franke and Hormes, 1995; Okude et al., 1999). However, these assignments of the white-line and pre-edge peaks leave some questions unanswered. For example, the white-line peak assignment to the transition into a P(3p) antibonding orbital is an atomic orbital whereas such electronic transitions should be into molecular orbitals. Furthermore, the pre-edge peak assignment to a transition into a Fe(3d)-O(2p) molecular orbital (Franke and Hormes, 1995; Okude et al., 1999) apparently did not consider transition into a Fe(4p)-O(2p) molecular orbital. To more fully explore such possibilities, differences in XANES spectra for Fe/PO₄ and Al/PO₄ systems and the assignment of XANES spectral features are discussed below.

In Fe/PO₄ and Al/PO₄ systems, valence atomic orbitals of P, O, and metal [Fe(III) or Al(III)] mix to form molecular orbitals. Local molecular geometry of phosphate whether associated with Fe(III) or Al(III), and the symmetry of valence atomic orbitals (whether s, p, or d) dictates the extent of symmetry overlap. For example, phosphorus 3p orbitals (-14.86 eV) (default values from Caesar Software)

and oxygen 2p orbitals (-14 eV) (default values from Caesar Software) both have p-type symmetry and are closest in energy. Hence, these atomic orbitals form a P(3p)-O(2p) bonding molecular orbital that is most stabilized in energy (See Figs. 3.7a and 3.7b); likewise the P(3p)-O(2p) antibonding molecular orbital is most destabilized in energy (Figs. 3.7a and 3.7b). The low-lying bonding and lone pair molecular orbitals are occupied; only the antibonding molecular orbitals are available for electronic transition from P 1s orbital, and hence are considered here.

We now discuss the possible molecular orbitals formed in systems containing PO₄ associated with Fe(III) or Al(III). In Fe/PO₄ systems, Fe (3d, 4s, 4p), O (2s, 2p), and P (3s, and 3p) valence atomic orbitals are present (Fig. 3.7a). The O(2s) orbitals, being much lower in energy (-32.3 eV) (default values from Caesar Software) compared to energies of other valence atomic orbitals, do not significantly overlap with other atomic orbitals and hence were not considered for the formation of molecular orbitals. Due to the trends in the periodic table, the Fe(4p) orbitals are larger and more diffuse compared to the Al(3p) atomic orbitals. Hence, we expect better Al(3p)-O(2p)-P(3p) overlap than Fe (4p)-O(2p)-P(3p) overlap. Based on the energy and symmetry overlap of the atomic orbitals, we expect Fe(3d)-O(2p); Fe(4p)-O(2p); and P(3p)-O(2p) antibonding molecular orbitals in the order of increasing energy in Fe/PO₄ systems (Fig. 3.7b). Some Fe(4s) character may be mixed in with Fe(4p) character in the Fe(4p)-O(2p) antibonding molecular orbitals and some P(3s) character in P(3p)-O(2p) antibonding molecular orbital. In systems containing Al/PO₄, Al(3p)-O(2p); and P(3p)-O(2p) antibonding molecular orbitals (in the order of increasing energy) are expected (Fig. 3.3b). Although, molecular orbitals

in Fe/PO₄ and Al/PO₄ systems may be predicted qualitatively, the energy distribution of these orbitals is not clearly known.

The EH (extended Huckel) computed PDOS for Fe- or Al-phosphate complexes in idealized monodentate or bidentate geometries provide a trend for energy distribution of antibonding molecular orbitals and confirm the fundamental expectations from the qualitative picture described above. The EH calculations for PDOS in Fe-PO₄ complexes showed Fe (3d) (-12 eV to -8 eV), Fe (4p) (2 eV to 16 eV) (aggregation of Fe(4p) PDOS into a and b sets is discussed below), and P (3p) (16 eV to 23 eV) character in the order of increasing energy (Figs. 3.8a and 3.8b). Although, the O(2p) PDOS is not shown, it mixes with Fe(3d), Fe(4p) and P(3p) PDOS to form antibonding molecular orbitals. The PDOS denote the contribution to a molecular orbital from individual atomic orbitals; for clarity and in keeping with the bonding arguments, the antibonding molecular orbitals are discussed as inferred from the PDOS plots. The P(3p)-O(2p) antibonding molecular orbital was highest in energy as shown in Figs. 3.8a and 3.8b and the white-line peak was also the higher energy feature in XANES spectra. Thus, the white-line peak in XANES spectra was attributed to transition into a P(3p)-O(2p) antibonding molecular orbital as expected from the qualitative arguments above, and supported by EH model calculations.

The pre-edge peak in the XANES spectra for PO₄ associated with Fe(III) is present on the low energy side of the white-line peak. Model calculations showed Fe(4p) PDOS distributed on the low energy side of P(3p) PDOS (Figs. 3.8a and 3.8b), suggesting that the pre-edge peak must be due to transition into the Fe(4p)-O(2p) antibonding molecular orbitals. Previous studies on P K-XANES have

attributed this pre-edge feature to transition into a Fe(3d)-O(2p) hybridized orbital, however this orbitals is on the lower energy side of Fe(4p)-O(2p) antibonding molecular orbital (Figs. 3.8a and 3.8b). The latter orbital was apparently not considered in the previous literature (Franke and Hormes, 1995; Okude et al., 1999). Based on the energy distribution of Fe(3d), Fe(4p), and P(3p) PDOS (Figs. 3.8a and 3.8b), we expected to see three features in XANES spectra for PO₄ associated with Fe(III). Only two features, the white-line peak and pre-edge peak were observed (Fig. 3.2). Because the pre-edge peak attributed to the dipole allowed P 1s to Fe(4p)-O(2p) transition is weak in intensity, the dipole forbidden transition from P 1s to Fe(3d)-O(2p) orbital is expected to be even weaker and hence more difficult to observe.

Support for the above assignment of spectral features may be derived by comparison of Fe K-XANES experimental spectra for Fe-minerals in combination with computed molecular orbitals for Fe-O octahedron. Although, the starting point for electronic transition varies from Fe 1s in Fe K-XANES to P 1s in P K-XANES spectroscopy the same set of molecular orbitals are probed by Fe-K XANES and P K-XANES spectroscopy. The K-edge spectra for Fe³⁺ in oxygen coordination showed three features: a pre-pre-edge peak (7113-7113.7 eV), a pre-edge peak (7122 to 7123.3 eV), and a white-line peak (7128.8 to 7132.1 eV) (Waychunas et al., 1983; Seka and Hanson, 1969). These features were assigned to transitions into antibonding molecular orbitals based on the calculations by Tossell et al. (1974) and Seka and Hanson, (1969). The pre-pre-edge peak was assigned to the transition into the Fe(3d)-O(2p) antibonding molecular orbitals, and the pre-edge peak was

assigned to the transition into the Fe(4s)-Fe(4p) antibonding molecular orbital (Waychunas et al., 1983). The white-line peak was assigned to a discrete transition from Fe (1s) to Fe (4p) antibonding orbitals (Waychunas et al., 1983). The three distinct features observed in the Fe K-edge spectra for Fe-minerals, and the energy separations between them lent support to the three groupings of orbitals obtained from our EH calculations for Fe-PO₄ monodentate and bidentate complexes. In Fe K-XANES spectra, the pre-edge peak on the lower energy side of the white-line peak was assigned to the transition into a Fe(4p)-Fe(4s)-O(2p) antibonding molecular orbital consistent with our assignment. The pre-pre-edge peak predicted by qualitative bonding arguments and supported by EH model calculations was indeed observed on the lower energy side of the pre-edge peak in Fe-K XANES spectra for Fe-minerals and attributed to transition into a Fe(3d)-O(2p) antibonding molecular orbital consistent with our assignment. All of the above arguments indicated that the pre-edge peak in XANES spectra for PO₄ associated with Fe is due to the dipole allowed transition of a P 1s electron to the unoccupied Fe (4p)-O(2p) antibonding molecular orbital.

The EH calculations for Al-PO₄ complexes showed that the P(3p) PDOS was shifted to lower energy compared to the P(3p) PDOS in Fe-PO₄ complexes (Figs. 3.8c and 3.8d). The P(3p) and Al(3p) PDOS overlap in Al-PO₄ complexes (Figs. 3.8c and 3.8d) such that a single set of Al (3p)-O(2p)-P(3p) antibonding molecular orbital is available for electronic transition from a P 1s core orbital, resulting in a single spectral feature in Al/PO₄ systems. XANES spectra for Al/PO₄ systems showed a single feature, the white-line peak, consistent with our arguments (Fig. 3.2). Due to

the energy separation between Fe(4p)-O(2p) and P(3p)-O(2p) molecular orbitals (Figs. 3.8a and 3.8b), both a pre-edge peak and the white-line peak was observed in Fe/PO₄ systems (Fig. 3.2).

Experimental Data Supporting the White-line Peak Assignment

In the previous section, the white-line peak in Fe/PO₄ was assigned to the transition of a P 1s electron into a P(3p)-O(2p) antibonding molecular orbital. In this section, we used experimental XANES and UV-visible data on Fe/PO₄ solutions (Fe/P molar ratio = 0 to 2) containing monodentate or bidentate complexes to support the white-line peak assignment. The single peak observed in the UV-visible spectra (Fig. 5) was ascribed to the transition from the nonbonding Fe-3d (*t_{2g}*) to antibonding Fe-3d (*e_g*) molecular orbitals.

The bonding in Fe-PO₄ complexes is a competitive binding of O with Fe versus P. Therefore, if the phosphorus (3p)-oxygen (2p) (P-O) bonding is optimized the metal [Al(3p) or Fe(4p) or Fe(3d)]-oxygen (2p) (M-O) bonding must simultaneously weaken. In a monodentate Fe-PO₄ complex, the phosphate molecule is free to rotate (See Fig. 3.1a); hence, the Fe-O bonding is optimized. Because oxygen competes for binding with Fe and P, optimal binding with Fe means that the P-O bonding will not be optimal. In a bidentate Fe-PO₄ complex, Fe-O bonding is strained because the PO₄ is fixed in space constrained by two of its oxygens bound to two atoms of Fe, and PO₄ cannot rotate freely. Therefore, the Fe-O bonding is not optimal and oxygen optimizes its bonding with P. Thus, in the bidentate Fe-PO₄ complex, the binding of O with Fe is not optimal and becomes weaker. The Fe-O

antibonding orbital is depressed in energy causing the P-O antibonding orbital to increase in energy. The reverse was true for a monodentate Fe-PO₄ complex. The EH computed PDOS for Fe-PO₄ complexes in idealized monodentate and bidentate configurations supported the qualitative bonding arguments described above (Figs. 3.8a and 3.8b). The EH calculations showed that a P(3p)-O(2p) antibonding orbital for the monodentate configuration is at energy ~16.5 eV, while that for the bidentate configuration is at ~20 eV (Figs. 3.8a and 3.8b). This shift of about 4 eV to higher energies in the bidentate Fe-PO₄ complex (Fig. 3.8b) is consistent with the higher energy shift in the white-line peak of FePO₄ solutions with increasing Fe/P molar ratio (Figs. 3.3 and 3.6). The EH calculations showed that the Fe(3d) and Fe(4p) PDOS was shifted to lower energies for Fe-PO₄ complexes in idealized bidentate configuration compared with monodentate configuration (Figs. 3.8a and 3.8b). Thus, change in bonding configuration (monodentate to bidentate) with increasing Fe/P molar ratio in aqueous Fe-PO₄ complexes should cause M-O bonding to weaken, and simultaneously P-O bonding to be strengthened.

If our white-line peak assignment to transition from a P 1s core orbital to a P(3p)-O(2p) antibonding molecular orbital is correct, we should see a shift in white-line peak to higher energies with increasing Fe/P molar ratio. The XANES spectra for Fe/PO₄ solutions showed a systematic shift in white-line peak toward greater energy, consistent with our assignment (Figs. 3.3a, 3.3b, and 3.6). In addition, the peak in the UV-visible spectra shifted toward lower energies with increasing Fe/P molar ratio (Fig 3.5). The shift in the white-line peak of XANES spectra is directly related to the shift to lower energy in the UV visible spectra with increasing Fe/P

molar ratio in Fe/PO₄ solutions. Because, the UV-visible spectra were caused by the transition into the M-O antibonding orbitals, the shift in the peak in UV-visible spectra to lower energies indicated a reduction in the energy of the M-O antibonding orbitals, which must occur if the P-O antibonding orbitals increase in energy.

Experimental Data Supporting the Pre-edge Peak Assignment

Although, the pre-edge peak in systems containing PO₄ associated with Fe(III) was assigned to transition into a Fe(4p)-O(2p) antibonding molecular orbitals, the split in the pre-edge peak into pre-edge peak a and pre-edge peak b in Fe/PO₄ solutions (Fig. 3.4) has not yet been discussed. The split in the pre-edge peak, and trends in the intensity of pre-edge peaks 'a' and 'b' with increasing Fe/P molar ratio are used to support our spectral assignment (Fig. 3.4).

In Fe-PO₄ complexes, the oxygens bound to Fe(III) are not all chemically identical. Instead, the molecular orbital formed from bonding of Fe(III) with oxygens bound to H atoms is expected to differ from the molecular orbital formed by bonding of Fe(III) to oxygen bridging between the Fe and P atoms. The EH calculations for model Fe-PO₄ complexes in idealized monodentate and bidentate configurations showed that the Fe(4p) PDOS was aggregated in two sets a and b (Figs. 3.8a and 3.8b). Based on the contribution from different oxygens bound to Fe(III), the two sets of Fe(4p)-O(2p) molecular orbital were assigned to Fe-OH and Fe-O(-P) antibonding molecular orbitals in order of increasing energy. The probability of transition into a Fe-OH orbital is expected to be weaker than the probability of transition into a Fe-O(-P) orbital because the electronic excitation into a Fe-OH antibonding molecular

orbital occurs thru space versus the electronic transition into a Fe-O(-P) antibonding molecular orbital occurring via bonds. Furthermore, the transition probability into a Fe-OH antibonding molecular orbital is expected to vary depending on the rigidity in space of the Fe-OH fragment with respect to the PO₄ fragment. In monodentate bonding configuration, the PO₄ fragment is free to rotate (See Fig. 3.1a). Hence, the Fe-OH fragment is not fixed with respect to the PO₄ fragment, diminishing the probability of transition from a P 1s orbital to a Fe-OH antibonding molecular orbital. Conversely, in the bidentate configuration, the Fe-OH are constrained by the oxygens in PO₄ tetrahedron, and the probability of transition from a P 1s to a Fe-OH molecular orbital should be enhanced compared to the transition probability in the monodentate bonding configuration.

The pre-edge peak 'a' assigned to the transition into a Fe-OH antibonding molecular orbital, increased in intensity as we approached the bidentate configuration at Fe/P molar ratio of 2, consistent with our assignment (Fig. 3.4). The EH calculations showed that the Fe-O(-P) antibonding molecular orbital overlapped with the P-O antibonding molecular orbital (Fig. 3.8a). Hence, the pre-edge peak 'b' should be absent in monodentate binding configurations. Our data showed that pre-edge peak 'b' is indeed absent from the Fe/PO₄ solutions at low Fe/P molar ratio (Fe/P = 0, 0.25), where monodentate binding is dominant consistent with our assignment (Fig. 3.4). The EH calculations for the bidentate configuration showed that the Fe-OH and Fe-O(-P) antibonding molecular orbitals were distinct from the P-O antibonding molecular orbitals (Fig. 3.8b). Thus, we expect to see two peaks on the lower energy side of the white-line peak. The XANES spectra for Fe/P molar

ratio >1.0 (more contribution from bidentate configuration) showed the presence of two peaks ~ 0.2 eV apart on the lower energy side of the white-line peak, consistent with bonding arguments (Fig. 3.4). The pre-edge peak 'b' assigned to a Fe-O(-P) antibonding molecular orbital is more intense due to a greater transition probability into this orbital (Fig. 3.4).

An increase in the density of unoccupied states is one factor causing an increase in the probability of transition, thus resulting in the increase in intensity of a peak. If the pre-edge peak is due to the transition of a P 1s electron to a Fe (4p)-O(2p) antibonding molecular orbital as we propose, then the intensity of this transition should increase with an increase in the concentration of Fe-O-P bonds. For example, in bidentate aqueous complexes, two Fe atoms are coordinated with phosphate while four Fe atoms are coordinated to phosphate in strengite. Our pre-edge peak assignment to transition from a P 1s core orbital to a Fe(4p)-O(2p) antibonding molecular orbital would predict an increase in XANES pre-edge intensity in going from monodentate aqueous complexes (Fe/P = 1) to bidentate aqueous complexes (Fe/P = 2) to strengite. Indeed the pre-edge peak for Fe(III) associated PO_4 increased in the order aqueous Fe/P = 1 < aqueous Fe/P = 2 < strengite (Figs. 3.2, 3.4) consistent with our pre-edge peak assignment.

The EH calculations for Al- PO_4 complexes in idealized monodentate and bidentate configurations also showed some Al(3p) PDOS distinct from the Al(3p) PDOS overlapping with P(3p) PDOS (labeled as a) (Figs. 3.8c and 3.8d). This separation was due to the Al bonded to bridging hydroxyls following similar arguments as for Fe- PO_4 complexes. Because the transition probability into Al-OH

orbital is very weak, the pre-edge feature was not observed in Al/PO₄ systems. The white-line peak in Al/PO₄ solutions is also expected to shift to higher energies with change in bonding from monodentate to primarily bidentate configurations similar to the shift observed in Fe/PO₄ solutions (Figs. 3.8c and 3.8d). However, we did not have experimental data to verify this trend.

The coordination of PO₄ on the surface of ferrihydrite is not definitively known. However, the pre-edge peak intensity for PO₄ sorbed on ferrihydrite (average of 200 to 1680 mmol kg⁻¹ spectra) (Fig. 3.2) was intermediate between the pre-edge peak intensity for primarily monodentate and bidentate configurations in Fe/PO₄ solutions, suggesting that PO₄ coordination on ferrihydrite at this concentration range was a combination of monodentate and bidentate configurations.

CONCLUSIONS

Based on bonding arguments supported by model EH computations, the white-line peak in P K-XANES spectra for Fe(III)/PO₄ systems was assigned to an electronic transition from a P 1s orbital into a P(3p)-O(2p) antibonding molecular orbital and the white-line peak in XANES spectra for Al(III)/PO₄ systems was assigned to an electronic transition from a P 1s orbital into a Al(3p)-O(2p)-P(3p) antibonding molecular orbital. XANES and UV-visible spectral trends for aqueous Fe-PO₄ complexes in known monodentate and bidentate configuration were consistent with our white-line peak assignment. Using a similar approach as for the white-line peak assignment, the pre-edge peak in XANES spectra for Fe/PO₄

systems (3 to 5 eV lower in energy than the white-line peak) was ascribed to an electronic transition from a P 1s into a Fe(4p)-O(2p) antibonding orbital. Greater pre-edge peak intensity in XANES spectra for strengite than the pre-edge peak intensity in XANES spectra for aqueous bidentate or monodentate Fe-PO₄ complexes was consistent with our pre-edge peak assignment.

REFERENCES

Beauchemin, S. and R.R. Simard. 1999. Soil phosphorus saturation degree: review of some indices and their suitability for P management in Quebec, Canada. *Can. J. Soil Sci.* 79:615-625.

Behrens, P. 1992. X-ray absorption spectroscopy in chemistry II. X-ray absorption near edge structure. *Trends in anal. Chem.* 11: 237-244.

Bellhausen, C.J., and H.B. Gray. 1965. *Molecular orbital theory*. W.A. Benjamin Inc., NY.

Best, P.E. 1966. Electronic structure of the MnO_4^- , CrO_4^{2-} , and VO_4^{3-} ions from the metal K X-ray spectra. *J. Chem. Phys.* 44: 3248-3253.

Bianconi, 1988. XANES. p 150-190. In D.C. Koningsberger and R. Prins (ed.) *X-ray absorption: principles, applications, techniques of EXAFS, SEXAFS, and XANES*. John Wiley & Sons, New York.

Biber, M.V., and W. Stumm. 1994. An in-situ ATR-FTIR study: The surface coordination of salicylic acid on Aluminum and Iron (III) oxides. *Environ. Sci. Technol.* 28: 763-768.

Durham, 1988. Theory of XANES analysis. p 51-85. In D.C. Koningsberger and R. Prins (ed.) X-ray absorption: principles, applications, techniques of EXAFS, SEXAFS, and XANES. John Wiley & Sons, New York.

Eng., P.J., T.P. Trainor, G.E. Brown, G.A. Waychunas, M. Newville, S.R. Sutton M.L. Rivers. 2000. Science. 288: 1029-1033.

Fendorf, S.E., D.L. Sparks, G.M. Lamble, and M.J. Kelley. 1994. Applications of X-ray absorption fine structure spectroscopy to soils. Soil Sci. Soc. Am. J. 58:1583-1595.

Filatova, L.N., M.A., Shelyakina, A.S. Plachinda, and E.F. Makarov. 1976. Dimerisation of iron (III) in aqueous solution in the presence of phosphate ions. Russ. J. Inorg. Chem. 21:1494-1497.

Franke, R., J. Hormes. 1995. The P K-near edge absorption spectra of phosphates. Phys. B. 216: 85-95.

Khare, N., D. Hesterberg, S. Beauchemin, and S.L. Wang. XANES analysis of adsorbed phosphate distribution between ferrihydrite and boehmite in mixed-mineral systems. Soil Sci. Soc. Am. J. (in press)

Marasinghe, G.K., M. Karabulut, D.E. Day, C.H. Booth, P.G. Allen, J.J. Buchner, N.M. Edelstein, and D.K. Shuh. 1997. EXAFS/XANES studies of iron phosphate glasses. SSRL Activity Report.

Parfitt, A.J., and, R.L. Atkinson, 1976. Phosphate adsorption on Goethite (α -FeOOH). *Nature*, 264:740-742.

Parfitt, R.L., R.J. Atkinson, and, R. St.C. Smart, 1975. The mechanism of phosphate fixation by iron oxides. *Soil Sci. Soc. Amer. Proc.* 39: 837-841.

Persson, Per, Nilsson Nils, and Sjoberg Staffan. 1995. Structure and bonding of orthophosphate ions at the iron oxide-aqueous interface. *J. colloid interface Sci.* 177: 263-275.

Ren, J., W. Liang, M.H. Whangbo. 1988. Crystal and electronic structure analysis using CAESAR. PrimeColor Software Raleigh. This book can be downloaded free of charge from the Web site <http://www.primec.com>

Sayers D.E., B.A. Bunker. 1988. Data analysis. p 211-253. In D.C. Koningsberger and R. Prins (ed.) *X-ray absorption: principles, applications, techniques of EXAFS, SEXAFS, and XANES*. John Wiley & Sons, New York.

Okude, N., M. Nagoshi, H. Noro, Y. Baba, H. Yamamoto, T.A. Sasaki. 1999. P and S K-edge XANES of transition-metal phosphates and sulfates. *J. Elec. Spect. And Related Phen.* 101-103: 607-610.

Pierzynski, G.M., T.J. Logan, S.J. Traina, and J.M Bigham. 1990a. Phosphorus chemistry and mineralogy in excessively fertilized soils: quantitative analysis of phosphorus-rich particles. *Soil Sci. Soc. Am. J.* 54:1576-1583.

Pierzynski, G.M., T.J. Logan, S.J. Traina, and J.M Bigham. 1990b. Phosphorus chemistry and mineralogy in excessively fertilized soils: descriptions of phosphorus-rich particles. *Soil Sci. Soc. Am. J.* 54:1583-1589.

Rose, J., A. Manceau, J.Y. Bottero, A. Masion, and F. Garcia. 1996. Nucleation and growth mechanisms of Fe oxyhydroxide in the presence of PO_4 ions. 1. Fe K-edge EXAFS study. *Langmuir.* 12:6701-6707.

Sallade, Y.E., and J.T. Sims. 1997. Phosphorus transformations in the sediments of Delaware's agricultural drainageways: II. Effect of reducing conditions on phosphorus release. *J. Environ. Qual.* 26: 1579-1588.

Seka, W., H.P. Hanson. 1967. Molecular orbital interpretation of X-ray absorption edges. *J. Chem. Phys.* 50:344-350.

Steinwand, S.J., J.D. Corbett, and J.D. Martin. 1997. Syntheses, crystal structures, and magnetic properties of $\text{Sc}_{19}\text{Br}_{28}\text{Z}_4$ compounds with $\text{Z}=\text{Mn}$, Fe , Ru , or Os . Structural and bonding trends in $\text{R}_{16}\text{X}_{20}\text{Z}_4$ -type oligomers. *Inorg. Chem.* 36:6413-6422.

Tejedor-Tejedor, M.I., and, M.A. Anderson, 1990. Protonation of phosphate on the surface of goethite as studied by CIR-FTIR and electrophoretic mobility. *Langmuir*, 6:602-611.

Teo., B.K. 1986. EXAFS:Basic principles and data analysis. Springer-Verlog, Berlin.

Tossell, J.A., D.J. Vaughan, and K.H. Johnson. 1974. The electronic structure of rutile, wustite, and hematite from molecular orbital calculations. *Am. Mineral.* 59: 319-334.

Waychunas, G., M.J. Apter, and G.E. Brown. 1983. X-ray K-edge absorption spectra of Fe minerals and model compounds: Near edge structure. *Phys. Chem. Minerals.* 10:1-9.

Whangbo, M.H. 2000. Perspective on "An extended Huckel theory. I. Hydrocarbons" Hoffmann R (1963). *J. Chem Phys* 39:1397-1412.

.

Figure Captions

Fig. 3.1 Metal (M = Fe or Al) phosphate clusters in different idealized bonding configurations used for extended Huckel computations are illustrated: a) monodentate complex; b) bidentate complex.

Fig. 3.2 Edge-normalized phosphorus K-XANES spectra for phosphate associated with Fe(III) in aqueous, sorbed (on ferrihydrite), and mineral (strengite) complexes versus phosphate associated with Al(III) in sorbed (on boehmite) and mineral (variscite) complexes.

Fig. 3.3 Phosphorus K-XANES spectra for aqueous Fe (III)-phosphate solutions at Fe/P molar ratios of 0 to 2 (50 mmol P kg⁻¹; pH~0.5). The intensity of the pre-edge feature increased with increasing Fe/P ratio and the white-line peak shifted toward higher energy: a) overall spectra in -10 to 25 eV relative energy range; b) rescaled white-line region.

Fig. 3.4 Pre-edge region in phosphorus K-XANES spectra for aqueous Fe (III)-phosphate solutions at Fe/P molar ratios of 0 to 2 (50 mmol P kg⁻¹; pH~0.5). Pre-edge peaks are denoted as a and b.

Fig. 3.5 UV-visible absorption spectra for aqueous Fe (III)-phosphate solutions (50 mmol P kg⁻¹; pH~0.5) at Fe/P molar ratios of 0 to 2. The peak shifted to lower energies with increasing Fe/P ratio.

Fig. 3.6 Energies of peaks in the phosphorus K-XANES spectra (white-line) and UV-visible spectra as a function of Fe/P molar ratio.

Fig. 3.7 Comparison of the energies of valence atomic orbitals and corresponding core orbitals (dotted), bonding molecular orbitals, (dashed), and antibonding molecular orbitals (solid) expected for Fe/PO₄ and Al/PO₄ systems: a) atomic orbital energies for Fe, Al, P, and O; b) P(1s) core orbitals and molecular orbitals.

Fig. 3.8 The projected density of states (PDOS) of antibonding molecular orbitals computed for Fe-PO₄ and Al-PO₄ in idealized monodentate and bidentate geometries using the Extended Huckel approximation: (a) monodentate FePO₄ complex; (b) bidentate Fe-PO₄ complex; (c) monodentate Al-PO₄ complex; (d) bidentate Al-PO₄ complex.

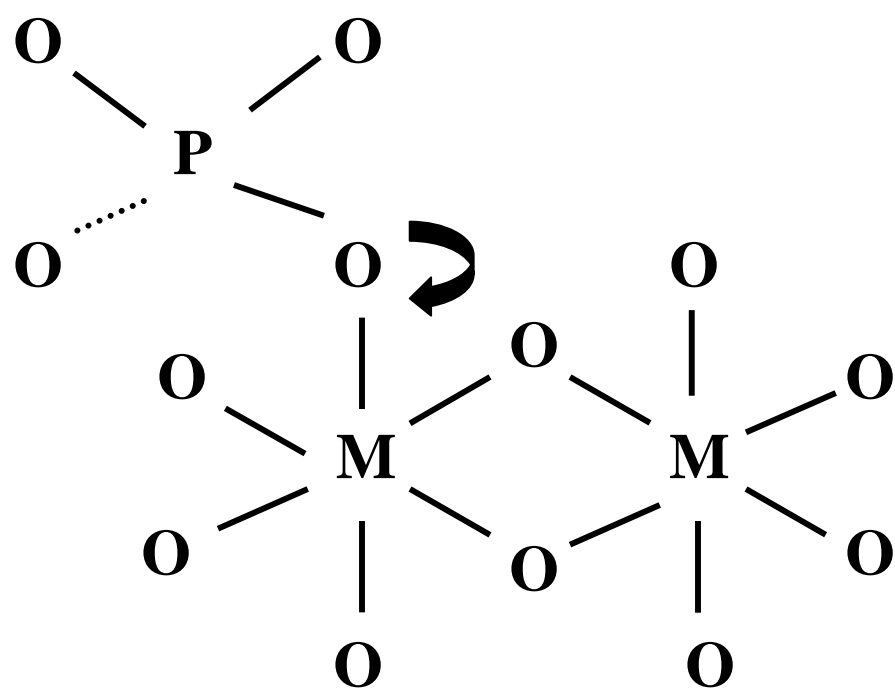


Fig. 3.1a

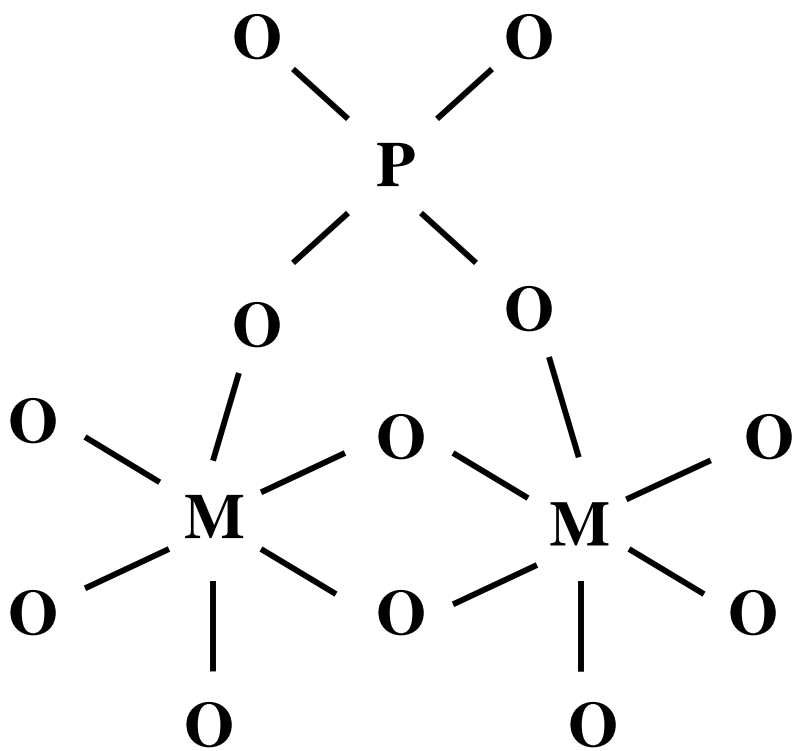


Fig. 3.1b

Normalized Fluorescence Yield

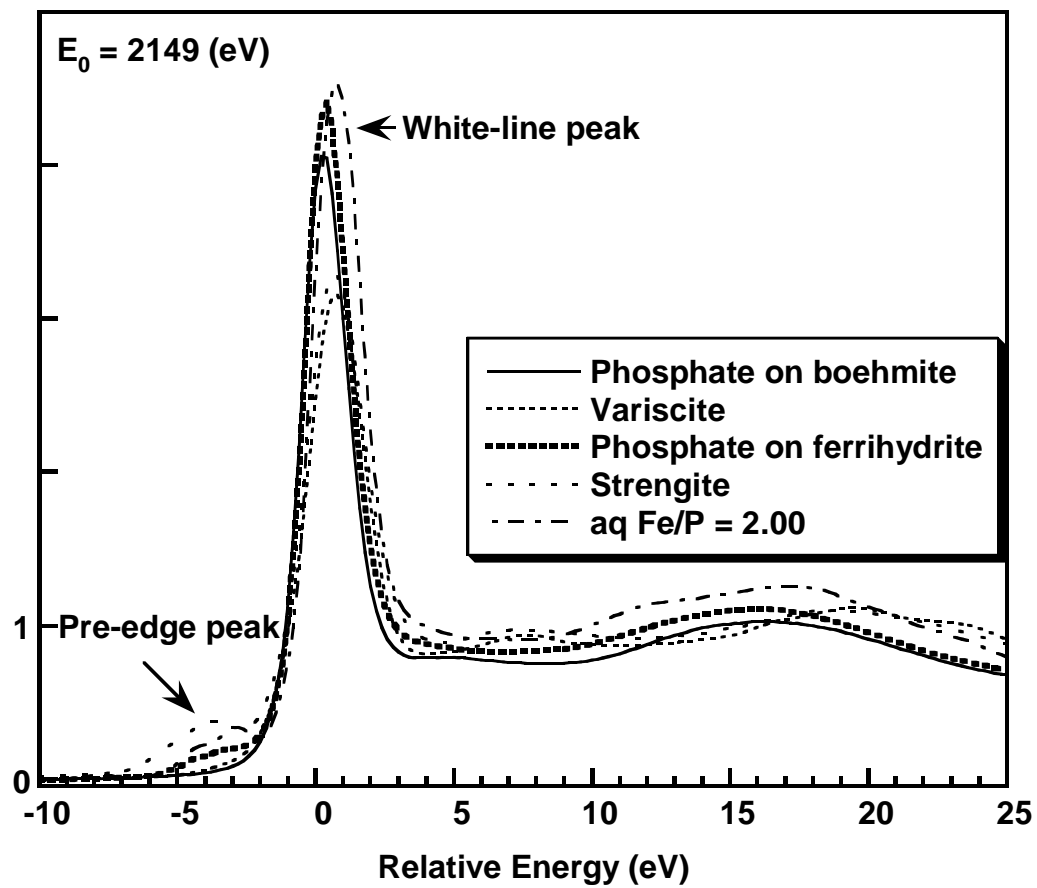


Fig. 3.2

Normalized Fluorescence Yield

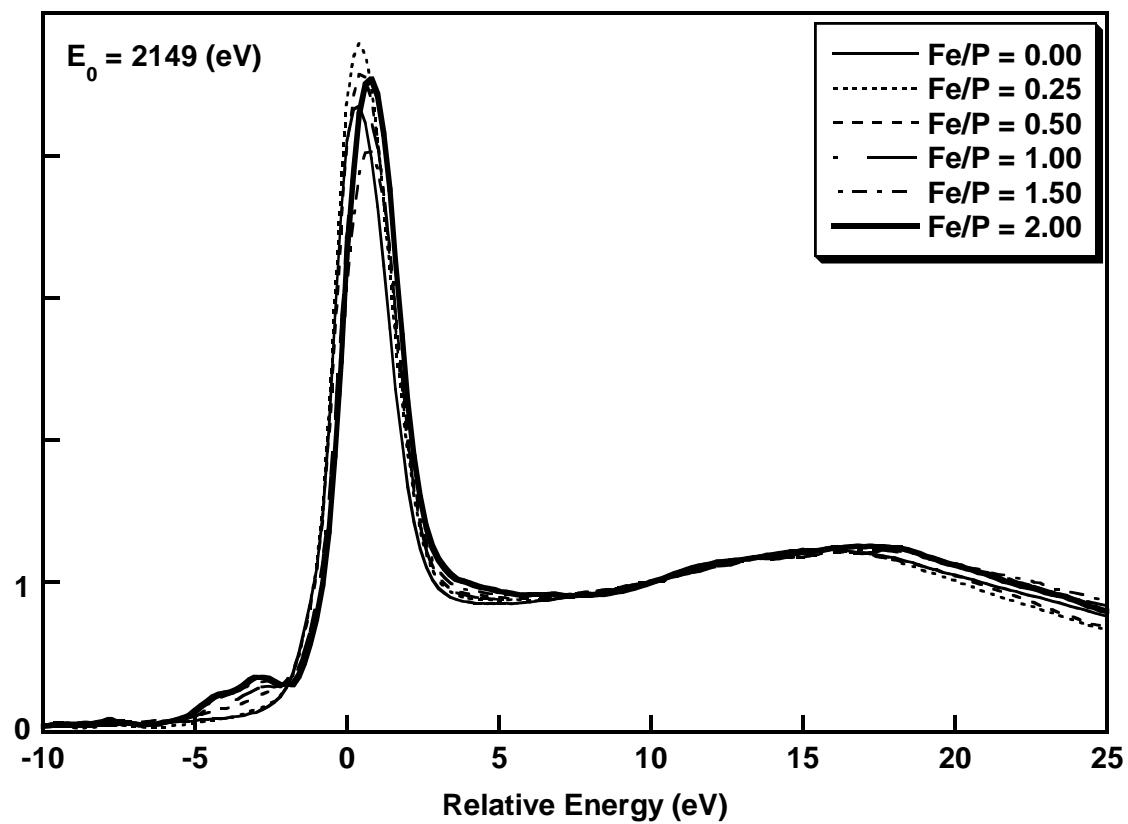


Fig. 3.3a

Normalized Fluorescence Yield

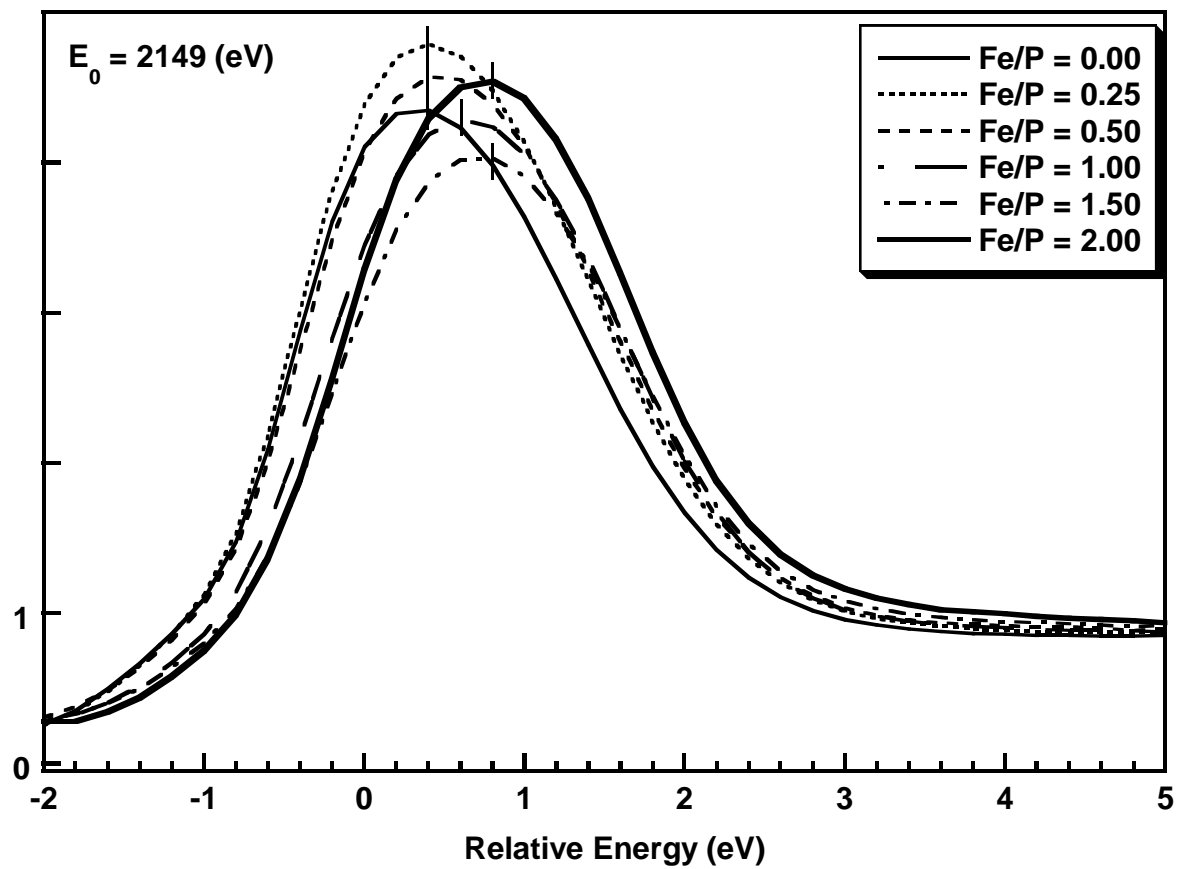


Fig. 3.3b

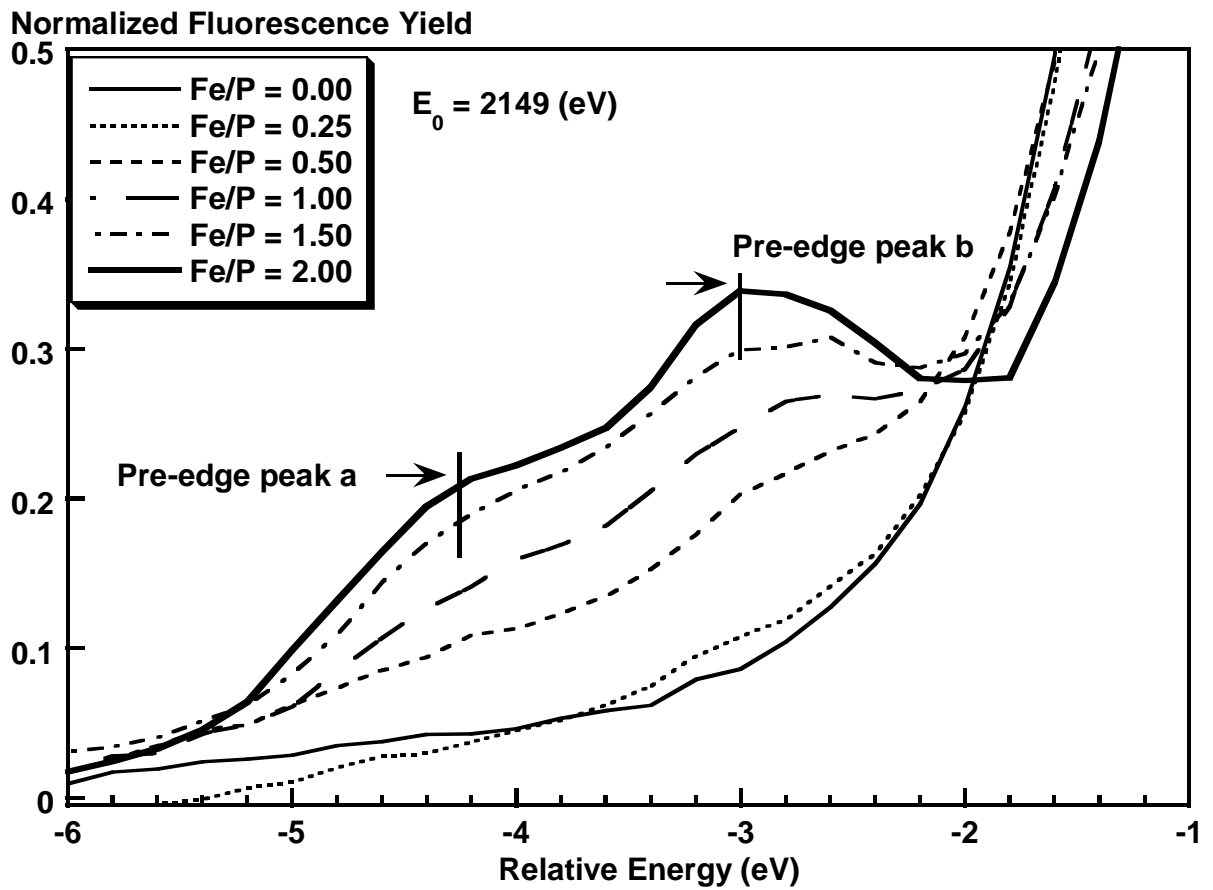


Fig. 3.4

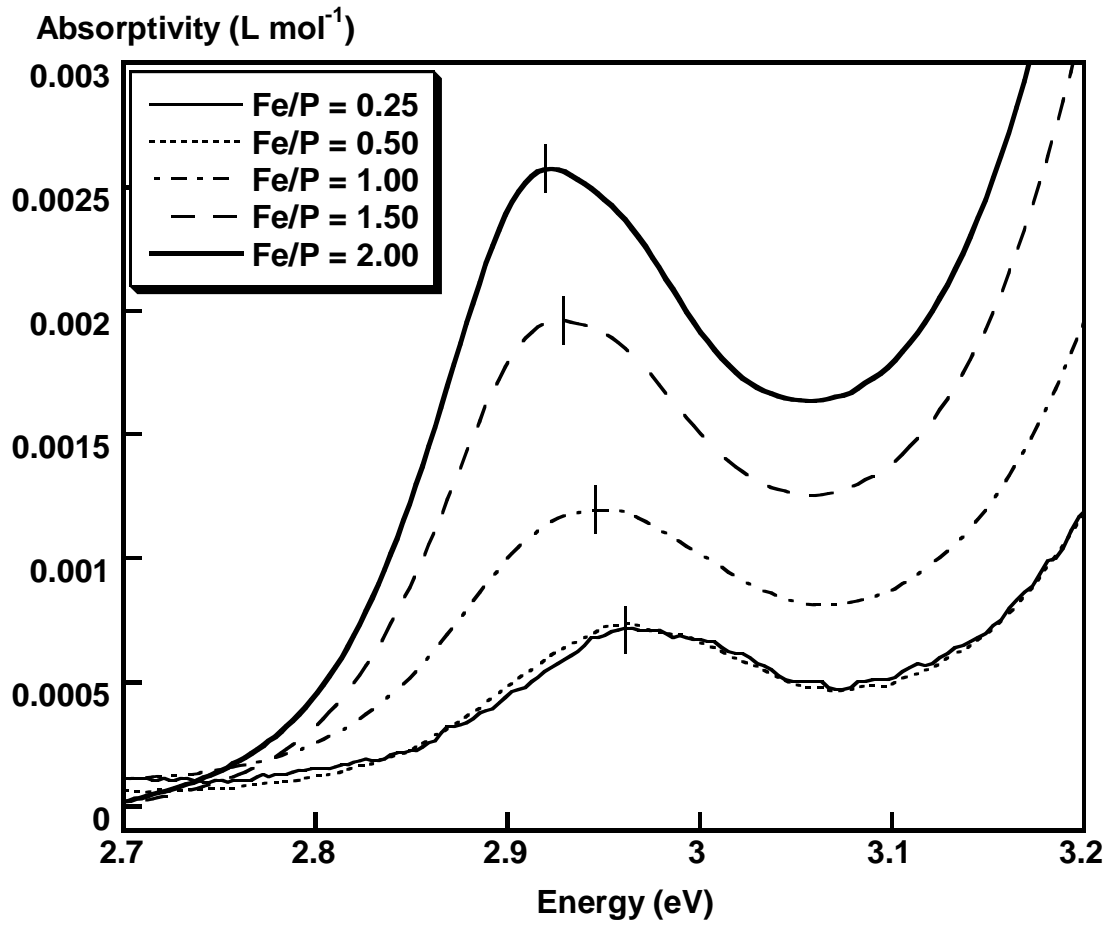


Fig. 3.5

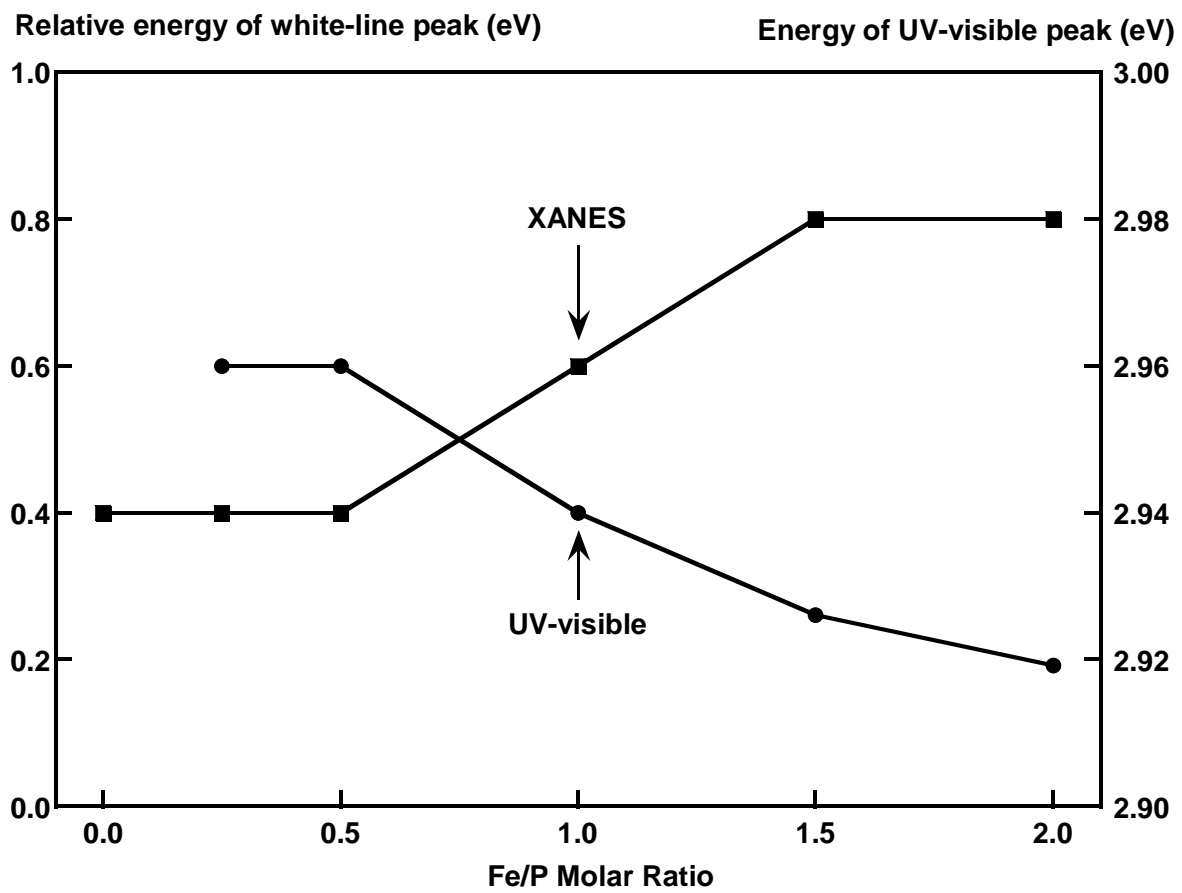


Fig. 3.6

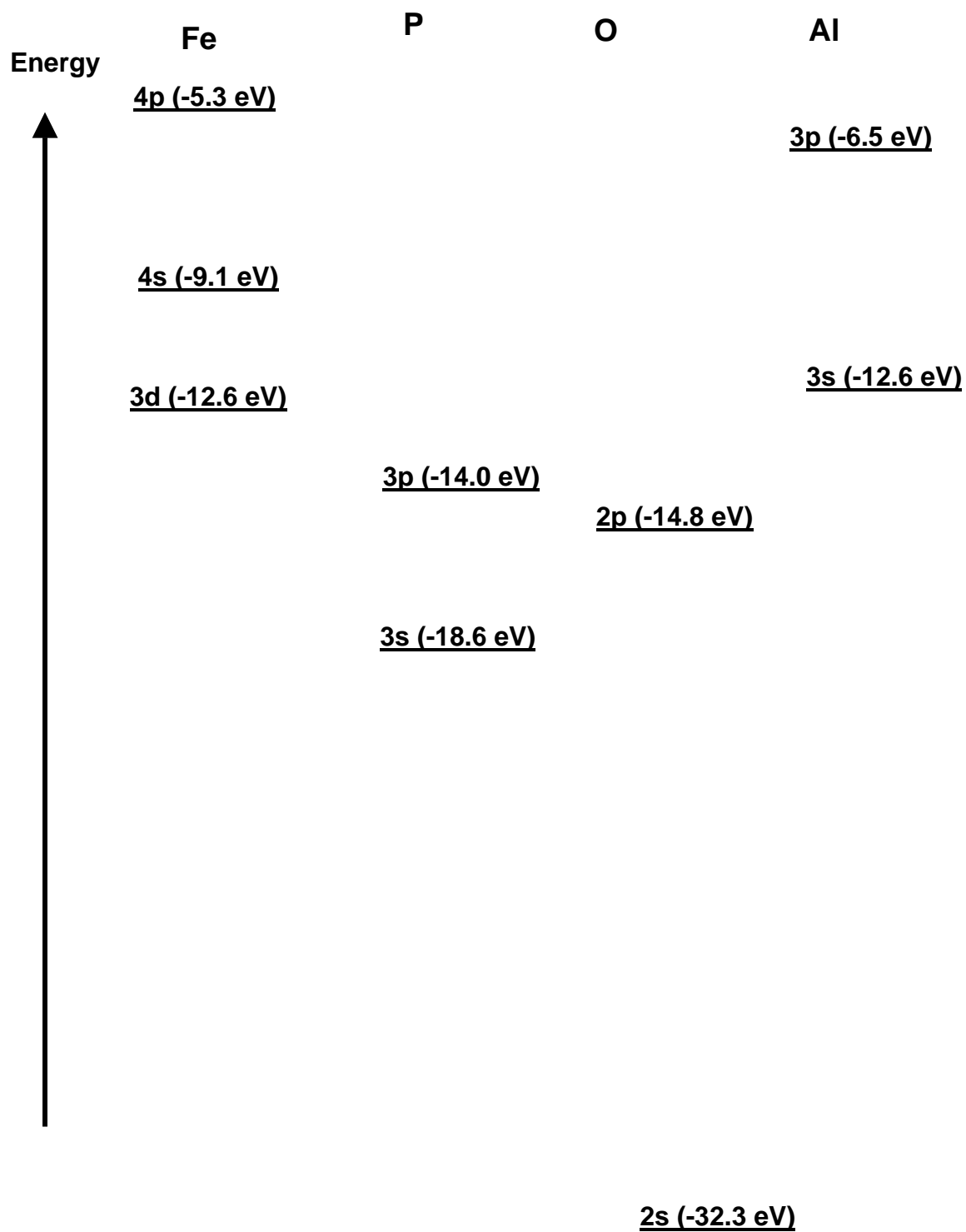


Fig. 3.7a

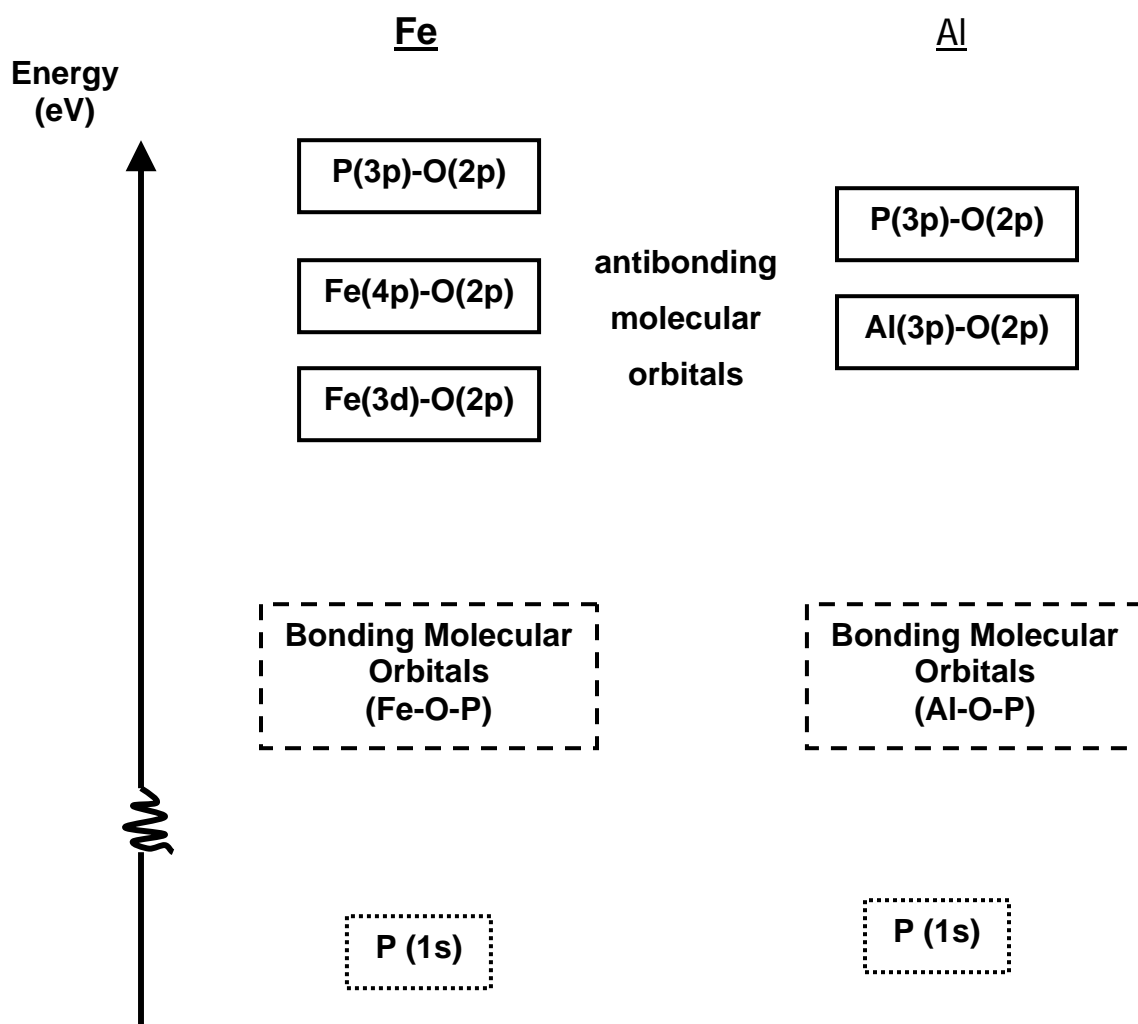


Fig. 3.7b

Projected density of states (arbitrary units)

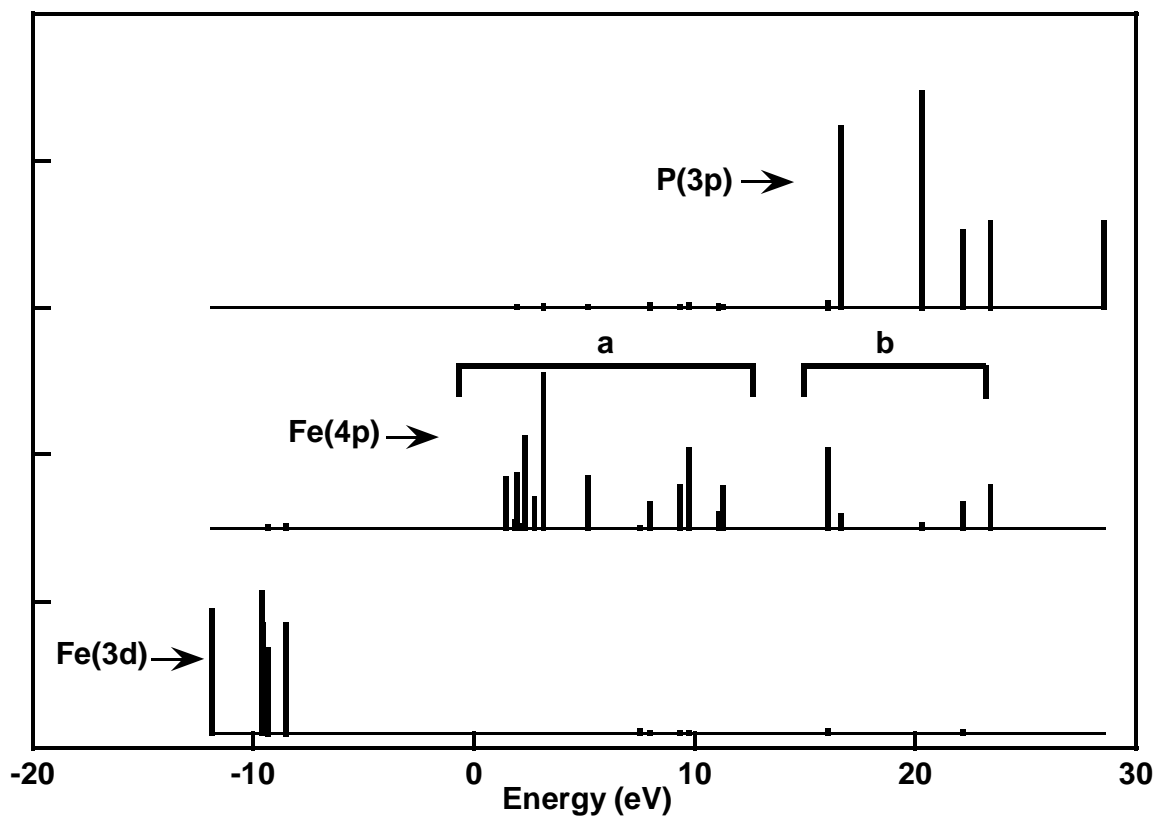


Fig. 3.8a

Projected density of states (arbitrary units)

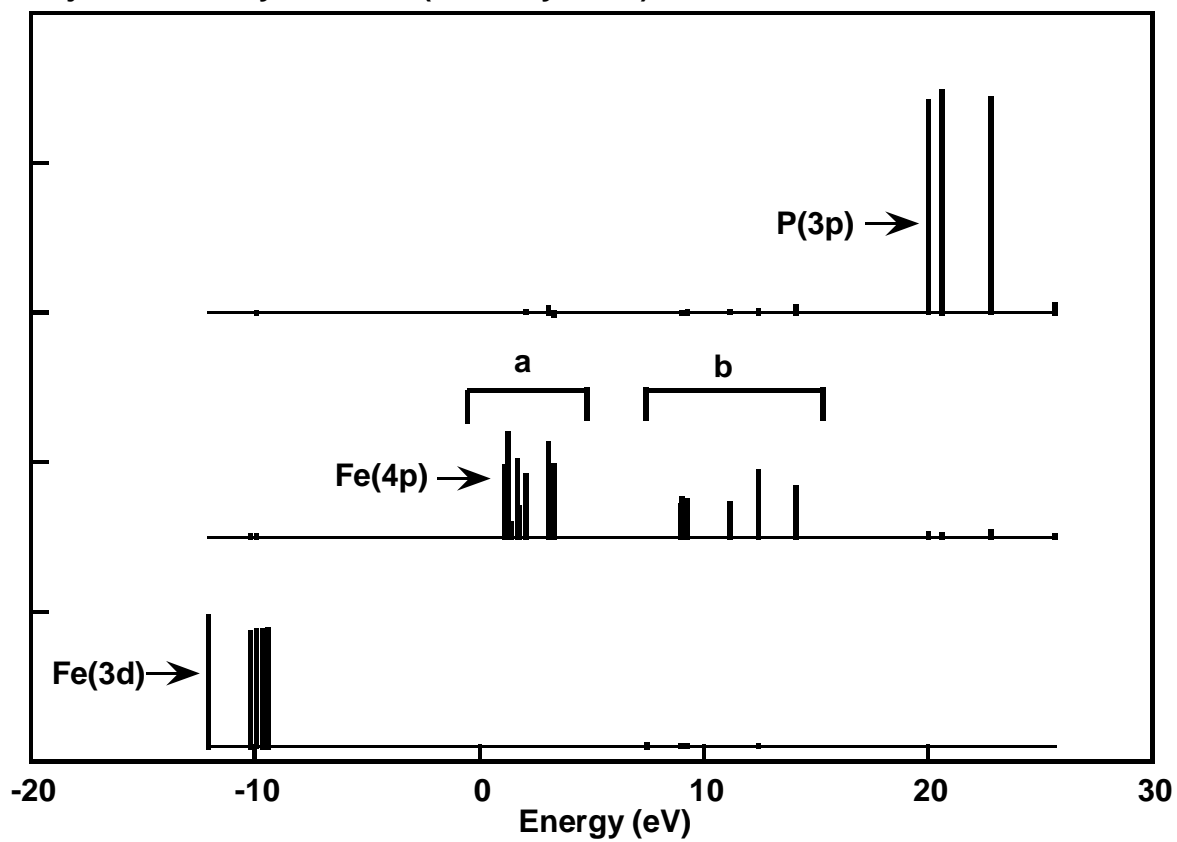


Fig. 3.8b

Projected density of states (arbitrary units)

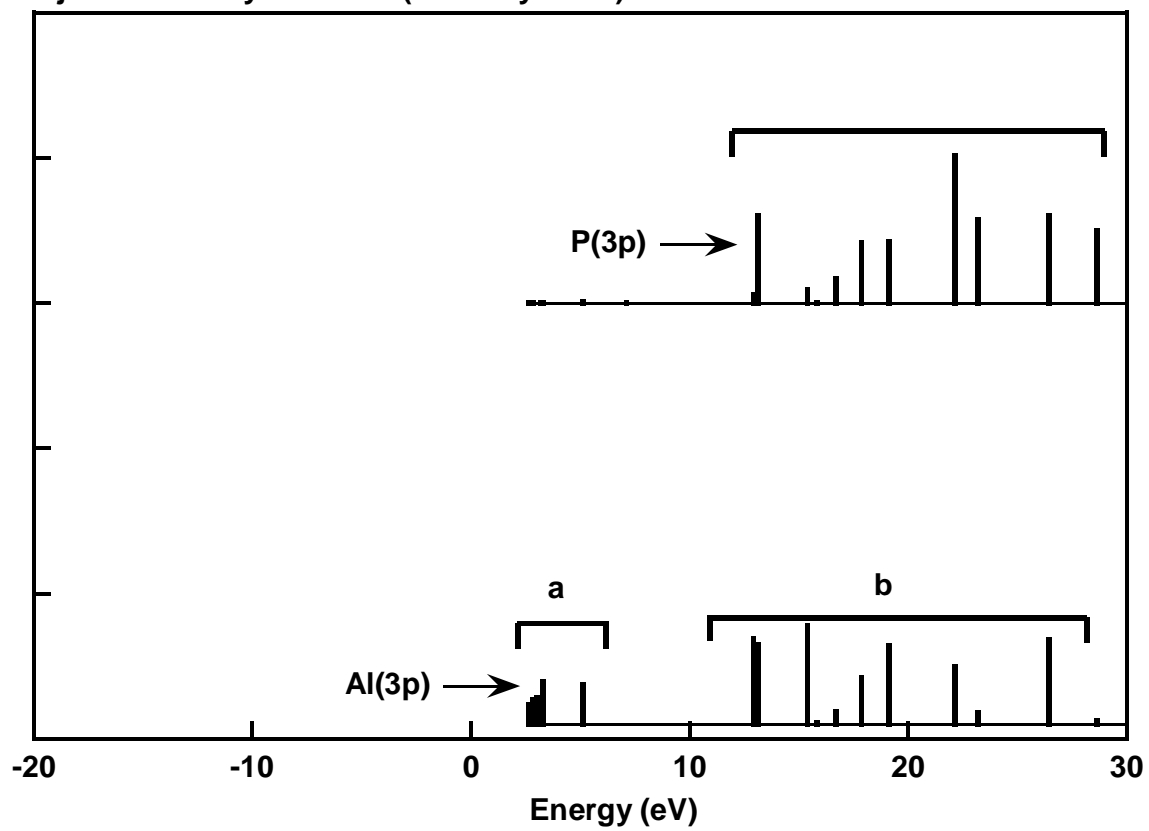


Fig. 3.8c

Projected density of states (arbitrary units)

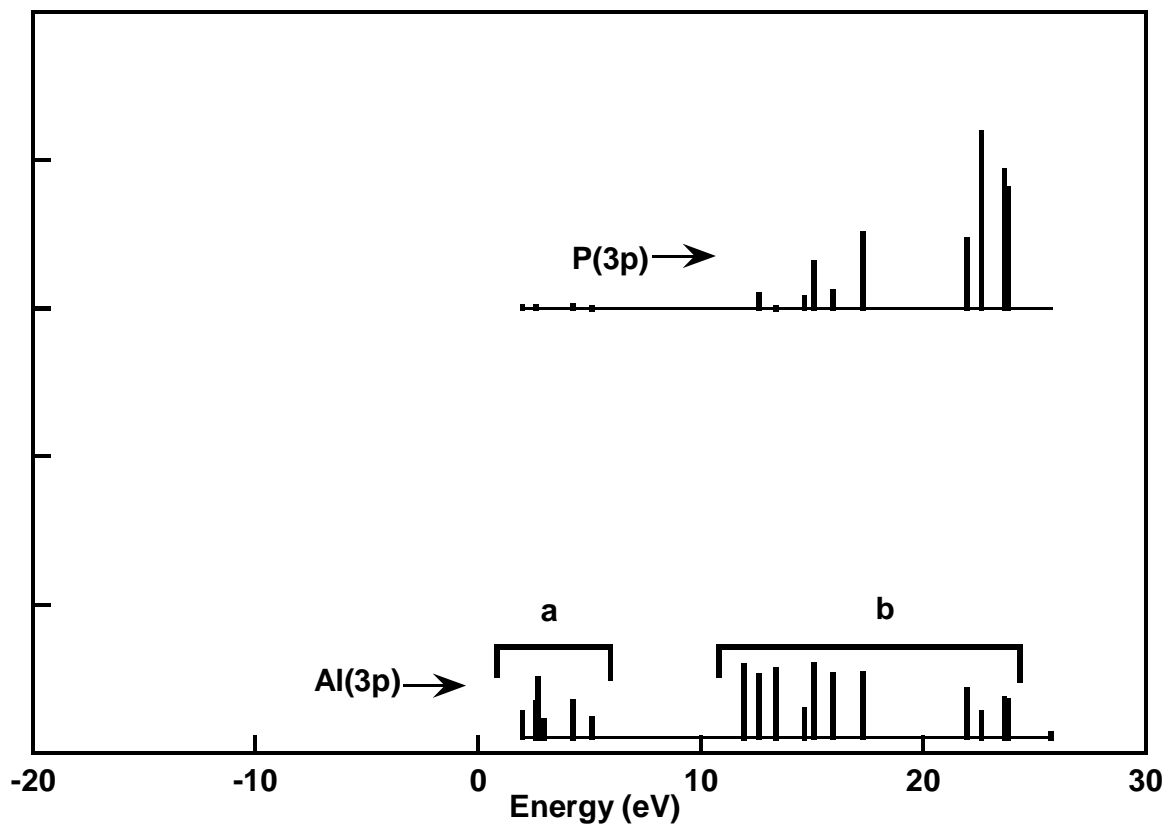


Fig. 3.8d

4. XANES INVESTIGATION OF METAL PHOSPHATE PRECIPITATION IN SINGLE AND BINARY MIXTURES OF Fe- AND Al-OXIDE MINERALS

INTRODUCTION

Phosphate sorption on Fe- and Al-oxide minerals has been studied for purposes of soil fertility and water quality because these minerals are considered the main P sorbents in acid soils (Pierzynski et al., 1990a; 1990b; Sallade and Sims, 1997; Beauchemin and Simard, 1999). Phosphate sorption studies on Fe- and Al-oxide minerals suggested that adsorption (surface complexation) or precipitation (e.g., surface precipitation) may occur (Ler and Stanforth, 2003; Johnson et al., 2002; Li and Stanforth, 2000; Nooney et al., 1998; Lookman et al., 1997; Tang et al., 1996; Lookman et al., 1994; Bleam et al., 1991; Martin et al., 1988; Willett et al., 1988; Bolan et al., 1985; van Riemsdijk and Lyklema, 1979; Veith and Sposito, 1977; Chen et al., 1973). Phosphate surface precipitation involves multiplayer surface coverage with phosphate and metal ions (Fe or Al) (Corey, 1981). Because some of the phosphate is buried under the particle surface and isolated from the exchange solution, occurrence of surface precipitation can inhibit phosphate desorption resulting in desorption hysteresis (Li and Stanforth, 2000). Furthermore, surface precipitation may increase the apparent sorption capacity of a mineral beyond that predicted by the density of surface binding sites (Van Riemsdijk and Lyklema, 1979, and Chen et al., 1973) Hence, it is important to distinguish adsorption from surface precipitation as the phosphate retention mechanism in Fe- and Al-oxide systems because surface precipitation (compared to strictly adsorption) can cause greater

amounts of phosphate to be associated with the oxide minerals and also retard its release.

Common approaches to studying phosphate surface precipitation on single mineral systems of Fe- and Al-oxides include macroscopic measurements and molecular scale spectroscopic measurements. As examples of macroscopic studies, changes in zeta potential of goethite at varying pH and phosphate concentrations indicated the formation of a phosphate surface precipitate (Li and Stanforth, 2000). The transition from adsorption to surface precipitation was not apparent in sorption isotherms, and the onset of surface precipitation occurred well before monolayer surface coverage at high pH values and at relatively low dissolved P concentrations ($5\text{-}15\ \mu\text{mol L}^{-1}$) (Li and Stanforth, 2000). Evidence for formation of x-ray amorphous variscite was shown in the reaction of $\text{Al}_2\text{O}_3 \cdot n\text{H}_2\text{O}$ with phosphate of varying acidity (Veith and Sposito, 1977). Van Riemsdijk and Lyklema (1979) reported the possibility of formation of potassium aluminum phosphate precipitate on the surface of gibbsite.

Spectroscopic techniques such as nuclear magnetic resonance (NMR) spectroscopy provided more direct (molecular-scale) evidence for surface precipitation in phosphate sorbed on Al-oxide minerals. For example, phosphate sorption in non-crystalline (non-xl) Al-hydroxide minerals investigated using NMR showed the formation of amorphous octahedral aluminum phosphate (Lookman et al., 1997). In addition, sorption of phosphate on Al_2O_3 studied using solid state NMR showed evidence for outer- and inner-sphere complexes and surface precipitation (Johnson et al., 2000).

While, zeta potential measurements are an indirect technique for determining surface precipitation, solid-state NMR spectroscopy (although direct) requires sample drying, which can alter the structure of surface species. For example, Bleam et al. (1991) found evidence for Al-PO₄ crystallites on the surface of boehmite, but discounted its significance because of possible artifacts of drying the samples.

X-ray absorption fine structure spectroscopy, including XANES and EXAFS, can be done in moist samples and hence are a non-invasive means for characterizing phosphate sorption in-situ. Investigating surface precipitation using P K-EXAFS is possible. However, significant improvement in signal to noise ratio is needed to fully exploit the EXAFS region at the P K-edge (Bradley et al., 1997). X-ray absorption near edge structure (P K-XANES) spectroscopy has recently been used to study phosphate sorbed on single minerals and in binary mixtures of ferrihydrite and boehmite (Chapter 2). Different spectral features have also been tied to specific electronic transitions of the core P electron (1s) to antibonding molecular orbitals (bound states) (Chapter 3). Because the molecular orbital energies and XANES spectral features were sensitive to the geometric configuration of phosphate associated with oxide minerals (Chapter 3), this technique has the potential to distinguish adsorption from surface precipitation.

The objective of this study was to investigate surface precipitation in single- and binary mixtures of Fe- and Al-oxide minerals as a function of sorbed phosphate concentration using a direct spectroscopic (XANES) approach. Unique aspects of this study were 1) to use XANES to determine the transition from adsorption to precipitation; 2) to study this transition in mixed-mineral systems in addition to

single-mineral systems. Although the transition from adsorption to surface precipitation has been characterized in single-mineral systems using NMR and zeta potential measurements, such studies have not been conducted in binary mixtures of Fe- and Al-oxides. Determination of surface precipitation in binary mixtures independently of characterizing surface precipitation in single mineral systems is important because it can provide insight into mineral-interaction effects on sorption. Single and binary mixtures of goethite/boehmite and ferrihydrite/non-xl Al-hydroxide were selected for this purpose. Goethite is ubiquitous in soils and sediments (Ler and Stanforth, 2003) while, ferrihydrite, boehmite, and non-xl Al-hydroxide represent poorly crystalline and non-xl analogs of Fe- and Al-oxide minerals in soils.

MATERIALS AND METHODS

Mineral Synthesis and Characterization

Two-line ferrihydrite was synthesized by hydrolyzing Fe(III) with KOH according to the method of Schwertmann and Cornell (1991). Goethite was synthesized by hydrolyzing $\text{FeCl}_2 \cdot 4\text{H}_2\text{O}$ with 1 M NaHCO_3 and oxidizing for 48 hours according to the method of Schwertmann and Cornell (1991). Poorly-crystalline boehmite was purchased from Reheis Co. (Berkeley Heights, NJ) in gel form under the trade name Rehydrigel HPA. Non-xl Al-hydroxide was synthesized by titrating a 0.25 M $\text{Al}_2(\text{SO}_4)_3$ solution with 1.5 M KOH solution (Prodromou and Pavlatou, 1995). Ferrihydrite, goethite, boehmite, and non-xl Al-hydroxide were characterized using x-ray powder diffraction. The x-ray diffraction pattern for non-xl Al-hydroxide showed

no peaks, confirming that it was x-ray amorphous. The x-ray diffraction pattern for ferrihydrite showed two broad peaks at 0.24 and 0.15 nm that are characteristic of 2-line ferrihydrite (Schwertmann and Cornell, 1991). Boehmite and goethite patterns showed no impurities. Boehmite, ferrihydrite, and non-xl Al-hydroxide minerals were stable in the time frame of experiments as determined by consistencies in maximum PO₄ sorption capacities measured 1 week after synthesis and again 1 year after synthesis.

Ferrihydrite, goethite and non-xl Al-hydroxide were washed thrice with 1 M KCl and further washed with 0.01 M KCl to bring to a 0.01 M KCl background electrolyte. Boehmite was purchased as a gel in deionized water and was also brought into a 0.01 M KCl background by adding a 1 M KCl solution. All minerals were stored as stock aqueous suspensions of known (measured) solids concentration in 0.01 M KCl (Chapter 2) containing 40.2 g ferrihydrite kg⁻¹, 14.1 g boehmite kg⁻¹, 30.2 g goethite kg⁻¹, and 53.7 g non-xl Al-hydroxide kg⁻¹. The mean crystallite dimensions of poorly-crystalline boehmite purchased from Reheis were previously determined to be 4.5, 2.2 and 10 nm along the crystallographic a, b and c axes, respectively; and the BET H₂O surface area was 514 m²g⁻¹ (Wang et al. 2003). Goethite synthesized by the above procedure is reported to produce acicular 100 nm long needles with BET surface area of 80 m² g⁻¹ (Schwertmann and Cornell, 1991). Although BET surface area for goethite was not measured for this sample, N₂ BET surface areas measured for previously synthesized batches varied from 80 to 180 m² g⁻¹.

Sorption Isotherms

Sorption isotherm experiments for ferrihydrite, goethite, boehmite, non-xl Al-hydroxide, goethite/boehmite and ferrihydrite/non-xl Al-hydroxide mixtures were conducted at pH 6.0 in 250-mL polycarbonate centrifuge bottles following the procedure described in Chapter 2. The goethite/boehmite and ferrihydrite/non-xl Al-hydroxide mixtures were prepared by mixing stock suspensions of individual components in 1:1 ratio by mass. Samples had a suspended solids concentration of 1.50 g kg^{-1} , constant ionic background of 0.01 M KCl, and total sample mass of $133.34 \pm 0.01 \text{ g}$. All aqueous solutions for sorption experiments (0.01 M KCl, 0.01 M HCl, 0.01 M KOH, and 0.01 M KH_2PO_4) were prepared using analytical grade reagents, and degassed (heated and N_2 purged), deionized water. All samples were shaken on a reciprocating water bath shaker at 1 s^{-1} for 42 hours at 22 °C. Additional isotherm data for the single and mixed-mineral systems were obtained on scaled down samples of 30 g total in 50 mL polycarbonate centrifuge tubes under identical experimental constraints and following an analogous procedure as outlined above and in Chapter 2. Isotherm data from both procedures were integrated.

XANES Data Collection and Analysis

Sample Preparation

For XANES analysis, each sedimented mineral sample from the 250-mL centrifuge bottles used for concurrent isotherm experiments was rinsed over in to 50-mL polycarbonate centrifuge tubes using a portion of its supernatant solution (to avoid changes in sorbed P), and centrifuged at $\sim 20,000 \times g$ for 15 minutes. A portion

(~0.2 g) of the sedimented mineral samples were mounted in acrylic holders and covered with 5 μm PP film to avoid desiccation as described in Chapter 2. Experiments were timed so that sample preparation was completed a maximum of five days in advance of XANES data collection.

Data Collection

Phosphorus K-XANES data acquisition was done at Beamline X-19A at the National Synchrotron Light Source, Brookhaven National Laboratory in Upton, NY. The electron beam energy was 2.6 GeV and the maximum beam current was 300 mA. The synchrotron radiation was monochromatized by a germanium [Ge(111)] monochromator. The monochromator energy was calibrated to 2149 eV at the maximum peak in the 1st-derivative spectrum at the white-line peak of a variscite sample diluted to 400 mmol kg⁻¹ in boron nitride (Hesterberg et al., 1999; Chapter 2). Spectra were collected in fluorescence mode using a PIPS (Passivated Implanted Planar Silicon) detector mounted into a He-filled sample chamber. XANES spectra were taken at photon energies between 2079 and 2248 eV with a minimum step size of 0.2 eV between 2099 to 2174 eV. Self-absorption effects were not considered to be important in the concentration range of our samples (as discussed in Chapter 2). Samples were analyzed in random chronological order to avoid any systematic trends in spectra due to beamline optics or decaying ring current between fills.

Data Normalization

The photon energy scale for all samples and standards was normalized to a relative energy scale by subtracting 2149 eV (Hesterberg et al., 1999). All individual scans were baseline corrected using a linear regression between -40 and -10 eV relative energy (Sayers and Bunker, 1988). To quantitatively analyze the pre-edge region of the spectra, the baseline for each individual scan was further refined by adjusting all the spectra to a common fluorescence yield value at -7 eV. After baseline correction and refinement, multiple scans for a given sample were ensemble averaged. To remove P concentration and detector response effects on the edge step, a single-point background normalization (Sayers and Bunker, 1988) was done using the fluorescence yield at the energy of the maximum peak between 10 and 18 eV in the first derivative XANES spectrum (edge normalized) (Chapter 2). The fluorescence yields over the entire spectrum were divided by the fluorescence yield at the given normalization energy.

Approach for distinguishing Adsorption vs. Surface Precipitation

White-line Peak Broadening as an Indicator of Precipitation

The broadening of the white-line peak in XANES spectra for PO_4 sorbed on Fe- or Al-oxide minerals was used as an indicator for formation of a mineral precipitate phase. White-line peak broadening was quantified by measuring the full width at half maximum height (FWHM) of the peak defined as the width of the white-line peak at half of its maximum height relative to the spectral baseline. The effect of a two dimensional adsorption phase versus a three-dimensional precipitate on

FWHM of the white-line peak for Al(III)-associated PO₄ was determined by comparing the energy distribution of the Al(3p) and P(3p) projected density of states (PDOS) for PO₄ sorbed on Al-oxide minerals and variscite as described in Chapter 3. Phosphate sorbed on an Al-oxide mineral was modeled by an Al-PO₄ cluster (AlO₅PO₄H₅)⁵⁻ in idealized monodentate configuration, and the variscite represented the AlPO₄ precipitate phase. Fractional coordinates for variscite were taken from the literature. Fractional coordinates for the monodentate Al-PO₄ cluster were calculated by assuming an ideal octahedral symmetry for Al-O, ideal tetrahedral symmetry for a PO₄ fragment, and Al-Al, Al-O bond distances in boehmite, and P-O bond distances in variscite. Extended Huckel (Whangbo, 2000) computed PDOS were obtained using the procedure described in Chapter 3.

Adsorption vs. Surface Precipitation

Adsorption vs. precipitation was assessed by trends in FWHM of white-line peak in XANES spectra for PO₄ sorbed on Fe- and Al-oxide minerals as a function of sorbed PO₄ concentration. The onset of PO₄ surface precipitation in mineral-mixtures was investigated by comparing trends in FWHM of white-line peak in XANES spectra for mixtures with trends in their respective single-mineral components.

Relative Distribution of PO₄ in Mixed-Mineral Systems

To determine the proportion of PO₄ associated with Fe(III) vs. Al(III), XANES spectra for goethite/boehmite and ferrihydrite/non-xl Al-hydroxide mixed-mineral

systems were fit in the pre-edge region (-6 to -1 eV) with single-mineral standards of PO₄ on the respective Fe-oxide or Al-oxide according to the procedure described in Chapter 2.

RESULTS AND DISCUSSION

Phosphate Sorption in Fe- or Al-oxide Mixtures

Sorption isotherms for goethite, boehmite, ferrihydrite, non-xl Al-hydroxide, and 1:1 mixtures of goethite/boehmite and ferrihydrite/non-xl Al-hydroxide (Figs. 4.1a and 4.1b) were L-curves that could be fit with Freundlich models (Sposito, 1984). The maximum levels of sorption observed were 580 (goethite), 850 (boehmite), 1860 (ferrihydrite), 3400 (non-xl Al-hydroxide), 710 (goethite-boehmite) and 2500 (ferrihydrite-non-xl Al-hydroxide) mmol kg⁻¹. Note that the isotherm data did not reach a plateau (asymptote) for any of the concentration ranges studied. Compared with the other systems, the isotherm for PO₄ on non-xl Al-hydroxide was more steeply sloping at the maximum observed level of sorbed PO₄. Similar to ferrihydrite/boehmite mixed-mineral systems (Chapter 2), the phosphate sorption isotherms for goethite/boehmite and ferrihydrite/non-xl Al-hydroxide mixed-mineral systems were intermediate between those of the respective single-mineral systems (Figs. 4.1a and 4.1b). However, the isotherm model derived as a weighted combination of Freundlich models for ferrihydrite and non-xl Al-hydroxide systems (see Chapter 2) predicted up to 16% more for the mixture of these minerals than was observed (Fig. 4.1b). For the goethite/boehmite mixtures, the combination

model varied by <2% from the Freundlich model fit to the mixed-mineral data (Fig. 4.1a).

P K-XANES spectra for Fe- or Al-oxide Mixtures

Representative XANES spectra for phosphate sorbed on goethite (100 to 580 mmol kg⁻¹), ferrihydrite (100 to 1680 mmol kg⁻¹), boehmite (100 to 850 mmol kg⁻¹), or non-xl Al-hydroxide (100 to 1800 mmol kg⁻¹), goethite/boehmite mixtures (100 to 660 mmol kg⁻¹) and ferrihydrite/non-xl Al-hydroxide mixtures (100 to 1230 mmol kg⁻¹) are shown in Figs. 4.2 and 4.3. The spectra were characterized by a strong white-line peak near 0 eV relative energy. In addition, the XANES spectra for PO₄ sorbed on goethite, ferrihydrite, and in mixtures showed a pre-edge feature on the low energy side of the white-line peak between -5 and -1 eV (Figs. 4.2 and 4.3). Because this pre-edge feature is due to a low probability transition of a phosphorus 1s electron into an Fe(4p)-O(2p) antibonding molecular orbital (Chapter 2), the feature indicates that PO₄ is coordinated with Fe(III) atoms in the second shell. Therefore, the feature provides direct evidence for inner-sphere surface complexation of phosphate on goethite and ferrihydrite (see Chapter 2) (Figs. 4.4a and 4.4b). This trend in pre-edge peak was similar to trends observed in ferrihydrite/boehmite mixtures (Chapter 2) and indicated a change in the distribution of Fe(III) and Al(III) in the second coordination shell of PO₄ (discussed below). There were also decreases in the white-line peak intensity with increasing concentration for some samples (Figs. 4.2 and 4.3) that were quantified on the basis of corresponding changes in FWHM of this peak (discussed later) (Figs. 4.2 and 4.3).

The White-line Peak as an Indicator of PO₄ Bonding Configuration

The white-line peak in P K-XANES spectra for PO₄ sorbed on Al-oxide minerals has been assigned to an electronic transition of a P(1s) electron into Al(3p)-O(2p)-P(3p) antibonding molecular orbitals (Chapter 3). The FWHM of the white-line peak was therefore a measure of the energy distribution of Al(3p)-O(2p)-P(3p) antibonding molecular orbitals. To understand the implications of white-line peak broadening (increase in FWHM), the energy distribution of Al(3p)-O(2p)-P(3p) antibonding molecular orbital in sorbed and precipitate Al/PO₄ phases were compared. Extended Huckel computed projected density of states (PDOS) (Whangbo, 2000) for P(3p) and Al(3p) were used to compare the energy distribution of Al(3p)-O(2p)-P(3p) antibonding molecular orbital. The width of overlapping Al(3p) and P(3p) PDOS for a monodentate bonded Al-PO₄ cluster and variscite are shown in Figs. 4.4a and 4.4b. The overlapping Al(3p) P(3p) PDOS for variscite spanned 23 eV (from 7 to 31 eV –Fig. 4b) and was ~13eV broader than for monodentate bonded AlPO₄ cluster (15 to 25 eV –Fig. 4.4a). This increase in width of overlap in Al(3p), P(3p) PDOS representative of Al(3p)-O(2p)-P(3p) antibonding molecular orbitals indicated that an increase in FWHM of the white-line peak is expected for a precipitate relative to an adsorbed phase. That is, the probability of a P(1s) electron being excited to an Al(3p)-O(2p)-P(3p) molecular orbital is higher over a greater energy range for variscite than for PO₄ adsorbed on Al-oxide as a monodentate surface complex. Therefore, for P K-XANES data normalized to a per-atom basis

(Sayers and Bunker, 1988), a broader (and less intense) white-line peak is predicted from the PDOS calculations for variscite.

The white-line peak in XANES spectra for PO_4 sorbed on boehmite remained essentially constant with sorbed PO_4 concentration but shifted by 0.2 eV to higher energy at 830 mmol kg^{-1} sorbed PO_4 concentration (Fig. 4.2, close-up of white-line peak shift not shown). The white-line peak in XANES spectra for PO_4 sorbed on non-xl Al-hydroxide or goethite/boehmite mixtures showed a systematic shift to higher energies (total observed shift = 0.2 eV for a 0.2 eV monochromator step size) with increasing sorbed PO_4 concentration (Figs. 4.2 and 4.3). However, the energy step size of the data (0.2 eV) was too great to determine systematic changes in white-line peak position. Nevertheless, based on the white-line peak assignment, a higher energy shift indicated that the energy of the Al(3p)-O(2p)-P(3p) antibonding orbital had increased. The bonding in Al- PO_4 complexes is a competitive binding of oxygen with Al vs. P (similar to bonding arguments for Fe- PO_4 complexes given in Chapter 3). The white-line peak shift to higher energies indicated that the phosphorus-oxygen bonding became stronger with increasing sorbed PO_4 concentration and the Al-O bonding became weaker. Weaker Al-O bonding would result if PO_4 is coordinated in a multidentate configuration (e.g., a bidentate surface complex or surface precipitate) on a mineral surface, or as a free precipitate (Chapter 3). Hence, the white-line peak shift to greater energy suggested that either bidentate surface complexation or surface precipitation could be occurring in the single-mineral systems of boehmite and non-xl Al-hydroxide.

Distribution of PO₄ in Mixed Mineral Systems

XANES spectra for PO₄ sorbed on Fe-oxide (goethite, ferrihydrite) and Al-oxide (boehmite or non-xl Al-hydroxide) differed in the pre-edge region (Figs. 4.2 and 4.3). As shown in Figs. 4.5a and 4.5b, the pre-edge for phosphate sorbed in mixed-mineral systems was intermediate in intensity compared to the respective single-mineral standards for phosphate sorbed on Fe- or Al-oxide minerals. Hence, linear combination fitting (LCF) analysis limited to the pre-edge region was used to determine the amounts of PO₄ associated with Fe or Al in mineral-mixtures (see Chapter 2). It is important to analyze if surface precipitation affects LCF analysis to determine quantitative PO₄ distribution between Fe- and Al-oxide minerals in mineral mixtures. The pre-edge feature was attributed to transition of a P(1s) electron to a Fe(4p)-O(2p) antibonding molecular orbital and is a quantitative measure of phosphate coordinated to Fe(III) in the second shell. The pre-edge intensity increases with increasing Fe-O-P bonding (Hesterberg et al., 1999; Chapter 3). Thus, formation of a surface (or free) precipitate would increase the intensity of the pre-edge feature. Phosphate sorbed on an Al-oxide mineral or Al-PO₄ mineral precipitate (such as variscite) showed no feature in the pre-edge region and the pre-edge region for these were essentially identical (Chapter 2). Hence, we can surmise that the pre-edge region in XANES spectra for PO₄ associated with Al(III) is identical both for adsorbed and surface precipitated phases. It is important to note that the phosphate associated with Al in mixed-mineral systems calculated using LCF analysis could represent phosphate adsorbed on the surface of boehmite (or Al-hydroxide), as well as Al-PO₄ precipitates on surfaces of Fe- or Al-oxides. Thus, it is

more proper to refer to the relative amounts of sorbed phosphate determined by LCF analysis as “PO₄ associated with Fe or Al” rather than PO₄ sorbed on Fe- or Al-oxide minerals.

XANES fitting results showed that the amount of PO₄ associated with Al(III) increased with increasing total sorbed PO₄ concentrations in the goethite/boehmite mixtures (Table 4.1, Fig. 4.6a). The relative distribution of PO₄ between Fe(III) and Al(III) in the ferrihydrite/non-xl Al-hydroxide mixtures followed a similar trend of increasing amounts of PO₄ associated with Al(III) with increasing total sorbed PO₄ concentration in the mixtures (Table 4.2, Fig. 4.6b). The relative PO₄ distribution on each single-mineral component for mineral-mixtures were compared to an apparent no-preference line assuming adsorption alone to be the PO₄ retention mechanism in these systems (see Chapter 2). In goethite/boehmite mixtures, the PO₄ distribution showed a marked deviation from the apparent no-preference line suggesting a preference for boehmite at sorbed PO₄ concentrations >400 mmol kg⁻¹ (Fig. 4.6a). In ferrihydrite/non-xl Al-hydroxide systems, PO₄ preferred non-xl Al-hydroxide at essentially all sorbed PO₄ concentrations. The behavior of PO₄ in the binary mixtures described above was in marked contrast to the trends observed in ferrihydrite/boehmite mixtures where PO₄ showed essentially no preference for either ferrihydrite or boehmite (Figs. 4.6a and 4.6b) (Chapter 2). A possible explanation for the apparent preference for Al(III) is that a Al-phosphate like surface precipitate formed in the mixed systems.

Adsorption vs. Surface Precipitation in Single-Mineral Systems

The FWHM of white-line peak in XANES spectra for phosphate sorbed on single Al-oxide minerals of boehmite or non-xl Al-hydroxide increased with increasing sorbed PO_4 concentrations (Figs. 4.7a and 4.7b) suggesting that Al-phosphate precipitation occurred. The regression models shown in Figs. 4.7a and 4.7b were significant for both of these systems ($p = 0.03$ for boehmite and $p < 0.01$ for Al-hydroxide). In agreement with our results for non-xl Al-hydroxide systems, Lookman et al. (1994) found evidence from NMR studies for Al-phosphate formation at higher adsorbed PO_4 concentration. Results from a diffuse reflectance IR study by Nanzyo (1984) also found that bulk Al-phosphate formed when reacting non-crystalline Al-hydroxide with phosphate.

In contrast to Al-oxide systems, XANES spectra for phosphate sorbed in Fe-oxide systems did not show broadening of the white-line peak (Figs. 4.7a and 4.7b), although data for goethite ($n = 3$) were limited. The FWHM of the white-line peak in XANES spectra for PO_4 sorbed on goethite or ferrihydrite did not show a trend with increasing sorbed PO_4 concentrations as indicated by non-significant ($p > 0.05$) linear regressions (Figs. 4.7b and 4.7a). Also, the XANES pre-edge features for these systems were less intense than the pre-edge feature observed in XANES spectra for FePO_4 (strengite), and the pre-edge intensity did not show a trend with sorbed phosphate concentration (Chapter 2). If increasing FWHM of the white-line peak in XANES spectra and intensity of the pre-edge feature are indicative of a 3-dimensional cluster or surface precipitate, then our data show no evidence for clustering or precipitation in the ferrihydrite and goethite systems. Our ferrihydrite

results are consistent with those of Willett et al., (1988) who found no evidence from a combination of infra-red spectrometry and electron micro-probe analysis for the formation of iron-phosphate when sorbing phosphate on the surface of ferrihydrite.

Adsorption vs. Surface Precipitation in Mineral Mixtures

The FWHM of white-line peak in XANES spectra for PO₄ sorbed in goethite/boehmite mixtures increased with increasing total sorbed PO₄ concentration significantly. These mixtures showed a trend in FWHM and (white-line peak energy shift, data not shown) similar to that in single-mineral systems of boehmite (Fig. 4.7a). Goethite, the second component in the goethite/boehmite mixtures showed no evidence for Fe-phosphate precipitation at sorbed PO₄ concentrations up to 550 mmol kg⁻¹ as discussed in the previous section. While the slope of regression of FWHM on sorbed P concentration for the goethite/boehmite mixture was not significantly ($p > 0.05$) different than that of boehmite, the regression intercept was between those for goethite and boehmite. Thus, the XANES results indicated that phosphate sorption in the 1:1 goethite/boehmite mixtures was essentially a combination of sorption in each of the separate components, with some form of Al-phosphate precipitation occurring. Also, the predicted sorption for the 1:1 goethite/boehmite mixtures based on a linear combination of Freundlich models for goethite and boehmite deviated by <2% from the Freundlich model for the mixed-mineral isotherm data (Fig 4.1a). The isotherm results were consistent with XANES results and suggested that mineral interactive effects with regards to phosphate sorption were minimal in the goethite/boehmite mixtures. At 660 mmol kg⁻¹

goethite/boehmite mixtures, the amount of PO_4 associated with Al(III) ($1150 \text{ mmol kg}^{-1}$) as predicted by XANES exceeded the maximum phosphate sorption capacity of boehmite (850 mmol kg^{-1}). As shown in Fig. 4.1a and the discussion above, the maximum observed P sorption by boehmite 850 mmol kg^{-1} included surface precipitation. We hypothesize that the XANES predicted excess PO_4 associated with Al(III) in goethite/boehmite mixtures may be due to Al(III) associated with sorbed PO_4 on the surface of goethite according to the surface precipitation model proposed by Ler and Stanforth. (2003). Regardless of the mechanism, XANES results apparently overpredicted the amount of phosphate associated with Al(III) (or boehmite) as a result of Al-phosphate precipitation.

In ferrihydrite/non-xl Al-hydroxide mixtures, the FWHM of the white-line peak in XANES spectra showed no significant trend with sorbed PO_4 concentration ($p \geq 0.05$), suggesting that no detectable surface precipitation occurred in this mixed-mineral system (Fig. 4.7b). Although white-line peak broadening indicated that (surface) precipitation occurred in single-mineral systems of non-xl Al-hydroxide, precipitation was apparently inhibited when this mineral was combined with ferrihydrite. The predicted sorption for the 1:1 ferrihydrite/non-xl Al-hydroxide mixture based on a linear combination of Freundlich models for the single-mineral systems (as described in Chapter 2) deviated positively from the Freundlich model fit for the isotherm data for dissolved PO_4 concentrations $>6 \mu\text{mol L}^{-1}$ (Fig. 4.1b). This trend makes sense if precipitation of Al-phosphate occurred in the single-mineral non-xl Al-hydroxide system (causing a greater level of PO_4 sorption beyond just adsorption), and not in the ferrihydrite/non-xl Al-hydroxide mixtures. Hence, our

results suggested that sorption in ferrihydrite/non-xl Al-hydroxide mixtures was not a linear combination of sorption in their respective single-mineral components consistent with XANES findings. Furthermore, the relative distribution of PO_4 as determined by XANES analysis of non-xl Al-hydroxide/ferrihydrite mixtures indicated an affinity preference of PO_4 for non-xl Al-hydroxide with increasing adsorbed PO_4 concentrations over the concentration range studied (Fig. 4.6b).

CONCLUSIONS

Phosphate was bound via an adsorption mechanism as an inner-sphere surface complex on goethite and ferrihydrite as indicated by a pre-edge feature in P K-XANES spectra. The trends in FWHM of the white-line peak of XANES spectra for phosphate sorbed on boehmite or non-xl Al-hydroxide showed evidence for Al-phosphate precipitation, probably as a surface precipitate. The XANES spectra for goethite/boehmite mixtures showed evidence for Al-phosphate precipitation, while no evidence for surface-precipitation was found in the ferrihydrite/non-xl Al-hydroxide mixtures. Based on XANES evidence, and sorption isotherms, the phosphate sorption in goethite/boehmite mixtures appeared to be a linear combination of phosphate sorption in single-mineral components. The ferrihydrite/non-xl Al-hydroxide mixtures did not appear to be a linear combination of phosphate sorption in their respective single-mineral components suggesting mineral interactive effects. Phosphate showed an affinity preference for non-xl Al-hydroxide with increasing adsorbed PO_4 concentrations in the non-xl Al-hydroxide/ferrihydrite mixtures.

REFERENCES

Bleam, W., P. Pfeffer, S. Goldberg, R.W. Taylor, and R. Dudley. 1991. A ^{31}P solid state nuclear magnetic resonance study of phosphate adsorption at the boehmite/aqueous solution interface. *Langmuir* 7:1702-1712.

Bolan, N.S., N.J. Barrow, and A.M. Posner. 1985. Describing the effect of time on sorption of phosphate by iron and aluminum hydroxides. *J. Soil Sci.* 36:187-197.

Bradley, S.M., S. Djajanti, S. Thomson, R.F. Howe. 1997. Soft X-ray absorption spectroscopy of microporous materials. SSRL activity report.

Chen, Yi S.R., J.N. Butler, and W. Stumm. 1973. Kinetic study of phosphate reaction with aluminum oxide and kaolinite. *Env. Sci & Tech.* 7: 327-332.

Corey, R.B. 1981. Adsorption vs. precipitation. p 161-183. *In* M.A. Anderson and A.J. Rubin (ed.) Adsorption of inorganics at solid-liquid interfaces. Ann Arbor Science.

Hesterberg, D.L., W. Zhou, K.J. Hutchison, S. Beauchemin, and D.E. Sayers. 1999. XAFS study of adsorbed and mineral forms of phosphate. *J. Synchrotron Rad.* 6:636-638.

Johnson, B.B., A.V. Ivanov, O.N. Antzutkin, and W. Forsling. 2002. ^{31}P Nuclear magnetic resonance study of the adsorption of phosphate and phenyl phosphates on $\gamma\text{-Al}_2\text{O}_3$. *Langmuir*. 18:1104-1111.

Li, L., and R. Stanforth. 2000. Distinguishing adsorption and surface precipitation of phosphate on goethite ($\alpha\text{-FeOOH}$). *J. Colloid Interface Sci.* 230:12-21.

Ler, A., and R. Stanforth. 2003. Evidence for surface precipitation of phosphate on goethite. *Environ. Sci. Technol.* 37:2694-2700.

Lookman, R., P. Gorbet, R. Merckx, and K. Vlassak. 1994. Phosphate sorption by synthetic amorphous aluminum hydroxides: a ^{27}Al and ^{31}P solid-state MAS NMR spectroscopic study. *Europ. J. Soil Sci.* 45:37-44.

Lookman, R., P. Gorbet, R. Merckx, and W.H. Van Riemsdijk. 1997. Application of ^{31}P and ^{27}Al MAS NMR for phosphate speciation studies in soil and aluminum hydroxide: promises and constraints. *Geoderma*. 80: 369-388.

Martin, R.R., R. ST. S. Smart, and K. Tazaki. 1988. Direct observation of phosphate precipitation in the goethite/phosphate system. *Soil Sci. Soc. Am. J.* 52: 1492-1500.

Nanzyo, M. 1984. Diffuse reflectance infrared spectra of phosphate sorbed on alumina gel. *J. of Soil Sci.* 35:63-69.

Nooney, M.G., A. Campbell, T.S. Murrell, X. -F. Lin, L.R. Hossner, C.C. Chusuei, and D.W. Goodman. 1998. Nucleation and growth of phosphate on metal oxide thin films. *Langmuir*. 14: 2750-2755.

Parfitt, R.L., R.J. Atkinson, and, R. St.C. Smart, 1975. The mechanism of phosphate fixation by iron oxides. *Soil Sci. Soc. Amer. Proc.* 39: 837-841.

Prodromou, K.P. and A.S. Pavlatou-Ve, 1995. Formation of aluminum hydroxides as influenced by aluminum salts and bases. *Clay Clay Minerals* 43:111-115.

Sayers D.E., B.A. Bunker. 1988. Data analysis. p 211-253. *In* D.C. Koningsberger and R. Prins (ed.) *X-ray absorption: principles, applications, techniques of EXAFS, SEXAFS, and XANES*. John Wiley & Sons, New York.

Schwertmann, U. and R.M. Cornell. 1991. *Iron oxides in the laboratory: preparation and characterization*. VCH Publ. Co., Weinheim, Germany.

Tang, Wei-Ping., O. Shima, and K. Ooi. 1996. A kinetic study of phosphate adsorption by boehmite. *J. Pharm. Sci.* 86: 230-235.

Van Riemsdijk W.H. and Lyklema J., 1979. The reaction of phosphate with aluminium hydroxide in relation with phosphate bonding in soils. *Colloids and Surfaces*, 1(1980) 33-44.

Veith, J.A., and G. Sposito. 1977. Reactions of aluminosilicates, aluminum hydrous oxides, and aluminum oxide with o-phosphate: The formation of X-ray amorphous analogs of variscite and montebasite. *Soil Sci. Soc. Am. J.* 41: 870-876.

Wang, S.L., C.T. Johnston, D.L. Bish, J.L. White, and S.L. Hem. 2003. Water-vapor adsorption and surface area measurement of poorly crystalline boehmite. *J. Colloid Interface Sci.* 260:26-35.

Whangbo, M.H. 2000. Perspective on "An extended Huckel theory. I. Hydrocarbons" Hoffmann R (1963). *J. Chem Phys* 39:1397-1412.

Willett, I.R., C.J. Chartres, and T.T. Nguyen. 1988. Migration of phosphate into aggregated particles of ferrihydrite. *J. Soil Sci.* 39:275-282.

Table 4.1: Phosphate associated with Fe and Al in 1:1 (mass basis) mixtures of goethite and boehmite calculated using linear combination fitting of edge normalized phosphorus K-XANES spectra †

Total Level of Sorbed PO ₄ (mmol kg ⁻¹)	% sorbed on Fe	% sorbed on Al	χ^2
100	58 ± 2	42 ± 4	0.0007
200	53 ± 2	47 ± 3	0.0006
300	45 ± 1	55 ± 2	0.0002
400	40 ± 1	60 ± 2	0.0002
500	28 ± 1	72 ± 2	0.0002
660	17 ± 2	87 ± 3	0.0005

†Standard errors shown were calculated by the fitting program (Kaliedagraph, Synergy Software Co., Reading, PA).

Table 4.2: Phosphate associated with Fe and Al in 1:1 (mass basis) mixtures of ferrihydrite and non-xl Al-hydroxide calculated using linear combination fitting of edge normalized phosphorus K-XANES spectra †

Total Level of Sorbed PO ₄ (mmol kg ⁻¹)	% Sorbed on Fe	% Sorbed on Al	χ^2
100	59 ± 6	41 ± 14	0.0067
200	22 ± 2	78 ± 3	0.0004
300	30 ± 1	70 ± 2	0.0003
400	18 ± 1	82 ± 3	0.0004
600	14 ± 1	86 ± 2	0.0002
1230	20 ± 0	80 ± 1	0.0001

†Standard errors shown were calculated by the fitting program (Kaliedagraph, Synergy Software Co., Reading, PA).

Figure Captions

Fig.4.1 Sorption isotherms for phosphate on single- and mixed-mineral systems (1:1 mass basis) at $\text{pH } 6.0 \pm 0.1$, along with Freundlich isotherm models. (a) goethite/boehmite systems; (b) ferrihydrite/non-xl Al-hydroxide systems. Data for the mixed mineral isotherm are also compared with mass weighted (1:1) linear combination of Freundlich models from the single-mineral systems (dashed line). Model parameters q_i and c_i denote the Freundlich model predicted sorbed and dissolved PO_4 concentrations respectively for boehmite (B), goethite (G), non-xl Al-hydroxide (A) ferrihydrite (F), and mineral mixtures (M), calculated from the data.

Fig. 4.2 Normalized, stacked phosphorus K-XANES spectra for phosphate sorbed on goethite, boehmite, or mixed-mineral systems at $\text{pH } 6.0 \pm 0.1$ at selected concentrations. Numbers in the legend denote adsorbed PO_4 in mmol kg^{-1} . A pre-edge feature between -5 and -1 eV relative energy is apparent in the goethite and mixed-mineral spectra.

Fig. 4.3 Normalized, stacked phosphorus K-XANES spectra for phosphate sorbed on ferrihydrite, non-xl Al-hydroxide, or mixed-mineral systems at $\text{pH } 6.0 \pm 0.1$ at selected concentrations. Numbers in the legend denote adsorbed PO_4 in mmol kg^{-1} . A pre-edge feature between -5 and -1 eV relative energy is apparent in the ferrihydrite and mixed-mineral spectra.

Fig. 4.4 The projected density of states (PDOS) computed for Al-PO₄ complex and variscite using the Extended Huckel approximation: (a) PDOS for monodentate Al-PO₄; (b) PDOS for the mineral variscite.

Fig. 4.5 Comparison of the pre-edge region for normalized XANES spectra for PO₄ sorbed in mixed-mineral systems at selected concentrations with spectra for averaged standards for PO₄ sorbed on Fe-oxide or Al-oxide at pH 6.0 ± 0.1. Numbers in the legend denote adsorbed PO₄ concentrations in mmol kg⁻¹: (a) goethite/boehmite mixtures; (b) ferrihydrite/non-xl Al-hydroxide mixtures.

Fig. 4.6 Concentration of PO₄ sorbed on the Fe-oxide component of Fe- and Al-oxide mixtures (as calculated from XANES fitting analysis) plotted as a function of total sorbed phosphate concentration for mixtures: (a) goethite/boehmite mixtures; (b) ferrihydrite/non-xl Al-hydroxide mixtures. The apparent no-preference line was determined based on the maximum observed sorption capacities of the single minerals in Fig. 1, assuming no surface precipitation (see Chapter 2). Regression fits to the data are also included.

Fig. 4.7 The full width at half maximum height (FWHM) of the white-line peak in XANES spectra for phosphate sorbed on mixtures, and the respective single-mineral components as a function of sorbed PO₄ concentration: (a) goethite/boehmite mixtures; (b) ferrihydrite/non-xl Al-hydroxide mixtures.

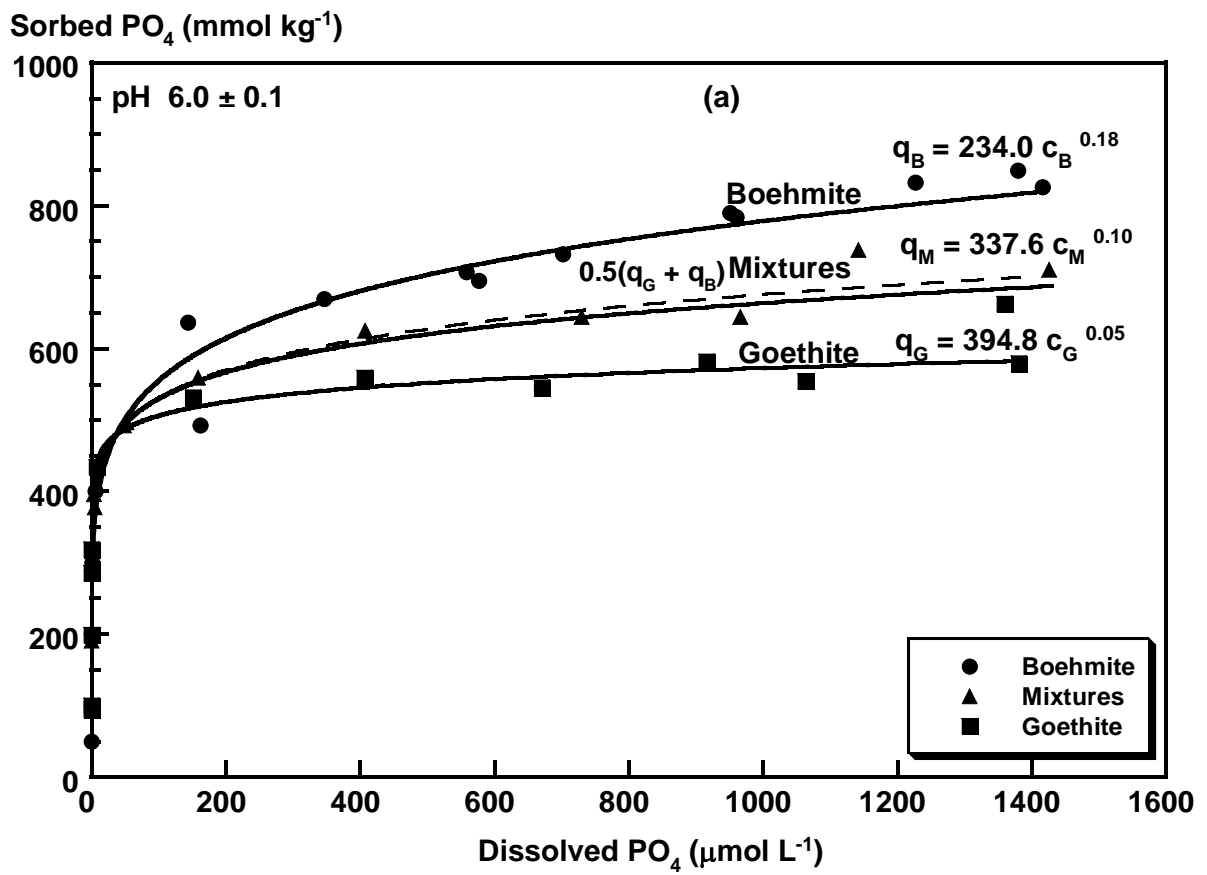


Fig. 4.1 a

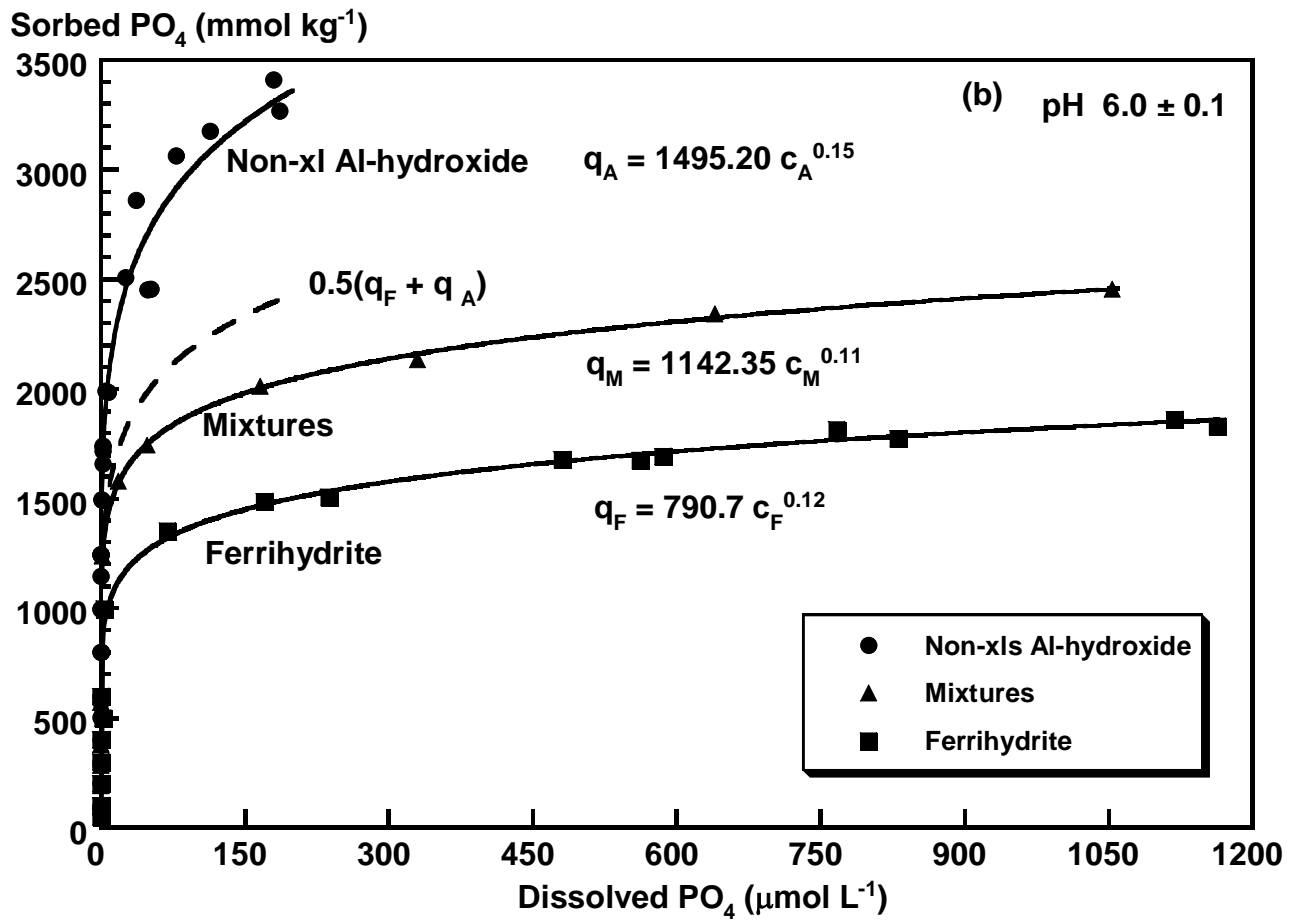


Fig. 4.1b

Normalized Fluorescence Yield

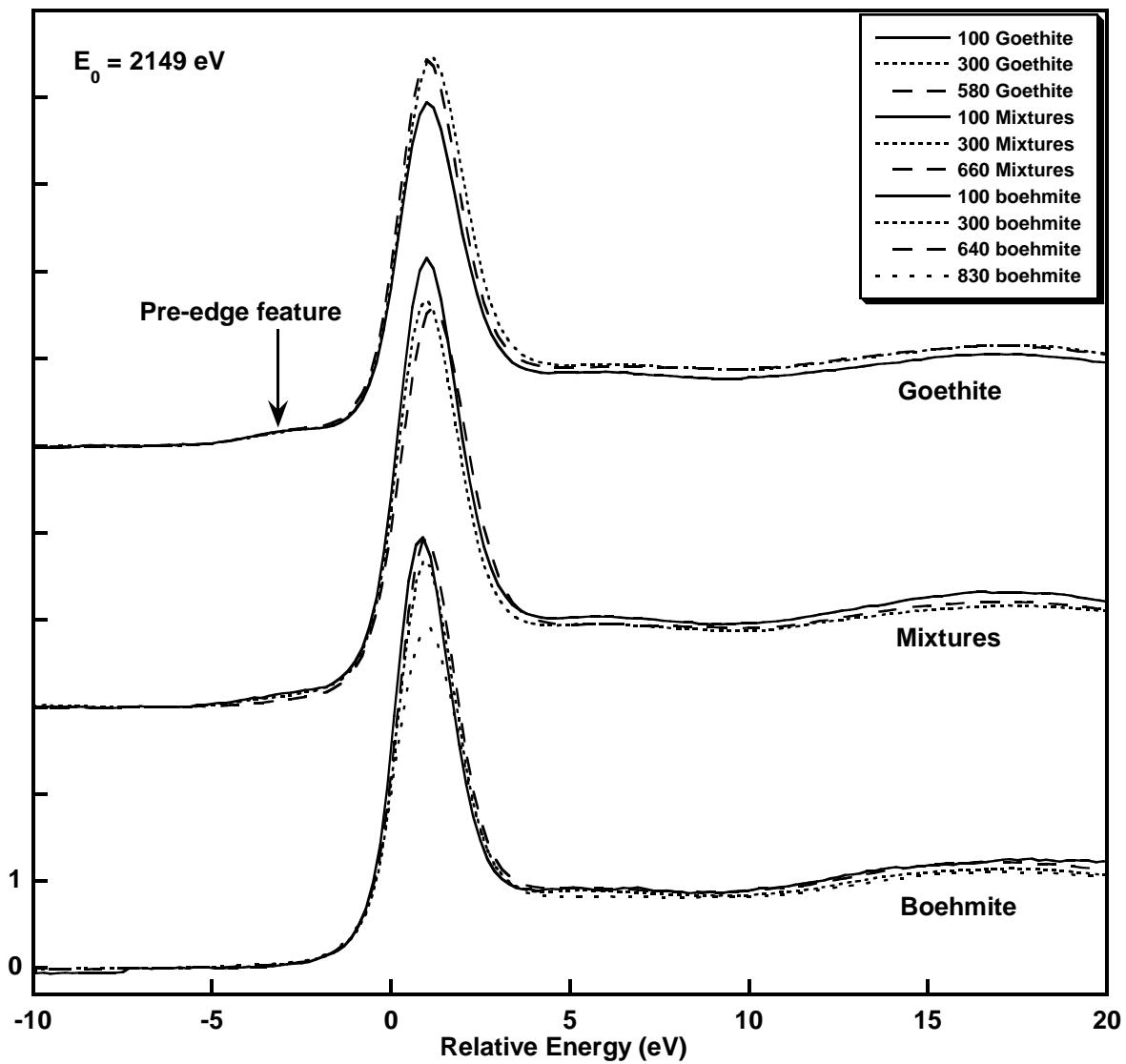


Fig. 4.2

Normalized Fluorescence Yield

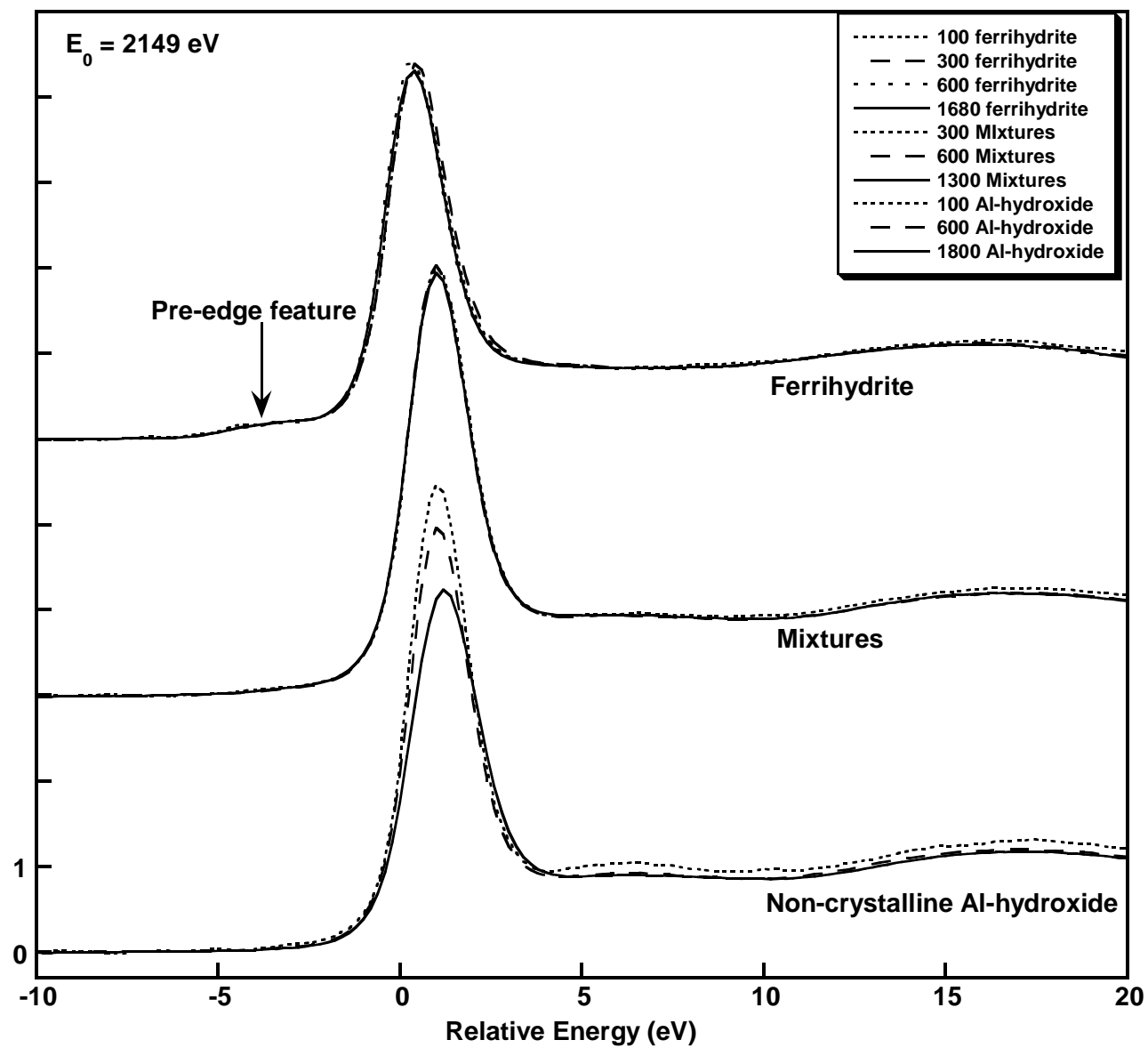


Fig. 4.3

PDOS (arbitrary units)

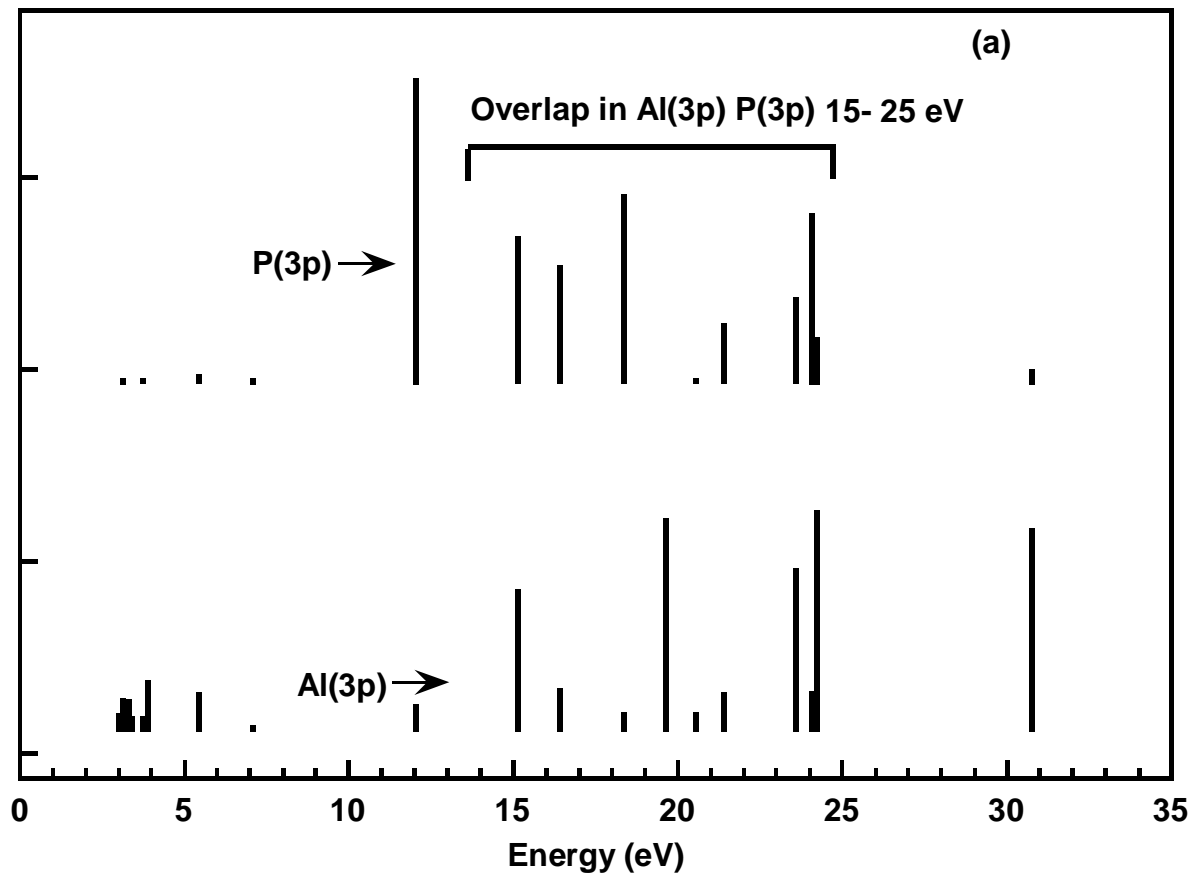


Fig. 4.4a

PDOS (arbitrary units)

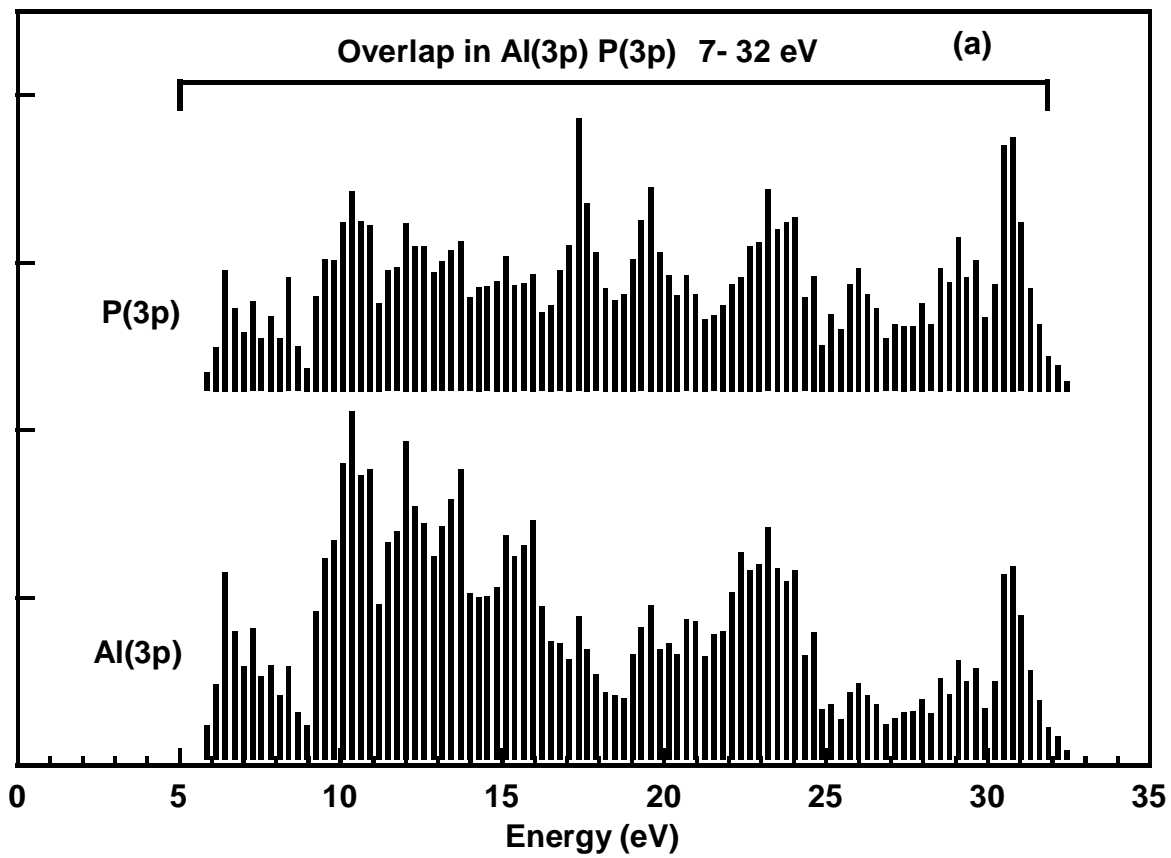


Fig. 4.4b

Normalized Fluorescence Yield

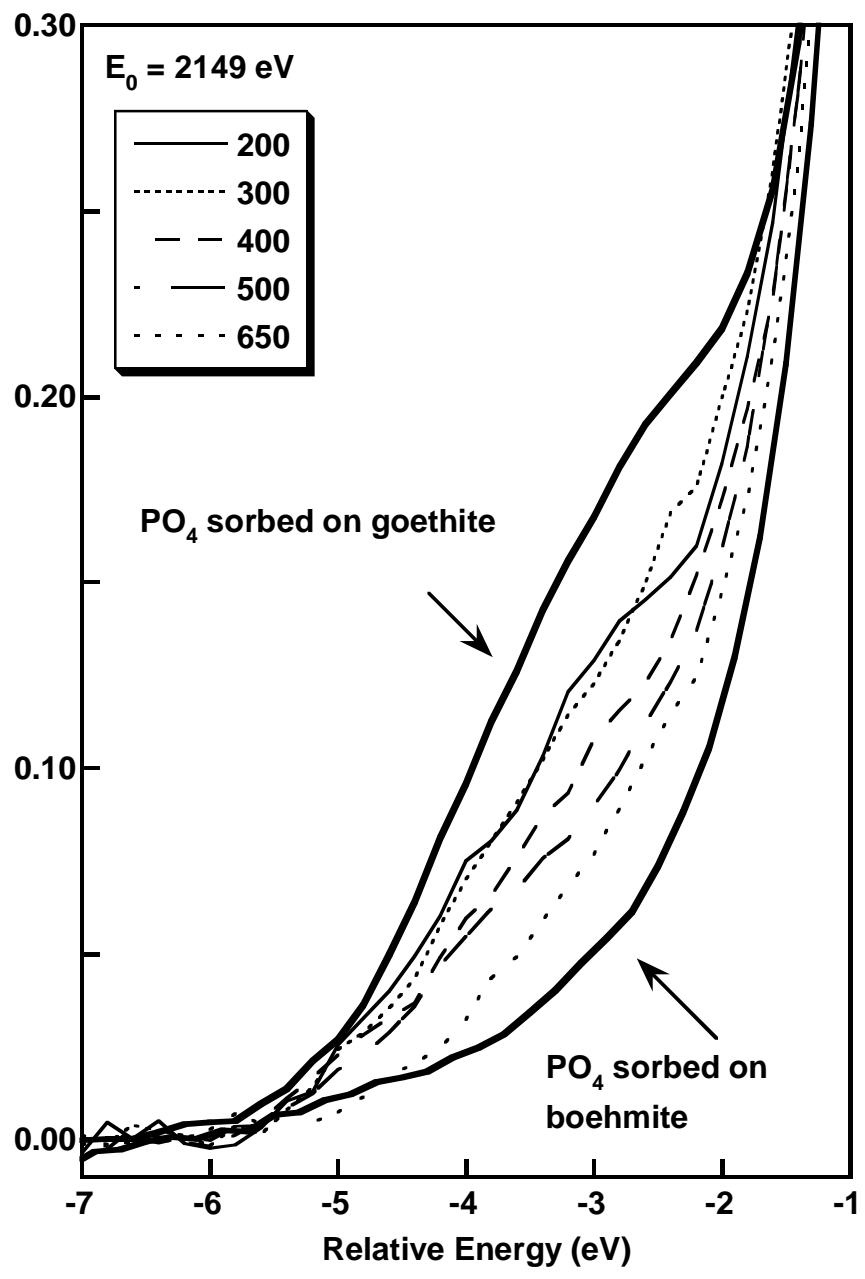


Fig. 4.5a

Normalized Fluorescence Yield

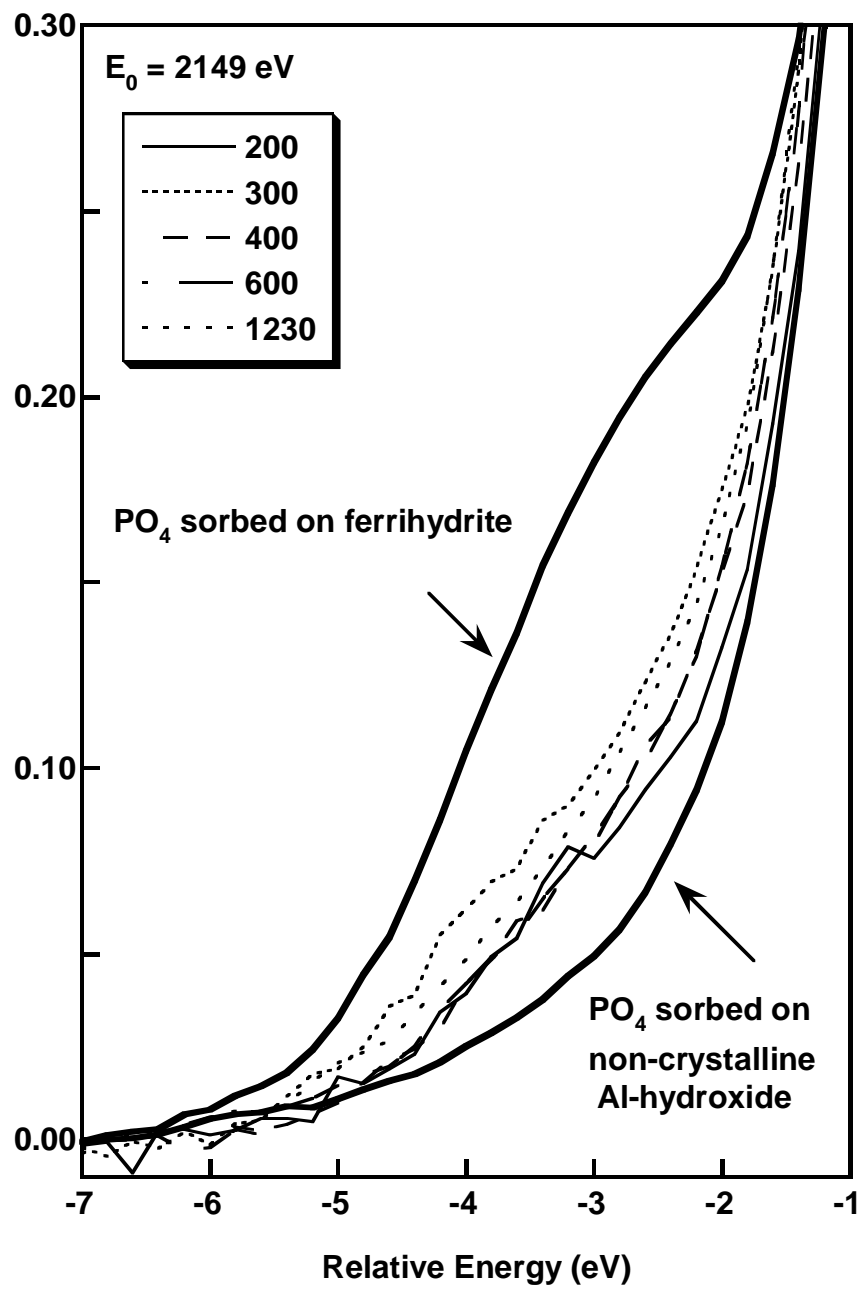


Fig. 4.5b

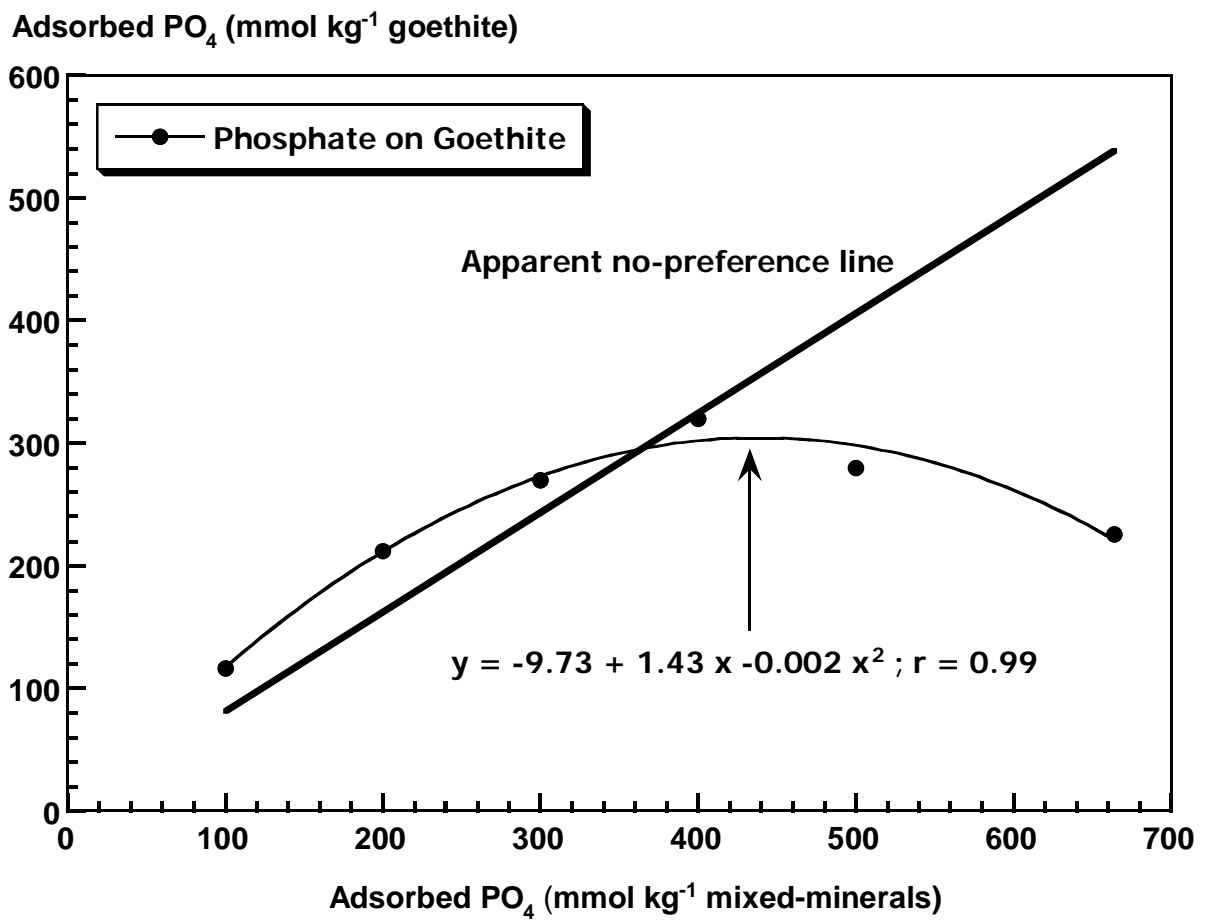


Fig. 4.6a

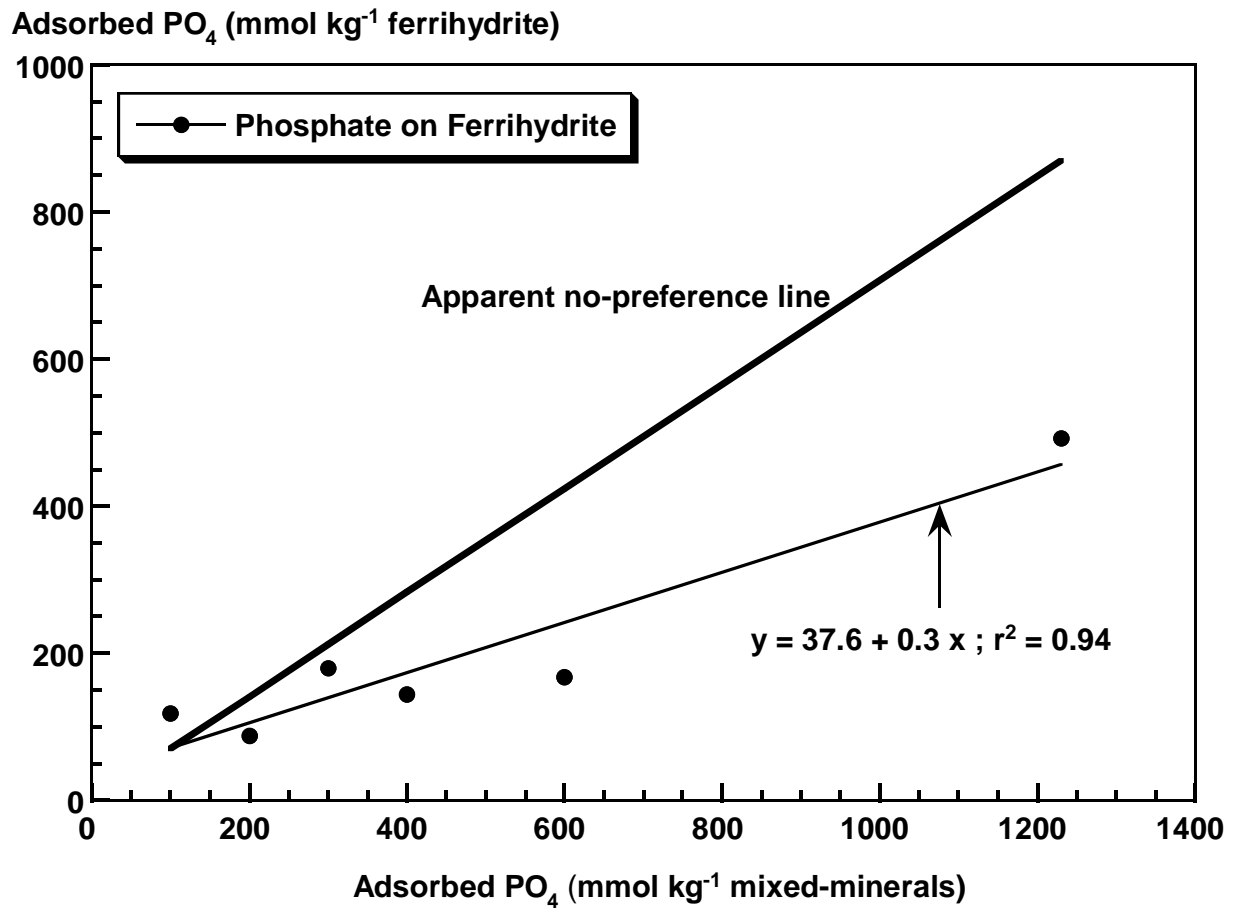


Fig. 4.6b

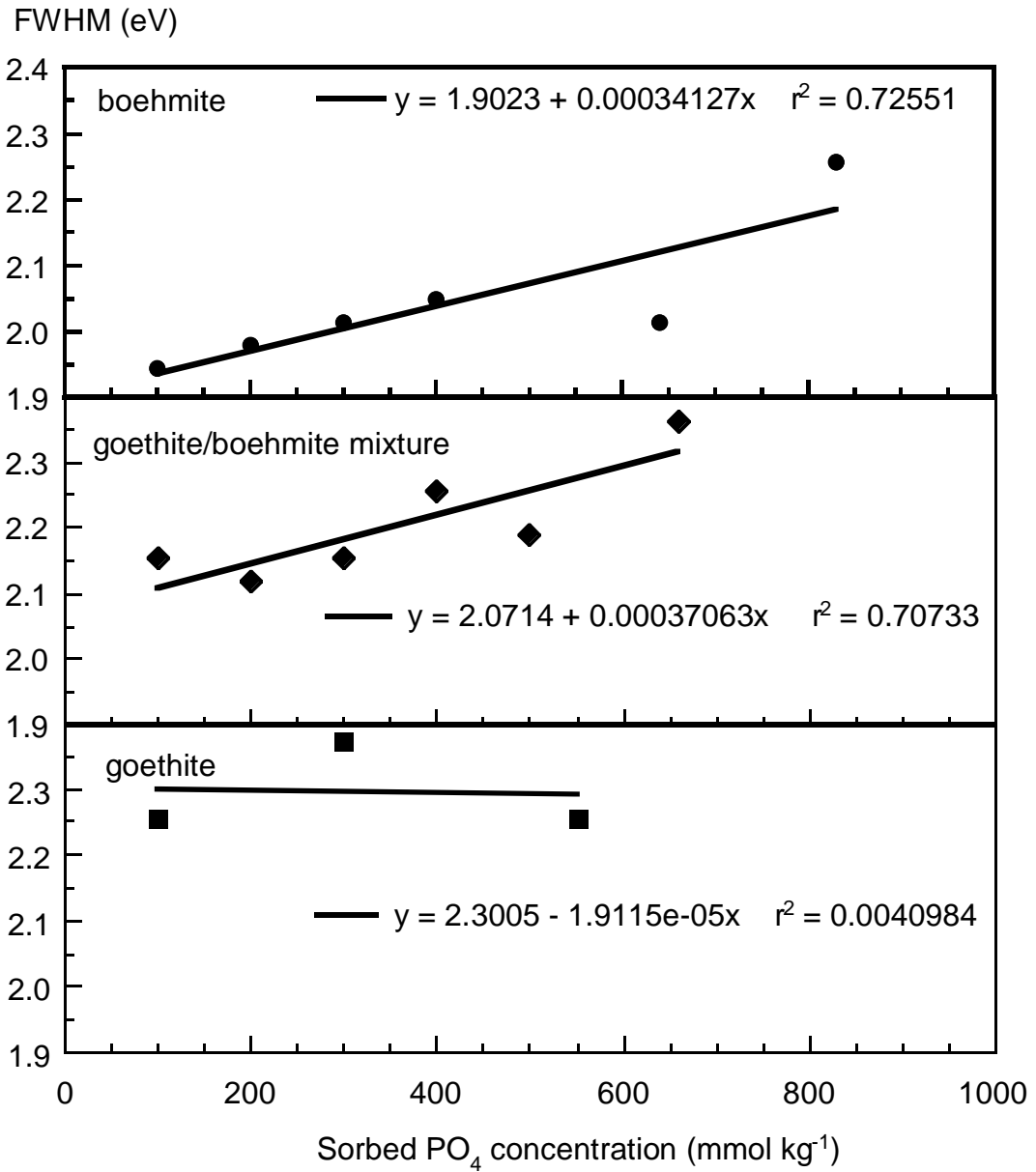


Fig. 4.7a

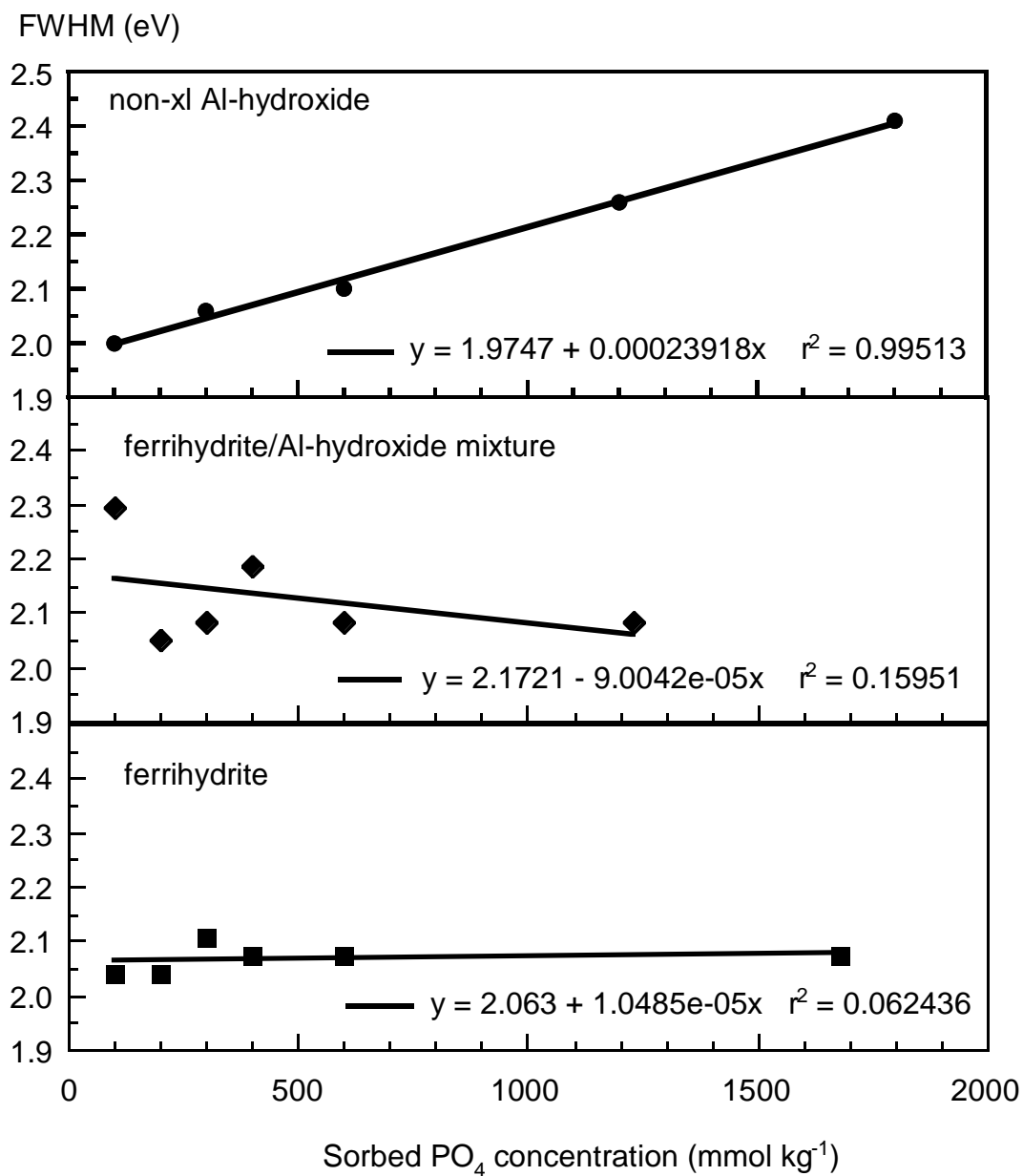


Fig. 4.7b

5. CONCLUSIONS and IMPLICATIONS

The purpose of this research was to characterize sorption in single- and mixed systems of Fe- and Al-oxide minerals at a molecular level using XANES spectroscopy. We successfully developed a technique to determine the quantitative distribution of PO_4 between Fe- and Al-oxide minerals in mixtures of these minerals. This technique was based on the difference in the pre-edge region of XANES spectra for PO_4 sorbed on Fe- versus Al-oxide minerals. Linear combination fitting analysis of XANES spectra (fitting limited to the pre-edge region) was used to quantitatively determine the amounts of phosphate associated with Fe-oxide versus Al-oxide minerals. Hence, phosphate distribution between Fe- and Al-oxide minerals could be determined in ferrihydrite/boehmite, goethite/boehmite, and ferrihydrite/non-xl Al-hydroxide mixtures. Furthermore, the relative affinity of each mineral in a mixture was estimated from the PO_4 distributions. In ferrihydrite/boehmite mixtures, PO_4 slightly preferred ferrihydrite at low sorbed PO_4 concentrations. At intermediate total sorbed PO_4 concentrations, phosphate had no preference for either mineral, while at 1310 $\text{mmol PO}_4 \text{ kg}^{-1}$ (near the maximum sorption capacity of 1420 $\text{mmol PO}_4 \text{ kg}^{-1}$), PO_4 preferred boehmite. These results indicated the presence of some high affinity phosphate binding sites on ferrihydrite. Similarly, a greater apparent affinity preference was found for phosphate on boehmite at $>400 \text{ mmol PO}_4 \text{ kg}^{-1}$ in goethite/boehmite mixtures, as was a trend of preference for non-xl Al-hydroxide in ferrihydrite/non-xl Al-hydroxide mixtures with increasing adsorbed P

concentration. For the goethite/boehmite mixtures, surface precipitation of an Al-phosphate may have skewed an estimate of relative affinity in favor of boehmite.

Based on bonding arguments supported by extended Huckel model computations, we attributed the white-line peak in XANES spectra for Fe-phosphate systems to the dipole allowed transition of a P 1s electron to a P(3p)-O(2p) antibonding molecular orbital. Similarly, the white-line peak in XANES spectra for Al-phosphate systems was attributed to the dipole allowed transition of a P 1s electron to a Al(3p)-O(2p)-P(3p) antibonding molecular orbital. XANES and UV-visible spectral trends in aqueous Fe-PO₄ complexes in known monodentate and bidentate bonding configuration were consistent with our white-line peak assignments. The pre-edge feature in PO₄ associated with Fe (for e.g. in FePO₄ minerals, or PO₄ sorbed on Fe-oxides) was assigned to the dipole allowed transition of a P 1s electron to a Fe(4p)-O(2p) antibonding molecular orbital; the absence of pre-edge feature for Al(III)-associated PO₄ was due to the overlap of Al(3p)-O(2p) and P (3p)-O(2p) antibonding molecular orbitals. The greater pre-edge peak intensity in strengite compared to aqueous monodentate and bidentate Fe-PO₄ complexes were consistent with our pre-edge peak assignment. Based on the EH computations, we also predicted the possibility of a third feature in P K-XANES spectra for P associated with Fe on the low energy side of the pre-edge feature due to a weakly allowed transition of a P 1s electron to a Fe(3d)-O(2p) antibonding molecular orbital. The above assignments strengthened the basis for distinguishing P associated with Fe versus Al. In addition, because the pre-edge feature was a quantitative measure of the

coordination of PO₄ with Fe(III) in the second shell, it provided direct evidence for inner-sphere complexation of PO₄ on Fe-oxides (goethite or ferrihydrite).

Based on trends in FWHM (full width at half maximum height) and energy shifts of the white-line peak in XANES spectra for PO₄ sorbed on boehmite or non-xl Al-hydroxide, surface precipitation occurred in single Al-oxide minerals with increasing sorbed PO₄ concentration. No evidence for surface precipitation was found in single-mineral systems of ferrihydrite or goethite. The evidence for adsorption as the binding mechanism in PO₄ sorption in Fe-oxides was consistent with its weaker pre-edge intensity compared to the mineral precipitate strengite (FePO₄·2H₂O). Surface precipitation occurred in goethite/boehmite mixtures due to a similar trend of white-line broadening and energy shifts as was observed in single-mineral systems of boehmite. In addition, the sorption in goethite/boehmite mixtures could be predicted (within 2%) as a linear combination of Freundlich model fits for goethite and boehmite. Hence, we concluded that sorption in goethite/boehmite mixtures was a linear combination of sorption in their respective components. No evidence for surface precipitation was found in the ferrihydrite/non-xl Al-hydroxide systems and the sorption isotherm data fitted as a linear combination of Freundlich model fits for ferrihydrite and non-xl Al-hydroxide deviated by 16% more than the observed sorption in the mixtures. Hence, we concluded that sorption in ferrihydrite/non-xl Al-hydroxide mixtures was not a linear combination of sorption in their respective components and that surface precipitation was inhibited in the mixtures due to mineral interactions.

This research therefore successfully determined solid state speciation in single- and mixed Fe- and Al-oxide systems. To the extent that the results from this study in binary mixtures can be extended to soils, we hypothesize that surface precipitation could play a role in phosphate sorption. More phosphate would likely be associated with Al-oxide rather than Fe-oxide minerals, simplistically implying less phosphorus release on reduction.